VIENNA UNIVERSITY OF TECHNOLOGY
DEPARTMENT FOR GEODESY AND GEOINFORMATION
RESEARCH GROUPS PHOTOGRAMMETRY & REMOTE SENSING

DISSERTATION

THE USE OF SAR BACKSCATTER TIME SERIES FOR CHARACTERISING RICE PHENOLOGY

Ausgeführt zum Zwecke der Erlangung des akademischen Grades

Doktor der technischen Wissenschaften

Unter der Leitung von

Univ.-Prof. Dipl.-Ing. Dr.techn. Wolfgang Wagner

E120.1

Department für Geodäsie und Geoinformation

Forschungsgruppe Fernerkundung

Eingereicht und der Technischen Universität Wien

Fakultät für Mathematik und Geoinformation

von

Duy Nguyen

Matrikelnummer: 1328707

Wien, im April 2018 .....

Unterschrift

VIENNA UNIVERSITY OF TECHNOLOGY
DEPARTMENT FOR GEODESY AND GEOINFORMATION
RESEARCH GROUPS PHOTOGRAMMETRY & REMOTE SENSING

DISSERTATION

THE USE OF SAR BACKSCATTER TIME SERIES FOR CHARACTERISING RICE PHENOLOGY

A thesis submitted in fulfillment of the academic degree of

Doktor der technischen Wissenschaften

Under the supervision of
Univ.-Prof. Dipl.-Ing. Dr.techn. Wolfgang Wagner

E120.1
Department of Geodesy and Geoinformation
Research Group Remote Sensing

Research conducted at TU Wien
Faculty of Mathematics and Geoinformation

by

Duy Nguyen
Matriculation number : 1328707

Vienna, April 2018

.....
Signature

Supervisor/Reviewer: Prof. Dr. Wolfgang Wagner

Department of Geodesy and Geoinformation, TU Wien

Gusshausstraße 27-29, 1040, Vienna, Austria

E-Mail: Wolfgang.Wagner@geo.tuwien.ac.at ……

Reviewer: Prof. Dr. Clement Atzberger

Institute of Surveying, Remote Sensing and Land Information, University of Natural Resources and Life Sciences ……

Peter-Jordan-Straße 82,1190 Vienna, Austria

E-Mail: clement.atzberger@boku.ac.at

Reviewer: Dr. Claudia Künzer

German Aerospace Center (DLR)

German Remote Sensing Data Center Land Surface ……

Oberpfaffenhofen, 82234 Weßling, Germany

E-Mail: claudia.kuenzer@dlr.de

Parts of the presented work have already been published in several peer-reviewed journal papers, which include:

Journal publications

Nguyen, D., K. Clauss, S. Cao, V. Naeimi, C. Kuenzer and W. Wagner (2015). *Mapping Rice Seasonality in the Mekong Delta with Multi-Year Envisat ASAR WSM Data*. Remote Sensing **7**(12): 15808.

Nguyen, D., A. Gruber and W. Wagner (2016). *Mapping rice extent and cropping scheme in the mekong delta using sentinel-1a data*. Remote Sensing Letters, 7, 1209-1218.

Nguyen, D and W. Wagner (2017). *European Rice Cropland Mapping with Sentinel-1 Data: The Mediterranean Region Case Study*. Water , 9, 392.

ERKLÄRUNG ZUR VERFASSUNG DER ARBEIT

AUTHOR'S STATEMENT

Hiermit versichere ich an Eides statt und durch meine Unterschrift, dass die vorliegende Arbeit von mir selbstständig, ohne fremde Hilfe angefertigt worden ist. Inhalte und Passagen, die aus fremden Quellen stammen und direkt oder indirekt übernommen worden sind, wurde als solche kenntlich gemacht. Ferner versichere ich, dass ich keine andere, außer der im Literaturverzeichnis angegebenen Literatur verwendet habe. Diese Versicherung bezieht sich sowohl auf Textinhalte sowie alle enthaltenden Abbildungen, Karten und Tabellen.

I hereby declare that I independently drafted this manuscript, that all sources and references are cited, and that the respective parts of this manuscript – including tables, maps, and figures – which were included from other manuscripts or the internet either semantically or syntactically are made clearly evident in the text and all respective sources are correctly cited.

Duy Nguyen

……

(Unterschrift/Signature)

ACKNOWLEDGEMENTS

I would like to thank everyone who made this dissertation possible. Special thanks go to my supervisor Wolfgang Wagner for his advice, also to Vahid Naeimi for guidance and supervision during my start in Vienna. Moreover, many thanks to Claudia Kuenzer for her support during my stay in DLR, Germany, to Kersten Clauss, Senmao Cao and Alexander Gruber for their brilliant co-authorship, to Ali Iftikhar for valuable comments and input that helped me whilst working on the thesis. Also, my gratitude and recognition is with to the entire GEO Remote Sensing Research Group for the unique working environment and extraordinary teamwork, to all the lectures of the Department of Photogrametry and Remote Sensing, Hanoi University of Mining and Geology for the unique support, hard work and research.

I would like to thank to everyone that I have not mentioned individually for their valuable input and helpful instructions. The teamwork on conferences, workshops, meetings is greatly appreciated. Furthermore, thanks to all scientists whom I have not had the opportunity to meet in person but inspired and guided me on the right path with my research.

Last but not the least, my sincere thanks to my soul father Nguyen Van Nghia, my mother Bui Thi Quy, my parents in law, Tran Van Son and Nhu Thi Lan Huong, my wife Tran Thi Huong Giang, for their continuing support and patience during this period. Thank you for their encouragement and believing in me, which helped me to pursue my research study towards the end.

KURZFASSUNG

Detaillierte Kenntnisse über die Fläche und die Lage der Reisanbaugebiete ist für jede Nation, dessen Wirtschaft von der Reisproduktion abhängt, von großer Bedeutung. Die Erforschung der Flächen der Reisanbaugebiete ist notwendig um die verschiedenen Faktoren und Auswirkungen des Reisanbaus zu untersuchen. Zu den Anwendungsgebieten zählen unter anderem Risikomanagement für die Versicherungsindustrie, Umweltberichtserstattungen, Ermittlung von Treibhausgasemissionen aufgrund von Reisanbau, die Analyse von Lebens- und Wasserzyklen, sowie Ernteprognosen.

Die wichtigste Quelle für Reisackerland-Aufzeichnungen sind satellitengestützte Mikrowellen-Instrumente, die Daten unabhängig von der Wolkenbedeckung erheben können. Ein Synthetic Aperture Radar (SAR) ist ein aktiver Sensor, der im Mikrowellenspektrum arbeitet. Die resultierenden Bilder reflektieren die Rückstreueigenschaften der Oberfläche, die durch die physikalischen (e.g. Oberflächenrauigkeit, geometrische Struktur, Orientierung) und elektrischen (e.g. Dielektrizitätskonstante, Feuchtigkeitsgehalt, Leitfähigkeit) Eigenschaften der Oberfläche und durch die Radarfrequenz des Sensors (e.g. L-, C-, X-Band) bestimmt werden.

Die multitemporale SAR Bildanalyse ist eine gängige Methode für die Überwachung der Reisanbaugebiete. Die starke Veränderung des SAR Rückstreuungssignals während der Wachstumsperiode bildet den Schlüsselparameter um Reisanbauflächen von anderen Landnutzungsflächen zu unterscheiden. Daraus entwickelte sich eine der wichtigsten Methoden für die Reisüberwachung auf der Grundlage von satellitengestützten Mikrowellen-Datensätzen. Aufgrund der starken Abhängigkeit des Signals vom Einfallswinkel gibt es bisher keine Studie, die das komplette Advanced Synthetic Aperture Radar (Envisat ASAR) Archiv zur kartografische Darstellung von Reisflächen nutzt. Des Weiteren ist das volle Potenzial der Sentinel-1 Mission für die Reisüberwachung (auf regionaler sowie kontinentaler Skala) immer noch Gegenstand laufender Forschung und noch nicht vollständig ausgeschöpft.

Diese Arbeit entwickelte eine multitemporale Methode zur Rückstreuungsanalyse, die darauf abzielt, Reisanbaugebiete zu klassifizieren und die Saisonalität von Reiskulturen zu bestimmen. Dafür wurde eine phänologische, SAR-basierte Methode vorgeschlagen und erfolgreich für die Reisüberwachung auf regionaler- und kontinentaler Skala umgesetzt. Die neue Methode hat sich als solide, schnell, und übertragbar erwiesen und ermöglicht, basierend auf historischen Daten von Envisat ASAR (Polarisation: horizontal-horizontal HH) und der aktuellen Sentinel-1 SAR Mission (Polarisation: vertikal-horizontal VH), eine objektivere Identifikation von Reisflächen sowie der Stadien des Reisanbaus.

ABSTRACT

Detailed knowledge of the area and location of rice cropland is of great importance to any nation whose economy depends on rice production. Research in the field of rice cropland monitoring is necessary to investigate the different factors and effects of rice cultivation. Areas of application include risk management for the insurance industry, environmental reporting, and determination of greenhouse gas emissions from rice cultivation, analysis of life and water cycles, and crop forecasts.

Important sources of data for rice cropland records are space-borne active microwave instruments, due to the advantage of being non-susceptible to cloud cover. A Synthetic Aperture Radar (SAR) is an active imaging system operating in the microwave spectrum. The resulting images reflect the backscatter properties of the surface, which are determined by the physical (e.g., surface roughness, geometric structure, orientation) and electrical (e.g., dielectric constant, moisture content, conductivity) characteristics of the surface, and the radar frequency of the sensor (e.g., L-, C-, X-band).

Multi-temporal SAR image analysis is a common approach for rice cropland monitoring. High variations of SAR backscatter signal during the growing of rice crop in comparison with other types of land use and land cover is therefore the most important method for rice monitoring from space. However, no study so far was able to utilize the complete Advanced Synthetic Aperture Radar (Envisat ASAR) archive to map rice fields because incidence angle dependency affects the backscatter signal. In addition, the exploitation of the potential of the Sentinel-1 mission for rice monitoring (i.e., on regional and continental scales) is still subject to ongoing research.

This dissertation developed a time series backscatter analyzing method, aiming for classifying rice areas and determining the seasonality of rice crops. A phenology SAR-based approach is proposed and successfully applied for rice monitoring, allowing a more objective interpretation of rice areas from historical Envisat ASAR data (polarization: horizontal-horizontal HH) and the current Sentinel-1 SAR mission (polarization: vertical-horizontal VH).

CONTENTS

LIST OF ABBREVIATIONS AND ACRONYMS

1D	One-dimension
2D	Two-dimension
dB	Decibel
ALOS	Advanced Land Observation Satellite
ASAR	Advanced Synthetic Aperture Radar
ASAR WSM	Advanced Synthetic Aperture Radar Wide Swath Mode
AW	Autumn Winter (crop)
DOY	Day Of Year
EO	Earth observation
EODC	Earth Observation Data Centre for Water Resources Monitoring
EOS	End of Season
ENVISAT	Environmental Satellite
ERS	European Remote Sensing Satellite
ESA	European Space Agency
FAO	Food and Agricultural Organization
FOV	Field Of View
GIS	Geographic Information System
GPS	Global Positioning System
GSO	General Statistics Office of Vietnam
HH	Horizontal transmit and Horizontal receive
HV	Horizontal transmit and Vertical receive
IW	Interferometric Wide
JERS	Japanese Earth Resources Satellite
LAI	Leaf Area Index
LOS	Length of Season
MKD	Mekong Delta
MODIS	Moderate Resolution Imaging Spectroradiometer
MMU	Minimum Mapping Units
NDVI	Normalized Difference Vegetation Index

NEST	Next ESA SAR Toolbox
PALSAR	Phased Array type L-band Synthetic Aperture Radar
RADAR	Radio Detection And Ranging
RMSE	Root Mean Square Error
RS	Remote Sensing
SA	Summer Autumn (crop)
SAR	Synthetic Aperture Radar
SRTM	Shuttle Radar Topography Mission
SPOT	Systeme Probatoire d'Observation de la Terre
SOS	Start of Season
TSX	TerraSAR-X
VH	Vertical transmit and Horizontal receive
VV	Vertical transmit and Vertical receive
WS	Winter Summer (crop)

LIST OF TABLES

LIST OF FIGURES

CHAPTER 1

INTRODUCTION

Global food security is a central challenge in the 21st century due to the continuously increasing population and the limited land available for agriculture. The first issue is finding a viable way to feed the growing population, as it is expected to reach around 9.7 billion in 2050, compared to 7.3 billion in 2015 (FAO 2015). The second issue is finding ways of how to adapt to climate change. The World Bank estimated that climate change could cut crop yields by more than 25% by 2050. Today, rice is a primary source of food for more than half of the world's population (Kuenzer and Knauer 2013). Also, about 160 million hectares of land (i.e., 12% of the world's cultivated land) is used for rice production (FAOSTAT 2015), most of which are located in Asia (Figure 1.1). These regions (i.e., South and Southeast Asia) produced more than 90% of the global rice yield in 2015 (FAOSTAT 2015). The top four rice producers in 2016 were China, India, Indonesia, and Pakistan (Figure 1.2), while African and European countries needed to import rice from other countries (Elert 2014, FAOSTAT 2015). Efforts to address this food security issue require accurate geospatial data of rice planting areas and production.

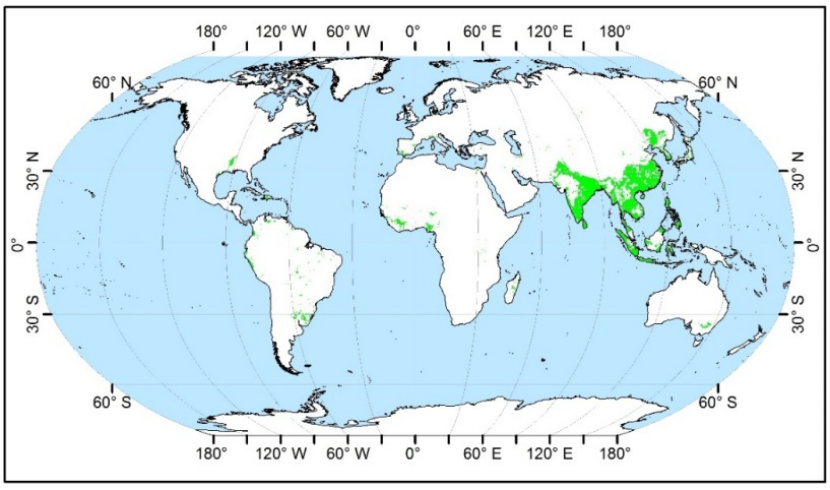

Figure 1.1. A map of lowland rice cropland extent over the world (modified from Monfreda et al., 2008).

Rice agriculture is mostly irrigated and consumes 24%–30% of the global freshwater resources (Kumar et al., 2012). Active urbanization, industrialization, changing patterns of precipitation, and rising global temperature affected the land and water resources for rice production (de Mirande et al., 2015). Furthermore, rice cropland is one of the most important sources of methane, which is emitted into the atmosphere, and it is an essential variable for modeling regional bio-geochemical cycles and climate (Van et al., 2012). Therefore, studies on the extent of rice cropland on regional and continental scales are vital for food security, water resource management, and environmental monitoring.

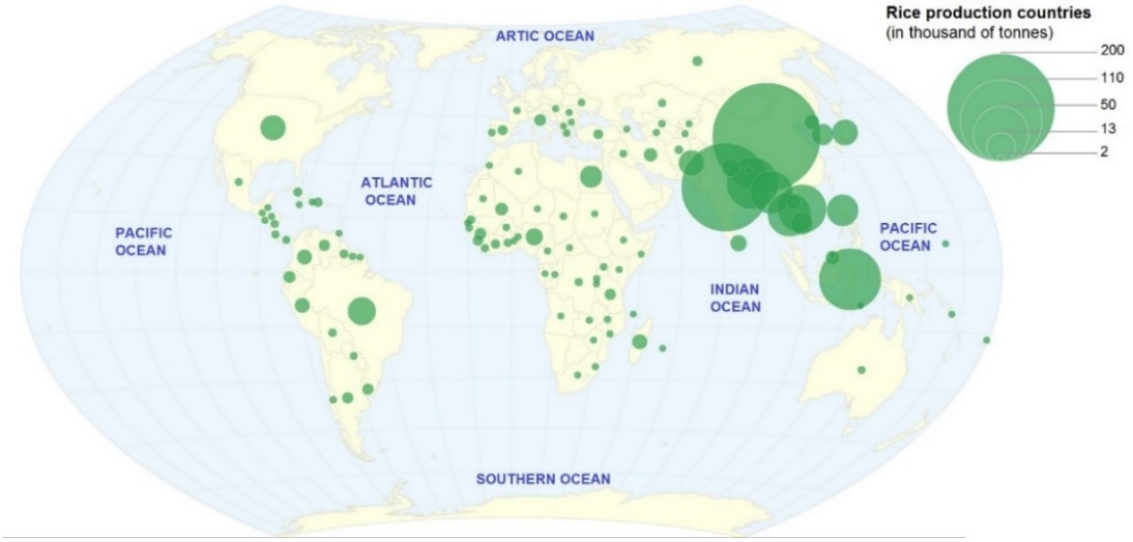

Figure 1.2. Rice production countries in 2016 (FAO 2016).

Traditionally, field visits and interviews with farmers have been the most widely used methods for estimating the extent of rice-cultivated areas. The methodology is based on annual/seasonal sample surveys using a number of sample clusters that are distributed over the country for measuring cultivated areas during the crop growing season. Each cluster is visited several times and the data are analyzed by regional statistical offices. This method provides invaluable data for understanding historical trends in rice cultivated area. However, field visits are time-consuming, sometimes imprecise, costly, inconsistent, and labor-intensive (Reynolds et al., 2000, Prasad et al., 2006).

The emergence of remote sensing techniques in the late 20th century introduced a new era for our understanding of rice cropland distribution and variation. Especially for large scales (e.g., continental and global), rice cropland extent mapping using remote sensing is a practical, economical, and efficient approach due to its consistency, reproducibility, and data coverage in regions where ground knowledge is limited. Today, satellite-based optical and microwave radar instruments are the most important data sources for rice monitoring (Kuenzer and Knauer 2013, Mosleh et al., 2015, Dong and Xiao 2016).

Optical satellite sensors provide multi-temporal and multi-spectral reflectance data over croplands that can be used for deriving time-series of vegetation indices (VIs). The reflectance spectrum of a rice crop canopy is the result of a complex relationship between its biophysical and biochemical attributes (Yang and Cheng 2001, Yang et al., 2007). A number of studies have been undertaken to explore the ability of optical remote sensing instruments to identify rice areas (Xiao et al., 2005, Prasad et al., 2006, Nguyen et al., 2012, Singha et al., 2017). However, different varieties of rice might show similar temporal spectral responses. In addition, in most cases, under real-world conditions, the water surrounding the plant influences the spectral reflectance of rice. The water regime system thus has an important impact on the canopy reflectance spectra. Furthermore, cloud cover (i.e., exceeds 70% of the time in tropical regions) (Nelson et al., 2014) and coarse spatial resolution (i.e., in the range 500 m to 1 km when considering continuous datasets) limit the usability of optical imagery for rice cropland monitoring (Fang et al., 1998, Xiao et al., 2005, Xiao et al., 2006, Xie et al., 2008).

Microwave-based remote sensing techniques have the advantage of not being susceptible to cloud cover. Numerous studies have been conducted in order to assess the potential of Synthetic Aperture Radar (SAR) systems operating at different frequencies bands for rice cropland monitoring, including L-band (Wang et al., 2009, Ling et al., 2010), C-band (Toan et al., 1997, Bouvet et al., 2009, Lam-Dao et al., 2009, Fan et al., 2011, Nguyen et al., 2015, Nguyen et al., 2016), and X-band (Lopez-Sanchez et al., 2011, Pei et al., 2011, Inoue and Sakaiya 2013). The low temporal resolution of L-band SAR data (e.g., JERS and ALOS) and the high

price of commercial X-band SAR data (e.g., TerraSAR-X and TanDEM-X) have so far limited the use of L-band and X-band data for large-scale rice cropland monitoring. Therefore, C-band SAR is at present the most commonly used frequency for rice monitoring.

The goal of this thesis is to exploit the use of dense C-band SAR time series for rice cropland monitoring. The thesis is divided into five chapters. Chapter 1 is an introduction to both the study object *rice crop* and our main means of observation, the Synthetic Aperture Radar (SAR). Herein, the importance of rice, the basic principles of active microwave remote sensing, and general scattering mechanisms that determine the signal-target interactions are briefly introduced. Chapter 1 also presents several SAR-based multi-temporal rice crop monitoring methods and explains why C-band SAR is our primary data source for continuous year-round observation. The specific objectives, a summary of the research articles, and the scientific impact are explained at the end of Chapter 1. In the following chapters (i.e., Chapter 2, Chapter 3, and Chapter 4), the related scientific publications are presented. The thesis closes with Chapter 5 that includes a discussion of the feasibility and future directions for long-term and large scale rice monitoring with C-band SAR-based time series analysis.

1.1. Statement of the research problem

This thesis aims to examine the use of C-band SAR time series for rice cropland monitoring. It is motivated by the following questions: (1) What are appropriate methods for analyzing SAR time series for rice cropland monitoring? (2) Which kind of rice phenology parameters can be retrieved from SAR time series? (3) Can SAR-based time series approach be used for rice monitoring in large areas (i.e., regional and continental)? These questions have been addressed in three published research articles, which form the core of this thesis: (1) Mapping rice seasonality in the Mekong Delta with multi-year Envisat ASAR WSM data, (2) Mapping rice extent and cropping scheme in the Mekong Delta using Sentinel-1A data, (3) European rice cropland mapping with Sentinel-1 data: the Mediterranean region case study.

An essential contribution of this PhD thesis is to present the potential of current and upcoming C-band SAR missions for monitoring rice cropland at different scales, over different climatic regions, and to discuss the benefits and drawbacks of the presented methods.

1.2. Context of the scientific publications

This thesis and the included scientific publications present methods for rice cropland monitoring based on active microwave remote sensing. The important aspects of rice cropland monitoring are the acquisition and interpretation of SAR time series and the sequential extraction of rice phenological parameters from it. This task is strongly related to earth observation (EO) methodologies. EO is the gathering of information about planet Earth's physical, chemical and biological system via remote sensing technologies supplemented by ground-based observations (i.e., in-situ measurements), encompassing the collection, analysis, and presentation of data (Europe Commission-JRC). An active SAR is an imaging system operating in the microwave spectrum. The resulting images represent the backscatter properties of the surface, which are determined by the characteristics of the surface (e.g., surface roughness, dielectric constant, and moisture content), and the technical specifications of the sensor (e.g., L-, C-, and X-band) (Ulaby et al., 1982). The following section (i.e., Section 1.3) gives a summary of the concept of a radar system and scattering mechanisms.

1.3. Physical mechanisms for scattering

In microwave remote sensing the distinction between different objects on the ground is caused by the difference in the signal strength received by the microwave receiver device (i.e., antenna or sensor). The measurement of received signal strength is thus the most important measurement in remote sensing devices. Any return signal received by the receiver device can be considered as a combination of basic scattering mechanisms. The characterization of the scattering mechanisms has its application in rice cropland monitoring. The basic principles of radar and general scattering mechanisms that the signal-target interactions are described in this section.

1.3.1. Radar equation

The fundamental relation between the characteristics of the radar, the target, and the received signal is called Radar Equation. The associated scattering-geometry from an isolated radar-target is shown in Figure 1.3, along with the parameters that are involved in the radar equation (Ulaby et al., 1982).

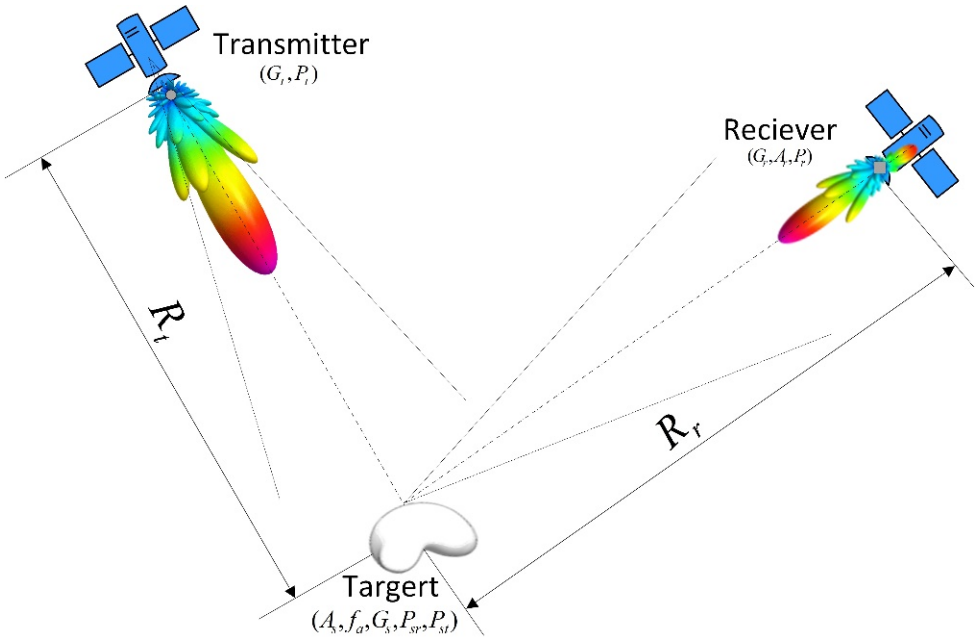

Figure 1.3. Geometry of and quantities involved in the radar equation.

$$P_r = \frac{P_t G_t A_r}{(4\pi R_t R_r)^2} G_s A_s (1 - \kappa_a) \quad (1.1)$$

where P_t and P_r are transmitted and received power by the antenna with gain G_t . A_r is the effective aperture of the receiving antenna and A_s is the effective area of the incident beam intercepted by the scatterer. κ_a is the fraction absorbed by the target with gain G_t. R_t is the distance between radar transmitter and target and R_r is the distance between target and radar receiver.

Since the quantities G_s, A_s , and κ_a cannot be measured individually, a new quantity called the radar cross-section is introduced which combines all properties of the scatterer i.e.:

$$\sigma = G_s A_s (1 - \kappa_a) \quad (1.2)$$

The final form of the radar equation for a single transmission and reception antenna simplifies to: ($R_t = R_r = R;\ G_t = G_r = G$)

$$P_r = \frac{PG^2\lambda^2}{(4\pi)^3 R^4}\sigma \tag{1.3}$$

The average value of the individual sub-targets cross-sections per unit area is defined as differential scattering coefficient (or backscatter cross-section):

$$\sigma^0 = \left\langle \frac{\sigma_i}{\Delta A_i} \right\rangle \tag{1.4}$$

The backscatter cross-section is usually expressed in dB, which is given by:

$$\sigma^0(dB) = 10log\sigma^0(m^2m^{-2}) \tag{1.5}$$

The resulting coefficient, σ^0, reflect backscatter properties of the surface, which are determined by the physical (e.g., surface roughness, geometric structure, and orientation) and electrical (e.g., dielectric constant, moisture content, and conductivity) characteristics of the surface, and the radar observation parameters (i.e., frequency, polarization, and incidence angle of the electromagnetic waves emitted) (Ulaby et al., 1982). Such signal characteristics can be used to obtain a number of important geophysical and biophysical parameters.

1.3.2. Scattering mechanisms

Because of the low frequency (long wavelength) power transmission, microwaves interact with plants and soils in a very different way to optical waves. In the visible and infrared spectral domains, the wavelength is very short compared to the size of the target (e.g., the leaves and stems of plants or soil particles). The strength of the reflected signal is a mainly driven by the chemical composition of the target. In the microwave domain, the wavelength is on the order of the target size. The basic principles that the signal-vegetation interactions are described in this section.

1.3.2.1. General scattering mechanisms.

When an electromagnetic wave impinges upon the boundary surface between two media, usually a portion of the incident energy is scattered upward, and the rest is transmitted forward into the lower medium. If the penetration-depth of the wave into the lower medium is small (or if the medium is completely homogeneous), one

speaks of the surface-scattering problem, since scattering takes place only at the surface boundary. Surface roughness determines the angular distribution of surface scattering, as shown in Figure 4a. The greater the roughness of a surface, the more the incident radiation will be backscattered to the radar. Natural surfaces, which act primarily as surface-scatterers for waves at microwave-frequencies, are water, soil (with the exception of very dry soil such as desert sand). On the other hand, if the lower medium is inhomogeneous and penetration depth is high, then a portion of the transmitted wave scattered backward by the in-homogeneities may cross the boundary surface into the upper medium again. In this case, scattering takes place within the volume of the lower medium, and one speaks of volume-scattering (Figure 1.4b). Vegetation-canopies and dry snow packs are examples of natural media that act primarily like volume-scatterers.

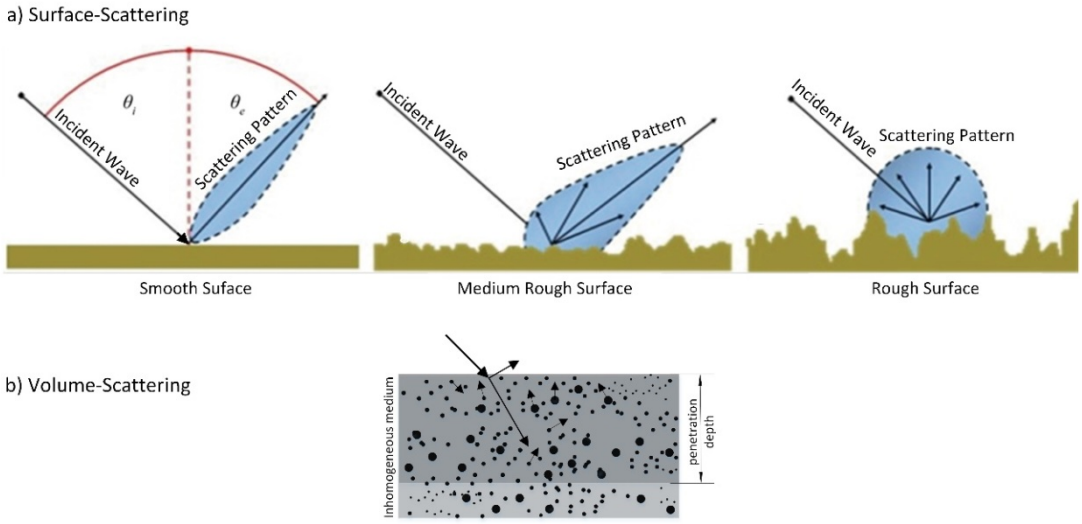

Figure 1.4. Surface and volume scattering patterns.

(modified from Ulaby et al., 1982)

Both surface- and volume-scattering are usually present in scattering from natural terrain. However, it is convenient to ignore one or the other of these whenever one is much smaller than the others. For example, in the microwave region, the sea has a high absorption and is therefore treated as a homogeneous medium capable of surface-scattering only (e.g., in calm conditions). At optical wavelengths, however, the dielectric constant of sea-water is much smaller, and small particles in water can make volume-scattering important.

1.3.2.2. Signal interactions with vegetation.

A crop is a (low) vegetation layer over a soil surface. From the electromagnetic point of view, it is a layer of scatterers bounded by air in the upper part and by a homogeneous surface in the lower part. As shown in Figure 1.5, scattering contributions from a vegetation-canopy over a soil-surface come from vegetation volume, soil surface, and vegetation-soil interaction. Correspondingly, we formulate the total backscatter coefficient as the sum of three parts:

$$\sigma^o_{canopy} = \sigma^o_v + T^2\sigma^o_s + \sigma^o_{int} \quad (1.6)$$

where the subscripts denoted the volume-, surface-, and interaction (volume-surface and surface-volume)- contributions; σ^o_v : direct backscattering from plants (leaves, stalks and ears); σ^o_s: direct backscattering from soil; σ^o_{int} : soil-plant interactions; T: the transmission factor.

These three scattering terms dependent on (a) the type and condition of the vegetation layer: healthy vegetation, with higher water content, has higher dielectric constant than drier or dead vegetation. The presence of dew or moisture increases the dielectric constant of vegetated surfaces; (b) the roughness and condition of the ground layer (soil surface properties): the micro- and mesoscale surface roughness (relative to the radar wavelength) and the soil moisture (dielectric constant). Rough surfaces have a notably higher backscatter than smooth surfaces. The backscatter coefficient is dependent on the soil moisture content of the uppermost soil layer, and (c) the wavelength and polarization of the incident microwave energy.

Radar backscatter of agricultural vegetation is sensitive to the structure of the canopy and the underlying soil properties. The surface is characterized by a changing amount of vegetation and the presence of water. The most important parameters accountable for the strength of backscatter are usually the height of vegetation layer, vegetation biomass per canopy area, gravimetric water content, and vegetation (plant) structure (Ribbes and Le Toan, 1999, Dong et al., 2006).

In the case of rice crop, there is a layer of water over the soil layer during the growth cycle; two things can happen: (1) it can significantly reduce, even

eliminate, any surface roughness; and (2) it can significantly increase the reflection coefficient of the surface layer. In terms of microwave scattering: (1) the elimination of any surface roughness means that all the energy is forward scattered, eliminating the surface backscattering (σ_s^o) in Equation (1.6); and (2) the increased forward scattering and higher reflection coefficient lead to significant increases in the water-plant interaction terms (σ_{int}^o). Le Toan et al. (Le Toan et al., 1997) gave a general description of the different scattering mechanisms for a rice crop (Figure 1.6), that the total backscatter signals were expressed as the sum of the following terms:

(1) Direct scattering from the canopy (i.e., from leaves or ears)

(2) Reflectance at the water surface followed by single scattering from scatterer (canopy-water multiple scattering).

(3) Opposite pathway to (2).

(4) Reflectance by a boundary followed by a single scattering from the scatterer and further followed by the reflection of the boundary (water-canopy-water multiple scattering).

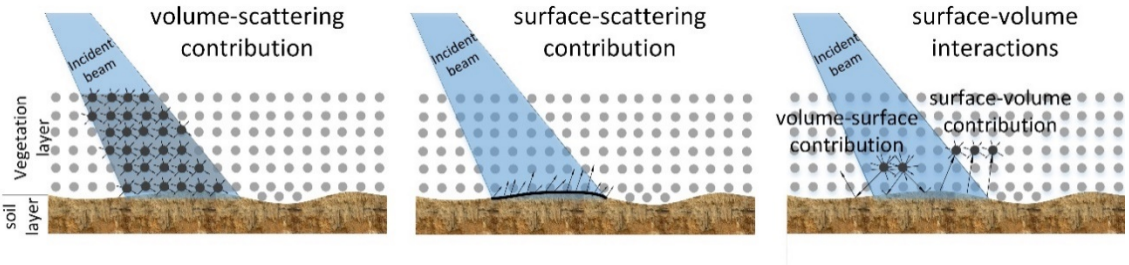

Figure 1.5. Surface and volume scattering patterns.

Understanding the microwave backscatter of rice crop as a function of crop growth is essential for the development of reliable and robust methods to estimate crop growth parameters (Choudhury et al., 2007). Also, the chosen radar frequency bands (wavelength), the polarization and incidence angles influence to the backscatter signal. The following section (i.e., Section 1.4) will describe the details of the general backscatter mechanisms of rice, the temporal dynamics of backscatter during the growing period for different frequencies, polarizations, and incident angles. Rice monitoring approaches based on SAR time series are also addressed.

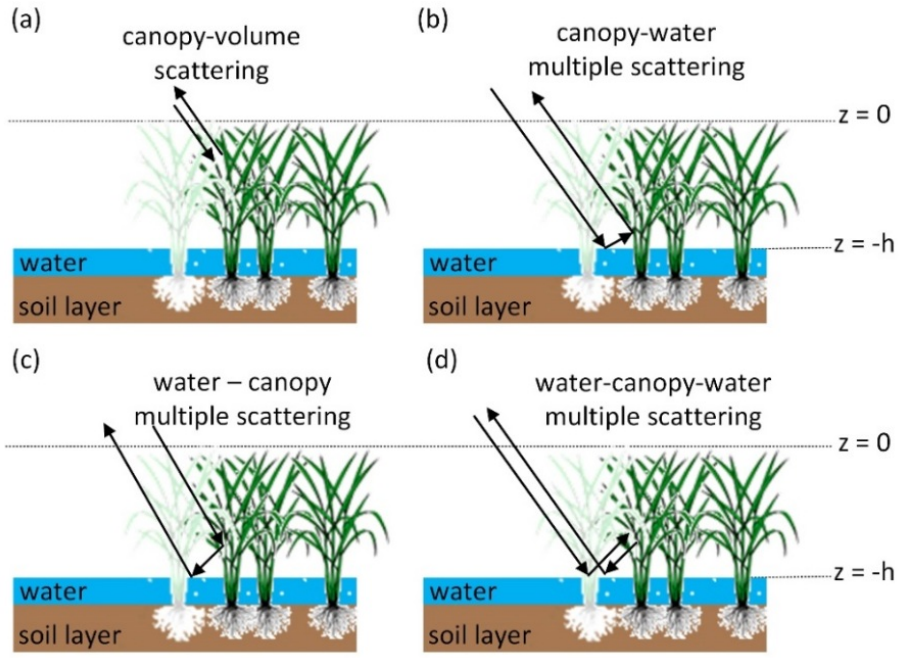

Figure 1.6. The main scattering mechanisms involved in the wave-rice canopy interaction (modified from Le Toan et al., 1997).

1.4. SAR-based rice crop characterization and mapping

1.4.1. Characteristics of microwave backscattering from rice fields over growth stages

In general, a large dynamic range of microwave backscatter values, which varies from the seeding/pre-transplanting to the pre-harvesting stage, can be observed in the case of rice crops (Figure 1.7). During the sowing period, when rice is sown directly into flooded soils (2-5cm water), radar backscatters from rice fields are low due to specular reflectance from the water surface. During the growing period, which consists of the vegetative stage, reproductive stage, and ripening stage, the vegetative stage is characterized by a rapid increase in rice plants height, tiller and leaf number. In addition, free space between rice stems is decreased, and therefore, radar backscatter increases rapidly during this stage. The following reproductive stage includes the panicle initiation, heading, and flowering processes. In this stage the plants stop increasing in height, biomass, and the leaves start to wither and die. Ripening is the final stage with its milk, dough, and mature grain processes. These processes coincide with changes in plant morphology that influence the interaction

with light and microwaves and thus can be observed with remote sensing data. In this period, radar backscatter intensity begins to level off. In the fallow period, when the rice fields are almost bare or flooded, radar backscatter values from rice fields are very low again. This temporal backscatter pattern is unique to rice crops; variations in backscatter over the growing season for rice are much more pronounced than in any other agricultural crop (Chen and McNairn, 2006, Choudhury et al., 2007).

A detailed description of the backscatter theoretical model of rice can be found in (Tsang et al., 1995, T. Le Toan et al., 1997, Wang et al., 2005, Koay et al., 2007, Wang et al., 2009, Zhang et al., 2014, Liu et al., 2016). In these studies, two alternative approaches were used to describe the scattering mechanisms and to predict the backscattering coefficient from rice crops. One approach was based on electromagnetic theory, which was, in general, computationally intensive and overlooked the complex electromagnetic interactions due to the use of a single layer to model the rice canopy (Le Toan et al., 1997, Wang et al., 2005). Another approach was based on radiative transfer theory, where the scattering mechanisms from the rice canopy was modeled as multiple-layers of needle-shaped scatterers with underlying water surface (Koay et al., 2007, Liu et al., 2016). These studies explored backscattering models as a function of canopy height, leaf width, and density of leaves, leaf area index, and leaf angle. The modeling results from different frequency bands, such as X-band (Le Toan et al., 1989), C-band (Wang et al., 2005) and L-band (Wang et al., 2009), and from different polarizations, such as HH (Wang et al., 2005), VV (Le Toan et al., 1989), and HH/VV/VH, (Liu et al., 2016), were in good agreement with theoretical models and in-situ observations (Figure 1.8). However, in practice, it is not trivial to use these numerical models to directly retrieve rice crop information, since many parameters, such as the number of branches, density of leaves, and leaf area index, are required for computation. Moreover, these approaches, in spite of their complexity, are all site-dependent and they might not accurately describe the interaction between the electromagnetic wave and the Earth's surface.

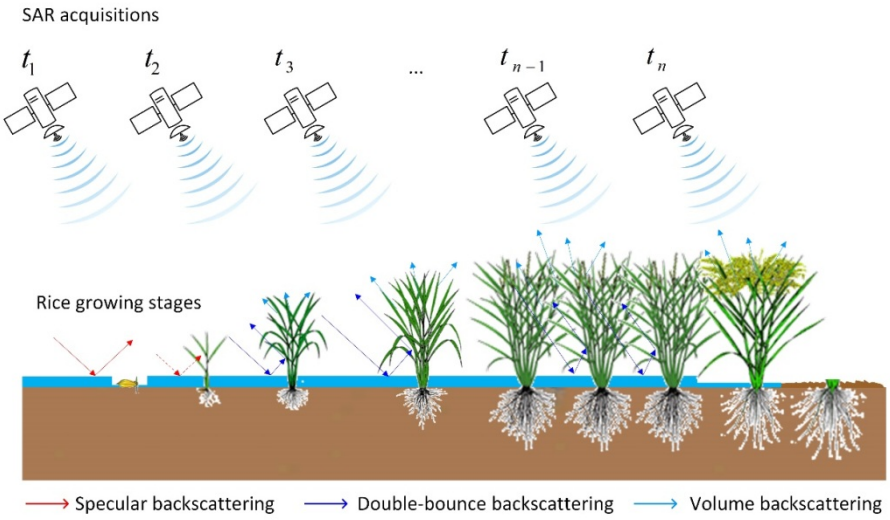

a) Dominating backscatter mechanisms at different stages of rice growth.

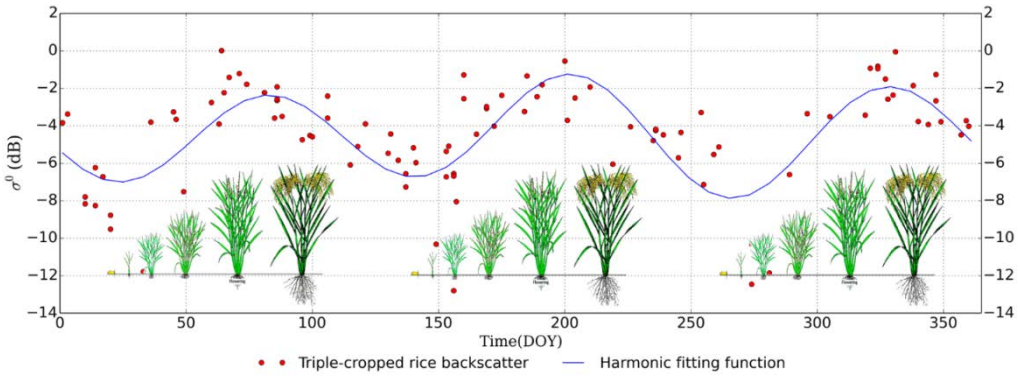

b) SAR backscatter behavior in relation to rice-growing stages for triple-cropped rice based on a multi-year Envisat ASAR WS time series.

Figure 1.7. SAR backscatter behavior in relation to rice-growing stages.

Relationships between radar backscatter and rice using ground-based scatterometers and the other radar data (i.e., space-borne) has also been investigated in several studies including (Lim et al., 2007, Lam-Dao et al., 2007, Le Toan et al., 1997, Bounman, 1991, Inoue et al., 2002, Prevot et al., 1993, Kim et al., 2008). Inoue et al. (Inoue et al., 2002) performed the assessment of each biophysical variable of rice by analyzing a comprehensive dataset of backscattering coefficients in five frequency bands (i.e., Ka, Ku, X, C, and L), full polarizations (VV, VH, HV, and HH), and four incidence angles (i.e., 25°, 35°, 45°, and 55°) during rice growth cycle. Kim et al. (Kim et al., 2008) examined the temporal behavior of the radar backscatter from rice crops during the growth period at multi-frequency (L-, C-, and X-band) with varied angular responses (i.e., 30°, 40°, 50°, and 60°).

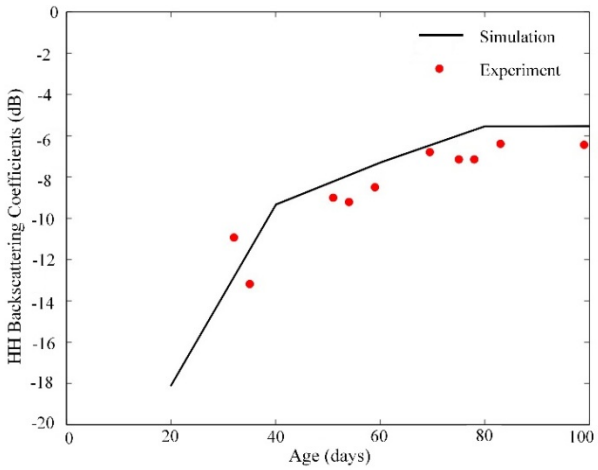

Figure 1.8. Comparison between the simulated σ^{o}_{HH} and RADARSAT (C-band) data as a function of rice age (θ = 23°) (modified after Wang et al., 2005).

Figure 1.9 presents the temporal variations of radar backscattering at different configurations of the radar observation parameters (i.e., different incidence angles and polarizations for different bands), as observed by Kim et al. (Kim et al., 2008). Similarly to the conclusions from this figure, Inoue et al. (Inoue et al., 2002) also found that the VV polarization in the L-band has little sensitivity at steeper incident angles (i.e., 25° and 35°), but shows more dynamic seasonal change at larger angles (i.e., 45° and 55°). By contrast, the backscattering coefficient in the X-band during the ripening period reversed with the incident angle, from decreasing (i.e., at 25°) to increasing (i.e., at 55°). The observed X-band response may be attributed to the penetration depth and canopy structure. Among the major results, these studies concluded that for the C-band, the rice field structure (i.e., planting density) has less effect on the return signals compared to the L-band. C-band backscattering coefficients at HH and VH/HV polarization and at medium incidence angles (30°, 40°) have been also strongly recommended for use for the characterization of rice agriculture in SAR-based rice monitoring projects. The VV polarization, on the other hand, was less well correlated with plant variables than the other polarizations in most case. This may be interpreted by the process that HH- and cross-polarizations penetrate more effectively into canopies and consequently have greater seasonal changes than the VV does. However, most studies on rice backscattering characterization were verified based on ground-based scatterometer data and very limited space-borne SAR data (Le Toan et al., 1997, Wang et al., 2005). The main

reason has the most likely been the limited availability of space-borne SAR observations at the same frequency, polarization, and incidence angle.

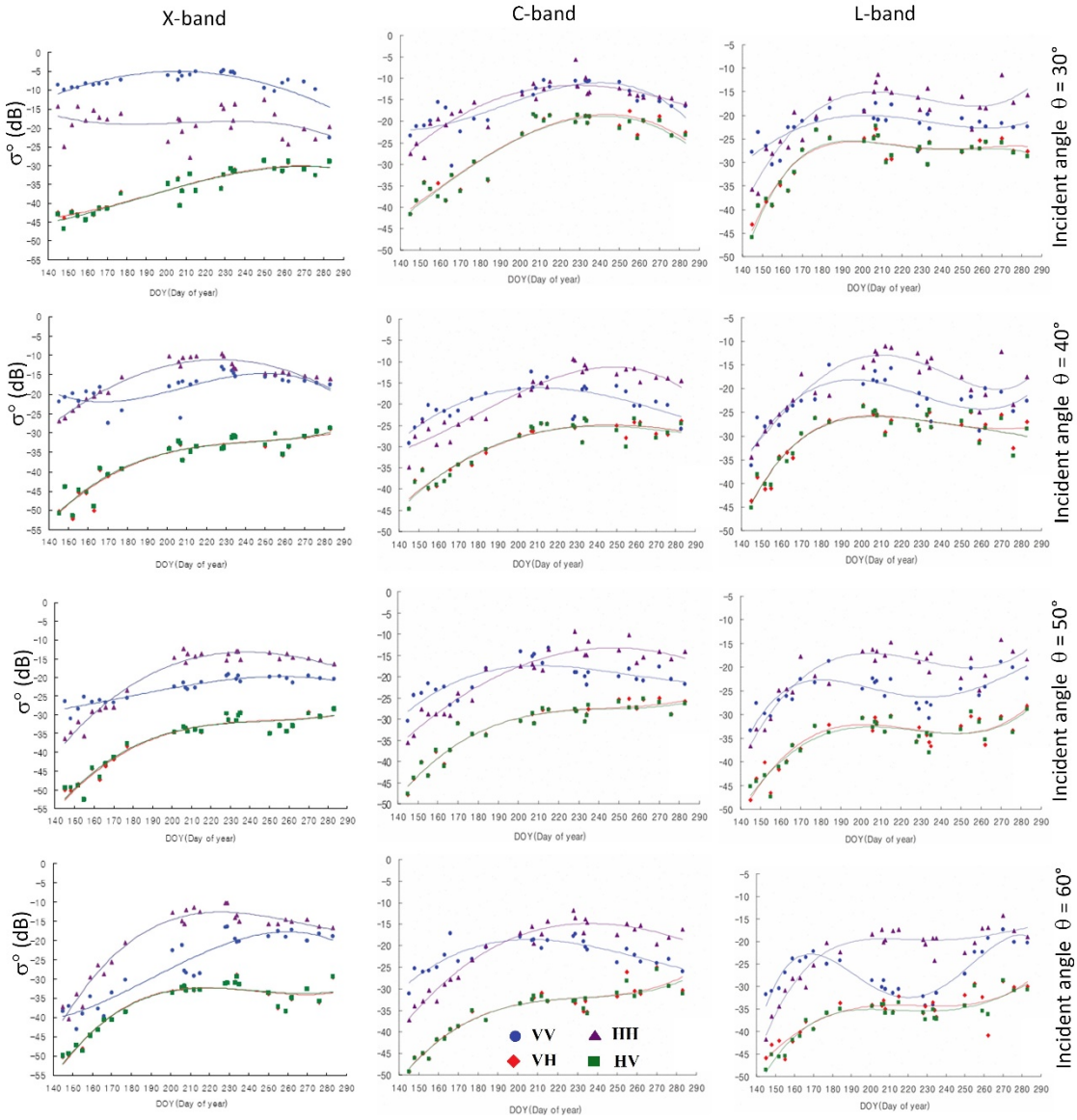

Figure 1.9. Temporal variations of backscattering coefficients at different polarization and incident angle 30°, 40°, 50°, 60° for the X, C, and L bands (modified from Kim et al., 2008).

Recently, SAR data availability has increased tremendously with the launch of Sentinel-1A (S-1A) on April 3rd, 2014 and Sentinel-1B (S-1B) on April 25th, 2016, which are operated within the European Commission's Copernicus program (Potin et al., 2012). The Sentinel-1 mission is designed for continuous near-real-time (NRT) land monitoring and provides dual-polarized (VV/VH) SAR images over

entire Europe (i.e., the Interferometric Wide swath mode) every four days and globally at least every 12 days. Furthermore, the free, full, and open data policy adopted by the Copernicus programme will make Sentinel-1 data a valuable resource accessible to the broader science community and accelerate progress in geophysical research in general and paddy rice cropland monitoring in particular.

1.4.2. SAR-based rice mapping approaches

A wide range of research articles has proved the usefulness of SAR data for the mapping of rice cropland extent and the biophysical characteristics of rice (Aschbacher et al., 1995, Le Toan et al., 1997, Liew et al., 1998, Ribbes and Le Toan, 1999, Inoue et al., 2002, Chen and McNairn, 2006, Chen et al. 2007; Bouvet et al., 2009, Bouvet and Le Toan, 2011, Rossi et al., 2015). In those studies, two common methods of SAR-based rice mapping have been implemented over multiple study areas using different SAR sensors: (1) single-polarization-based and (2) multiple-polarizations-based. In the first method, single polarization backscatter data with high temporal density is utilized to monitor variations of rice over its growth phases. The method requires data from sensors aboard satellites with a short revisit time. The first notable results have been published by Liew et al. (Liew et al., 1998), who derived backscatter change from ERS-2 (i.e., VV-polarization) time series and classified eight different rice-cropping schemes according to their temporal backscatter behavior. Ribbes and Le Toan (Ribbes and Le Toan 1999) also applied a mapping approach based on the temporal change of backscatter from RADARSAT-1 data (i.e., HH-polarization). The results were compared to available maps and found to have a high accuracy of 87%. Bouvet et al. (Bouvet et al., 2009) were the first to employ the multi-temporal method to produce a map of rice-cropping schemes and areas for the whole Mekong Delta with the use of Envisat ASAR wide swath data. They achieved this by aggregating horizontally polarized SAR time-series classifications from three satellite tracks since temporal coverage for a single track has not been dense enough to achieve high classification accuracy. The derived seasonality map had a reported accuracy of 75.8% compared to a reference dataset created from dual-polarization ASAR data. Thus,

so far, no study has utilized the complete Envisat ASAR archive for the particular region (i.e., Mekong Delta) due to the effect of incidence angle on SAR backscatter.

In the second method, SAR observations from different polarizations are compared to each other for determination of rice plant growth phases. Polarization ratios are commonly used for the mapping of paddy fields (Chen et al., 2007, Lam-Dao et al., 2007, Bouvet et al., 2009). Chen et al. (Chen et al., 2007) tested various ratio combinations of Envisat ASAR images polarized in HH and HV from different dates. It was stated that a simple threshold, in their case at 7 dB, could be used on the ratio image to highlight rice fields. Lam-Dao et al. (Lam-Dao et al., 2007) also used Envisat ASAR ratios (HH/VV), but from a single date in the middle of the crop cycle. In their approach, a pixel was classified as rice if two thresholds were valid: HH/VV > 3 dB and VV backscatter coefficient < –7 dB. A maximum difference of 7% was achieved between classification results and agency statistical data. Studies based on the second method, employing backscatter response from different polarizations, show the capability of distinguishing rice from other land cover and detecting its growth stages with less temporal coverage than the single-polarization. However, the approach is dependent on the availability of sensors with multi-polarized (dual- or quad-polarization) data capabilities. Selection of an appropriate method for SAR-based rice mapping is essentially determined by the data availability and sensor selection.

1.5. Study objectives

So far, few studies have used dense SAR time series for rice cropland monitoring. For this purpose, it is necessary to study the temporal SAR backscatter behavior of rice stages throughout the growing season. The objective of this PhD thesis is to analyze and interpret time series of SAR data for improving our understanding of backscatter dynamics over rice crop areas during the growth cycle. This thesis also aims to further develop phenology-based classification methods for dense SAR time series and to exploit the new capabilities of ESA's novel Sentinel-1 C-band sensor for rice cropland monitoring on regional and continental scales.

The objectives of the three research articles upon which this PhD thesis is based are:

I. Developing a SAR–based time-series analysis approach for rice cropland monitoring

The specific objectives of this publication are:

(a) Evaluating the assumptions underlying multi-year Envisat ASAR WS backscatter analysis and investigating their relation to the development stages of rice.

(b) Proposing an approach that utilizes multi-year Envisat ASAR WSM backscatter to monitor rice cropland extent.

(c) Identifying/defining a set of SAR-based time-series parameters for estimating rice cropland phenology.

II. Investigating the potential of Sentinel-1 VH polarization data for rice cropland monitoring

The specific objectives of this publication are:

(a) Time series Sentinel-1 C-band backscatter analysis for mapping and cropping scheme in the Mekong Delta region

(b) Implementing a modification of phenology-based method to utilize VH polarization imagery for mapping rice cropland monitoring.

III. Investigate the transferability of the proposed methods from regional scale to continental scale

The specific objectives of this publication are:

(a) Generalizing the phenology-based method to allow for the transfer to larger areas with diverse environmental conditions like areas over Europe.

(b) Utilizing high-density Sentinel-1 backscatter (VH polarization) for mapping rice cropland extent at the continental scale.

(c) Demonstrating the robustness and transferability of the proposed method over different study regions.

1.6. Summary of the publications

1.6.1. Publication I: Mapping Rice Seasonality in the Mekong Delta with Multi-Year Envisat ASAR WSM Data

In this publication, we presented a novel approach to rice mapping by combining multi-year (i.e., 2007 to 2011) and multi-track (i.e., 15 tracks) SAR wide swath acquisitions. Considering data availability for the selected region (i.e., Mekong Delta), we chose to perform the multi-temporal backscatter analysis method on C-band Envisat ASAR data for rice mapping. This novel approach led to a significant increase in the temporal density by using all available observations compared to previous studies that employed narrow swath multi-polarization data or only detected the temporal change within single tracks. The approach relied on two propositions. First, we supposed that the backscatter changes over time exhibited by different rice-cropping schemes remained stable over the observation period. This entails that no changes in the cropping scheme, no change in land cover and no significant alterations in the growing seasons took place during the 2007 to 2011 period. Second, we presumed the distribution and amount of sample points to be sufficient to fulfill the criteria of the sampling theorem. The average sampling of ASAR WSM observations is 1.5 to 2 measurements per week with a maximum two-week time gap between observations in some limited periods of the year. Therefore, it is supposed that the ASAR WSM weekly sampling (i.e., averaging 7-day intervals) is capturing all rice crop variations throughout the year as at least one measurement per week is occurring. The compositing of backscatter measurements has the advantage of reducing random noise errors inherited in the ASAR WSM data from atmospheric attenuation and speckle noise.

Effects of different incidence angles and temporal density of acquisitions have been tackled by temporal averaging (i.e., weekly sampling) and incidence angle normalization based on statistical methods. A Gaussian filter was then selected for temporal filtering as it showed satisfying coincidence with the reported number of rice crops, visible as distinct peaks, as well as their approximated heading dates compared to the reference data. The phenology patterns (translating and heading time) from time series backscatters were well observed over rice-cropped sections

in the study area. For the next step, the smoothed backscatter time series were used for determination of key seasonality parameters over all rice-growing areas. Building on the methodology developed by Jönsson and Eklundh (Jonsson and Eklundh 2002), we defined following phenological parameters: Start of Season (SOS) defined on the inflection point in σ^o_{smooth} time series where the second derivative equals 0 and changes from negative to positive; End of Season (EOS) as inflection point in σ^o_{smooth} time series where the second derivative equals zero and changes from positive to negative; Length of Season (LOS) as the difference between start and end of season. Classification was finally performed with a rice crop phenology decision-tree classifier based on previous studies.

The classification results were compared to the 2005 and 2010 land-use maps, and reported an overall accuracy of 85.3% with a kappa coefficient of 0.74. Our data is highly correlated with official rice area statistics (R^2 of 0.98). Seasonality parameters extracted from the time series have been used to produce maps of the temporal distribution of the beginning of the first and second cropping season, end of second and last growing season, as well as the length of the first and second cropping season. We found good agreement in the spatial distribution of single, double and triple rice-cropping schemes compared to previous studies in the Mekong Delta that reported cropping scheme maps with accuracies similar to our product.

The limitation of our method in this publication is that no yearly rice maps of the Mekong Delta can be produced based on Envisat ASAR data. This is less a limitation of the method, however, but more a reflection of lack ASAR data coverage. Sentinel-1 has the ability to cover our study area with a repeat cycle of 12 days and could be used for timely rice mapping and seasonality detection in the Mekong Delta.

We tested this approach in the Mekong Delta, but it should be also applicable to paddy rice areas worldwide demonstrating a distinct temporal backscatter change. Previous studies and theoretical models have shown that this holds true for all rice fields that are flooded before direct seeding or transplantation of rice seedlings.

1.6.2. Publication II: Mapping rice extent and cropping scheme in the Mekong Delta using Sentinel-1A data

This study demonstrates the potential of Sentinel-1A for mapping regional rice cultivation extent and for deriving rice phenological parameters (i.e., the starting date, heading date, and the length of the growing season). VH-polarized backscatter has been found to be more sensitive to rice growth than VV-polarized backscatter.

Sentinel-1A IW Level 1 (L1) GRDH (ground-range detected, high resolution) product was used in this study. Analyses were based on Sentinel-1A data acquisitions during the "*spring*" 2015/2016 season (i.e., from October 2015 to March 2016), which cover the entire Mekong Delta area. L1 data was pre-processed using ESA's open source Sentinel-1 Toolbox.

Multi-temporal backscatter observations at different polarizations have been analyzed to (1) investigate the backscattering characteristics of rice at different polarizations (i.e., VV and VH); (2) derive rice phenological parameters including the starting date, heading date, and the length of the growing season; and (3) delineate rice-cultivated areas. The temporal evolution of rice backscatter coefficients (i.e., mean and standard deviation) inside the rice fields were used for analyzing changes of SAR backscatter at different polarization during rice growth period. VV-polarized backscatter is larger than VH-polarized backscatter, and backscattering coefficients (both polarizations) gradually increase during the growing period until they reach their maximum at the end of the reproductive state. This is followed by a significant backscatter decrease during the maturation state. While VV-polarized backscatter reaches a first maximum (i.e., approximately 30 days after sowing), then drops with a strong subsequent depression (i.e., approximately 20 days after the first maximum), VH-polarized backscatter shows a monotonic increase without such depression until it reaches its maximum (i.e., approximately 70 days after sowing). The depression in VV backscatter is probably related to the disappearance of standing water in this period. The VH signal, on the other hand, seems to be less affected by such changes in standing water conditions and is thus expected to better represent the actual rice-growth cycle. We,

therefore, limit subsequent analyses to VH backscatter measurements only. A decision tree approach has been used to map rice-cultivated areas in the Mekong Delta region during the 2015/2016 *"spring"* season with a classification accuracy of 85.3% (with respect to a 2015 reference land use map) and a kappa coefficient of $\kappa = 0.74$. The estimated extent of delineated rice cultivated areas is in good agreement with official rice area statistics (i.e., coefficient of determination $R^2 = 0.98$). Finally, this study has pointed out that water supply is one of the most critical parameter influencing rice classification accuracy. This study was, to our best knowledge, the first Sentinel-1A-based analysis for mapping rice-cultivated area and for estimating rice phenological parameters at a regional scale.

1.6.3. Publication III: European Rice Cropland Mapping with Sentinel-1 Data: The Mediterranean Region Case Study

The goal of this study is to evaluate the potential and transferability of a phenology-based classification strategy developed by Nguyen et al. (Nguyen et al., 2016) over a regional test site in the Mekong Delta to a continental scale (i.e., Mediterranean region). To achieve this objective, we used a dense time series stack of Sentinel-1 backscatter data as inputs to map rice paddy areas at fine spatial scale over eight study sites in six European countries (i.e., Portugal, Spain, Italy, France, Greece, and Turkey).

In this study, we accessed archived Interferometric Wide Swath (IW) mode Sentinel -1 data acquired during the rice crop growing cycle in 2015, from April to early November to completely cover every test site. Sentinel -1A SAR IW mode acquisitions come from eight different tracks, whereas each test site is covered by the same track. All the images were obtained from ESA as standard Level 1 GRD (ground-range detected) high-resolution images. Only Sentinel -1 IW acquisitions with VH polarization were selected for rice cropland classification.

For the identification of potential rice growing areas, our approach is to threshold the dynamic range backscatter image to identify image pixels that change more than the defined threshold value (dB). Threshold value selection depends on the nature and expected changes in the magnitude of VH backscatter and the SAR geometry (i.e., incidence angle). A generalized threshold for the rice fields can only

be determined if the optimum SAR data acquisition is guaranteed (i.e., SAR observations are available in the flooded and vegetative stages). Otherwise, the threshold must be optimized considering the data acquisition and the constraints of local crop calendar. Sentinel-1A satellite provides at least one acquisition after every 12 days over the selected study sites; after the launch of Sentinel -1B satellite the temporal sampling was improved to 5–6 days. Based on the visual interpretation of optical imagery for the selected period and expert knowledge acquired from the ancillary data, a threshold of 8.5 dB was used to extract the potential rice pixels referred to as $\sigma^{o}_{VH\_potential}$.

To provide a direct comparison, the classification results in all study sites (i.e., Seville and Valencia in Spain, and Thessaloniki in Greece) were evaluated by using the reference vector dataset from the same year 2015. Lombardia (Italy) and Camargue (France) were evaluated by using higher spatial resolution (SPOT 5, 10 meters). Google Earth Imagery and Sentinel-2 data were used to produce reference data to validate the classification results for the rest of study areas, with high accuracy (i.e., above 70%). For all the study sites, CLC from 2012 was also used for comparing and checking the consistency of classification results over all the study areas. Despite the limitations of the CLC data (e.g., there was a three years difference between CLC and Sentinel -1 datasets) the results suggested that the application of S-1 time series data for rice area mapping had produced consistent results for all the test sites with overall accuracies ranging from 77.7% to 98.9% (i.e., kappa average at 0.53).

One limitation highlighted by the study is the need for ancillary information about the time of land preparation and water supply to improve the classification in areas where the temporal signature for rice is unusual. Acquiring to such data would help to improve the accuracy of rice cropland monitoring at the continental scale using S-1 time series.

1.7. Scientific impact

The key findings and major scientific contributions of this PhD thesis are summarized as the following:

I. A novel approach for rice monitoring was developed by combining multi-year and multi-track Envisat ASAR wide swath acquisitions (HH polarization) into a normalized time series which can be used to investigate the temporal backscatter dynamics over paddy rice fields. Effects of different incidence angles and temporal acquisition density have been tackled by temporal aggregation and incidence angle normalization based on statistical methods.

II. The potential of Sentinel-1 for mapping regional rice cultivation extent and for deriving rice phenological parameters has been demonstrated. VH-polarized backscatter has been found to be more sensitive to rice growth than VV-polarized backscatter. This study is, to my best knowledge, the first Sentinel-1-based analysis for mapping rice-cultivated area and for estimating rice phenological parameters on a continental scale.

III. The study has derived phenological parameters of rice crops (i.e., beginning of the season, end of the season, and length of the season) and produced rice seasonality maps (i.e., single-, double-, and triple-rice crop) from SAR imagery. This information is expected to provide valuable information for farmers, agricultural managers, and agricultural insurance services.

1.8. Author contributions

1.8.1. Publication I: Mapping Rice Seasonality in the Mekong Delta with Multi-Year Envisat ASAR WSM Data

Duy Ba Nguyen, Wolfgang Wagner, and Vahid Naeimi conceived and designed the study. The algorithm was developed by Duy Ba Nguyen, and the experiments were implemented by Duy Ba Nguyen with guiding comments by Kersten Clauss and Claudia Kuenzer. SAR data pre-processing and geophysical parameters retrieval were performed by Vahid Naeimi and Senmao Cao. Duy Ba Nguyen wrote a first draft version of the manuscript and produced all graphics.

Kersten Clauss and Claudia Kuenzer analyzed and interpreted the preliminary results, suggested detailed improvements, and had a major contribution to the writing of the results, discussions and conclusion sections. All authors provided assistance in editing and organizing the manuscript.

1.8.2. Publication II: Mapping rice extent and cropping scheme in the Mekong Delta using Sentinel-1A data

Duy Ba Nguyen and Wolfgang Wagner conceived and designed the study. The algorithm was developed by Duy Ba Nguyen, and the experiments were implemented by Duy Ba Nguyen. SAR data pre-processing and geophysical parameters retrieval were performed by Duy Ba Nguyen. Duy Ba Nguyen wrote a first draft version of the manuscript and produced all graphics. Wolfgang Wagner and Alexander Gruber suggested detailed improvements and had a valuable contribution to the writing of the results, discussions and conclusion sections. All authors provided assistance in editing and organizing the manuscript.

1.8.3. Publication III: European Rice Cropland Mapping with Sentinel-1 Data: The Mediterranean Region Case Study

Duy Ba Nguyen and Wolfgang Wagner conceived and designed the study. The algorithm was developed by Duy Ba Nguyen, and the experiments were implemented by Duy Ba Nguyen with guiding comments by Wolfgang Wagner. SAR data pre-processing and geophysical parameters retrieval were performed by Duy Ba Nguyen. Duy Ba Nguyen wrote a first draft version of the manuscript and produced all graphics. Wolfgang Wagner suggested detailed improvements. All authors provided assistance in editing and organizing the manuscript.

CHAPTER 2

MAPPING RICE SEASONALITY IN THE MEKONG DELTA WITH MULTI-YEAR ENVISAT ASAR WSM DATA

Rice is the most important food crop in Asia, and the timely mapping and monitoring of paddy rice fields subsequently emerged as an important task in the context of food security and modelling of greenhouse gas emissions. Rice growth has a distinct influence on Synthetic Aperture Radar (SAR) backscatter images, and time-series analysis of C-band images has been successfully employed to map rice fields. The poor data availability on regional scales is a major drawback of this method. We devised an approach to classify paddy rice with the use of all available Envisat ASAR WSM (Advanced Synthetic Aperture Radar Wide Swath Mode) data for our study area, the Mekong Delta in Vietnam. We used regression-based incidence angle normalization and temporal averaging to combine acquisitions from multiple tracks and years. A crop phenology-based classifier has been applied to this time series to detect single-, double- and triple-cropped rice areas (one to three harvests per year), as well as dates and lengths of growing seasons. Our classification has an overall accuracy of 85.3% and a kappa coefficient of 0.74 compared to a reference dataset and correlates highly with official rice area statistics at the provincial level (R^2 of 0.98). SAR-based time-series analysis allows accurate mapping and monitoring of rice areas even under adverse atmospheric conditions.

2.1. Introduction: Remote Sensing-Based Rice Mapping

Vietnam is the sixth largest producer of paddy rice in the world and second largest exporter of milled rice after Thailand (FAOSTAT 2013). Rice is the single most important food crop in Vietnam, and rice export contributes a fifth to Vietnam's GDP (GSO 2014). The Mekong Delta—dubbed "Vietnam's Rice Bowl"—contains the majority of the area designated for rice agriculture. Mapping and monitoring of crop growth is therefore of high importance for food security, as well as economic and ecological planning.

Reliable detection of rice-cropping schemes requires analysis of dense time series in order to determine different physiological stages in the growth of the rice plant and distinguish rice from other crops as well as to discriminate between rice-cropping schemes. Authors of optical remote sensing-based rice studies have frequently emphasized the need of using sensors with very high revisit times in order to acquire a sufficient amount of cloud-free observations to create reliable time series (Xiao et al. 2002, Sakamoto et al. 2005, Xiao, Boles et al. 2005, Xiao et al. 2006, Chen et al. 2011, Peng et al. 2011, Chen et al. 2012, Leinenkugel et al. 2013, Son et al. 2014, Dong et al. 2015). Microwave-based remote sensing techniques, on the other hand, have the advantage of being non-susceptible to cloud cover. Numerous studies have been conducted to assess the potential of active microwave sensors for backscatter characterization in Mekong River Basin (Naeimi et al. 2013) and using Synthetic Aperture Radar (SAR) sensors for rice mapping (Aschbacher et al. 1995, Kurosu et al. 1995, Ribbes and Toan 1996, Toan et al. 1997, Ribbes 1999, Lam-Dao et al. 2009, Bouvet and Le Toan 2011). The first studies of rice mapping with space-borne SAR sensors have been undertaken with the European Remote Sensing Satellite 1 (ERS-1), showing promising results (Aschbacher et al. 1995, Patel et al. 1995, Ribbes and Toan 1996, Chakraborty et al. 1997, Toan et al. 1997).

The temporal variation of SAR backscatter, σ°, can be regarded as a function of rice crop growth. The annual variation of σ° from rice is higher than any other agricultural crop, thereby making SAR sensors valuable remote sensing tools for rice-crop mapping and monitoring (Aschbacher et al. 1995, Ribbes 1999). The theoretical background of the C-band microwave interaction with rice plants has been extensively described by Le Toan et al. (Toan et al. 1997), who compared the visible backscatter changes in ERS-1 SAR images over two test sites in Japan and Indonesia with backscatter modelled by means of Monte Carlo simulation. They have shown that wave–plant–water interactions are the primary backscatter mechanisms in flooded rice fields, in addition to direct scattering. Scattering from multiple reflections only have negligible contributions. These findings have been reaffirmed by Wang et al. (Wang et al. 2005), who arrived at the same conclusion

when comparing RADARSAT-1 data with Monte Carlo simulation-based HH backscatter models. These modelling efforts can be used to explain the distinct backscatter profile rice-growing areas emit over time. Before rice is sown, paddies are usually flooded for pest and vegetation control. This results in very low backscatter values due to specular reflection on the flat surface. Flooded rice paddies might, however, be influenced by strong winds which cause ripples and waves on the water surface and consequently increase backscatter. Over the course of the vegetative and reproductive phases, backscatter continuously increases until the vegetation growth reaches its maximum at the heading stage. During this time, the phenological development of the rice plant leads to an elongation of stems, increase in plant moisture and leaf area - generally an increase in biomass. This in turn increases the area available for reflection of the radar wave via double-bounce and direct volume scattering leading to an increase in measured backscatter. After the heading stage, plant moisture, leaf area and biomass start to decline, thus leading to a decline in σ° due to the reduction of the aforementioned scattering effects. This temporal backscatter behavior is illustrated in Figure 2.1 showing the C-band backscatter measurements from Envisat SAR measurements over a triple-cropped rice field in the Mekong Delta.

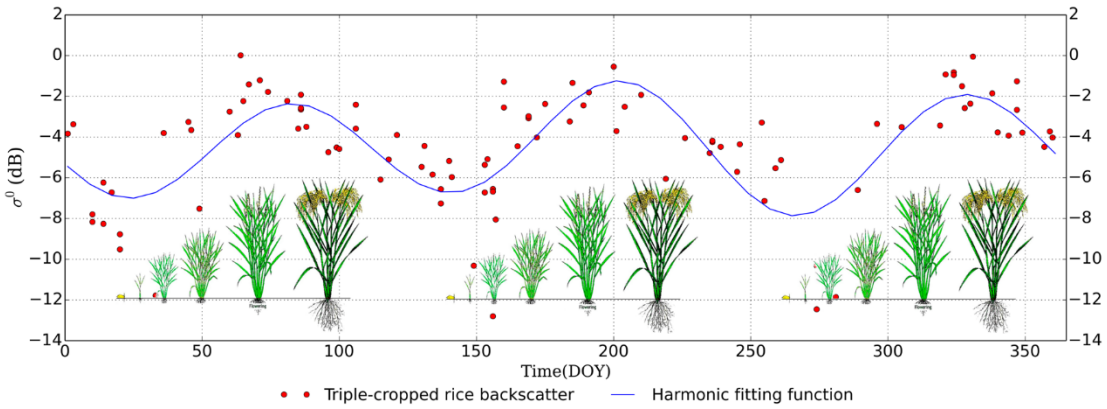

Figure 2.1. SAR backscatter behavior in relation to rice-growing stages (adapted from (Bouvet and Le Toan 2011), growing stage images from (IRRI 2015) for triple-cropped rice based on a multi-year ASAR WSM time series.

Basically, two common methods of SAR-based rice mapping have been implemented in multiple study areas using different SAR sensors. In one of the

methods, single polarization of backscatter data with high temporal density is utilized to monitor variations of rice plant over its growth phases. In the other method, backscatter observations from different polarizations are compared to each other for determination of rice plant growth phases. While the first method requires data from sensors aboard satellites with a short revisit time, the second one is dependent on sensors with dual- or quad-polarization capabilities. Method selection for SAR-based rice mapping is essentially determined by the data availability and sensor selection.

The backscatter images, acquired by the C-band SAR onboard ERS-1 with a repeat time of 35 days, were used in numerous SAR-based multi-temporal backscatter analyses for rice mapping case studies in Thailand (Aschbacher et al. 1995), Indonesia (Toan et al. 1997), Japan (Kurosu et al. 1995, Chakraborty et al. 1997, Toan et al. 1997), Vietnam (Soo Chin et al. 1998), Canada (McNairn and Brisco 2004, Jia et al. 2013) and India (Premalatha and Nageswara Rao 1994, Patel et al. 1995, Panigrahy et al. 1997). Methods developed for ERS-1 SAR data have been advanced and successfully transferred to RADARSAT-1 acquisitions at C-band with horizontal co-polarization and a 24-day repeat cycle (Shao et al. 1997, Panigrahy et al. 1999, Ribbes 1999, Shao et al. 2001, Li et al. 2003, Chakraborty et al. 2005, Choudhury and Chakraborty 2006). Joint analysis of ERS-1/2 and RADARSAT-1 data showed how polarization and incidence angle influence backscatter from paddy rice (Liewn et al. 1998). Comparative studies showed that C-, L- and X-band can be utilized for the multi-temporal method (Inoue et al. 2002, Suga and Konishi 2008). Rosenqvist (Rosenqvist 1999) highlighted the limits of L-band data since rice planted in slant range direction of the SAR instrument exhibits a dynamic σ° range of more than 20 dB compared to only a few dB if it is planted in azimuth direction caused by directional resonance and attenuation effects. Despite these limitations, rice mapping with L-band has been shown to work in several studies in southeastern China (Wang et al. 2009, Zhang et al. 2009, Ling et al. 2010).

The second common method exploits the fact that the vertical structure of the rice plant attenuates vertically polarized waves to a higher degree than horizontally polarized waves (Toan et al. 1997, Ribbes 1999). The potential of this behavior for

rice classification was initially explained by comparison of C-band ERS and RADARSAT-1 data, ground-based X-band measurements, as well as backscatter models (Toan et al. 1989, Toan, Ribbes et al. 1997, Ribbes 1999, Shao et al. 2001, Wang et al. 2005). Studies by Chen et al. (Chen et al. 2007)[48], Bouvet et al. (Bouvet et al. 2009) and Lam-Dao et al. (Lam-Dao et al. 2009) employed Envisat ASAR data to show that the ratio between HH and VV polarization on multi-temporal datasets can be used to classify rice areas with higher accuracy and less temporal coverage compared to the first method. Polarimetric decomposition of fully polarimetric RADARSAT-2 acquisitions showed promising results regarding not only the binary rice/non-rice classification of images but also the detection of rice's growth stages (Fan et al. 2011, Li et al. 2012, Yonezawa et al. 2012). Rice classification performance of TerraSAR-X (TSX) images over test sites in Spain and the theoretical models behind multi-polarization and X-band-based rice classification have been extensively described by Lopez-Sanchez et al. (Lopez-Sanchez et al. 2011, Lopez-Sanchez et al. 2014) as well as for the Mekong Delta (Gebhardt et al. 2012). Studies based on the second method, employing backscatter response from different polarizations, have shown the capability of distinguishing rice from other land cover and detecting its growth stages with less temporal coverage than the single-polarization, multi-temporal method for small study regions. Application of this approach on the regional or continental scale has been hampered by limited coverage of SAR sensors with dual- or quad-polarization capabilities.

SAR-based classification methods belonging to the two aforementioned categories have been proven to accurately map rice-cropping schemes under different growing regimes with a variety of sensors. The multi-temporal, single-polarization method has been applied far more often than the multi-polarization method, which is not an indicator of its superiority but rather highlights the limited availability of data suitable for the second method. Studies investigating the capabilities of the second method often underlined their superior accuracies compared to studies employing the first method.

These methods have been utilized for the Mekong Delta, and the first notable results have been published by Liew et al. (Soo Chin et al. 1998), who derived backscatter change from ERS-2 time series and classified eight different rice-cropping schemes according to their temporal backscatter behavior. Bouvet et al.(Bouvet et al. 2011) were the first to employ the multi-temporal method to produce a map of rice-cropping schemes and areas for the whole Mekong Delta with the use of Envisat ASAR wide swath data. They achieved this by aggregating horizontally polarized SAR time-series classifications from three satellite tracks since temporal coverage for a single track is not dense enough to achieve high classification accuracy. The resulting seasonality map has a reported accuracy of 75.8% compared to a reference dataset created from dual-polarization ASAR data. Efforts by Bouvet et al. (Toan et al. 1989) and Lam-Dao et al. (Lam-Dao et al. 2009) emphasized the performance of rice mapping with dual-polarization ASAR data in the Mekong Delta while employing a straightforward HH/VV ratio and achieving accuracies of up to 89.8%. Lam-Dao et al. (Lam-Dao et al. 2009) also showed the applicability of this method for X-band TerraSAR-X data as well as predicting crop yield by combining SAR images and survey data. However, limited availability of dual-polarization SAR data prohibited the implementation of this classification approach on a regional scale. Thus far, no study was able to utilize the complete Envisat ASAR archive for the Mekong Delta due to incidence angle effects on rice mapping. The goal of our study is therefore to classify rice areas and determine the seasonality of rice crops in the Mekong Delta by using phenological techniques applied on multi-year Envisat ASAR WSM time series from 2007 to 2011. This study builds upon methods initially developed by Nguyen et al. (Nguyen et al. 2015) over the Red River Delta, Vietnam.

2.2. Study Area: Mekong Delta

The Mekong Delta (MKD), Vietnam's southernmost region and home to over 18 million inhabitants, covers an area of about 40,000 km2 between 8.5°–11.5°N and 104.5°–106.8°E and consists of 13 provinces, as depicted in Figure 2. Due to its origin by accumulation of alluvial sediments from the Mekong River, the wide flat plain is mostly located below sea level and consists of fertile soils and, like all

deltas, it is vulnerable to a number of factors (Apel et al. 2012, Renaud et al. 2013). An intricate flood regime influences it, which used to be a single-peak pulse but is expected to change due to upstream regulatory measures (Kuenzer et al. 2013, Kuenzer et al. 2013). Irrigation and flooding of agricultural land is managed by a dense network of channels, dykes and gates.

A distinct dry season lasting from December until May caused by the northwest monsoon followed by a rainy season caused by the southwest monsoon typically lasting from June to December characterize the MKD, which experiences an average of 1800 mm precipitation per year. Large parts of the delta are flooded and covered in a new layer of sediments each rainy season; flood-controlled fields experience this every 3 to 4 years without interrupting the rice-cropping scheme (Nguyen et al. 2012).

This constant fertilization is the basis for the agricultural prosperity of the region where 62% of the land is used for agriculture, 15% aquaculture and 6% mangrove and melaleuca forest (GSO 2012). Since rice is by far the dominant crop, cultivated on 73.9% of the agricultural land, this region is often referred to as the "rice bowl of Vietnam." Towards the coast, rice cropland gives way to aquaculture of shrimp and fish as well as residual mangrove forest and hybrid land-use forms combining rice and shrimp farming or mangrove forest and shrimp farming. Aquaculture is the dominant land-use form in the southernmost part of the region and it is increasingly diminishing the remaining mangrove forests (Thu and Populus 2007, Kuenzer et al. 2011, Quoc Vo et al. 2015). Rice is grown in three distinct cropping seasons called "Đông-Xuân" or "Spring" from November to March, "Hè-Thu" or "Autumn" from April to August, "Thu-Đông" or "Winter" in inland areas from August to December and "Mùa" or "Main wet season" in coastal areas from July to February of the following year resulting in one to three rice harvests per year. Some
triple-cropped areas employ a short "Spring–Summer" season between Winter–Spring and Summer–Autumn. Choice of rice variety, cropping scheme and growing season implemented by farmers is highly dependent on the availability of

irrigation water and local water management practices leading to a spatially diverse distribution (Nguyen et al. 2012).

2.3. Data

The Advanced Synthetic Aperture Radar (ASAR) was a C-band sensor on the Envisat satellite which was launched on 1 March 2002; it had a 35-day repeat cycle and was operated by the European Space Agency (ESA) until April 2012. Multiple orbit paths can be used to observe the same area in a shorter time due to the side-looking nature of the ASAR instrument with different incidence angles ranging from 17° to 42°. For this study, we had access to almost all archived wide swath mode acquisitions from January 2007 through December 2011 that completely or partially cover the Mekong Delta. A total of 121 ASAR WSM HH polarization images at 150 m spatial resolution were available coming from different tracks (about 15 tracks in total): Track 32 (19 images); Track 183 (6 images); Track 304 (11 image); Track 412 (10 images); Track 97 (3 images); Track 147 (10 images); Track 377 (3 images); Track 75 (8 images); Track 490 (6 images); Track 261 (6 images); Track 118 (13 images); Track 219 (4 images), Track 104 (6 images), Track 262 (5 images) and Track 347 (12 images). We used Level-1b ground range-corrected data (ENVISAT.ASA.WSM_1P), which was generated by ESA from Level-0 data using the ScanSAR technique. Using scenes with partial coverage of our study area leads to an unequal spatial distribution of available data points for the creation of a time series. The amount of available acquisitions ranges from 80 to 113 with an average of 101 as shown in Figure 3a. In our multi-track, multi-year approach we combined the scenes according to their acquisition day of year (DOY) which leads to a time gap ranging from 1 to 16 days between available scenes with an average interval between 1.5 and 2.2 days. The total number of available scenes, averaged number of observations per week of year as well as the distribution of longest interval between the acquisitions are shown in Figure 2.3a–c, respectively.

A land-use map for the 13 provinces in our study area representing the year 2010 at the scale 1:50,000 has been provided by the General Department of Land Administration of Vietnam. The Vietnam Institute of Meteorology, Hydrology and Environment supplied us with a land-use map for the year 2005 at the scale

1:650,000. In addition, rice area statistics for each province have been collected by the General Statistics Office of Vietnam (Figure 2.2).

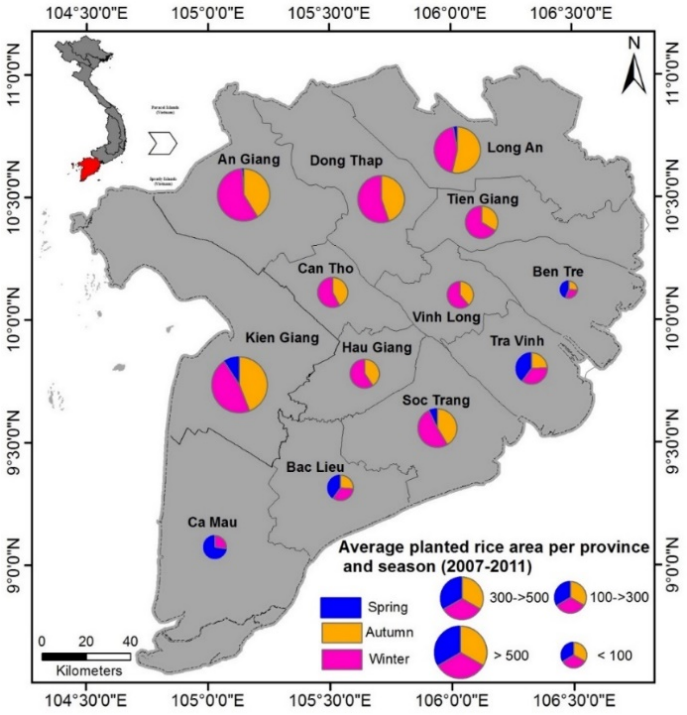

Figure 2.2. Planted rice area per province and season averaged for the period of 2007 to 2011 (Source: General statistics Office of Vietnam) (adapted from Bouvet et al. 2011).

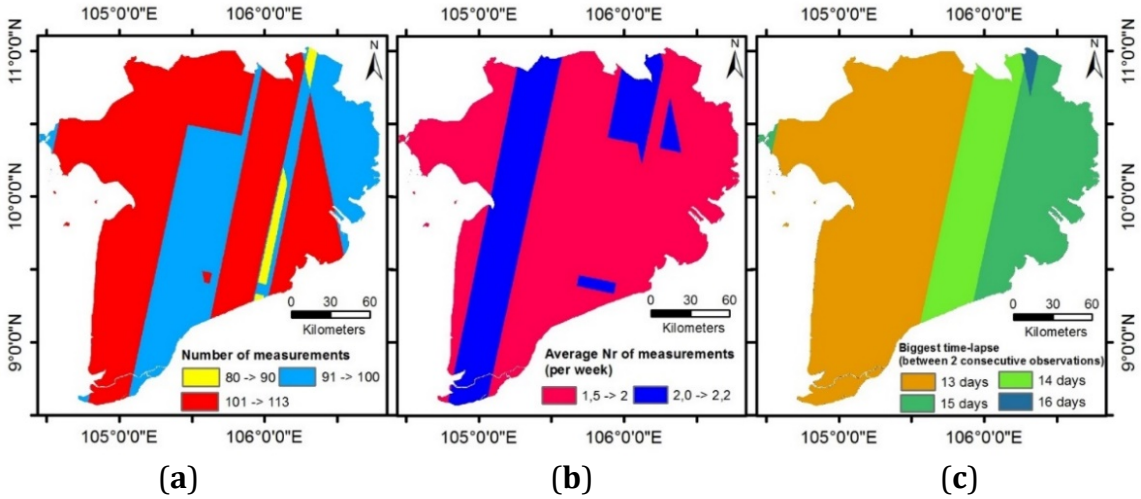

Figure 2.3. (a) Temporal and spatial distribution of available Envisat ASAR WSM scenes. (b) Average number of measurements per week. (c) Largest interval between DOY of ASAR WSM acquisitions from 2007 to 2011.

2.4. Methods and Data Analyses

Considering data availability for our study region, we chose to perform the multi-temporal backscatter analysis method on C-band Envisat ASAR data for rice mapping. We combined several ASAR WS mode acquisitions from multiple tracks to enhance temporal and spatial coverage, which has been also successfully applied in previous ASAR studies (Loew et al. 2006, Bouvet and Le Toan 2011). All Envisat ASAR WSM scenes were pre-processed using the open source software NEST (Next ESA SAR Toolbox). Pre-processing consisted of geocoding, radiometric calibration and resampling. The geocoding step involved a Range Doppler Terrain correction processing that used the elevation data from the 3 arc-second DEM product from the Shuttle Radar Topography Mission (SRTM) and DORIS orbit state vectors provided by ESA. In this process, data are resampled and geo-coded to a grid of 75m spacing to preserve the 150m spatial resolution according to the Nyquist sampling theorem (Loew et al. 2006). The data analysis in this study has been performed in six steps as illustrated in Figure 2.4: (1) ENVISAT ASAR pre-processing; (2) Backscatter normalization to a reference incidence angle (regression-based approach): $\sigma^\circ \rightarrow \sigma^\circ NOR$; (3) Time-series compositing and averaging: $\sigma^\circ NOR \rightarrow \sigma^\circ NOR\_average$; (4) Time-series smoothing with a Gaussian moving window filter: $\sigma^\circ NOR\_average \rightarrow \sigma^\circ smooth$; (5) Classification using a knowledge-based decision-tree approach; (6) Accuracy assessment based on the intersection of a 2005 and 2010 land-use map.

2.4.1. Incidence Angle Normalization

After pre-processing of the ASAR WSM scenes, the following parameters are obtained for each scene: sigma nought backscatter coefficient (σ°) expressed in decibels, and incidence angle (θ) expressed in degrees. The backscatter is not only influenced by the land cover but also the incidence angle. In order to detect changes in backscatter resulting from a change in surface status or land cover, it is necessary to remove incidence angle dependency of backscatter by normalizing all acquisitions to a common incidence angle. This was achieved by the approach described in (Pathe et al. 2009). In this method, long-term observations are used to

model backscatter behavior with respect to incidence angle by performing linear regression analysis (Nyquist 1928).

$$\sigma^0(\theta) = a + b\theta \quad (2.1)$$

where the θ is the incidence angle, σ° is the backscatter and b is the slope parameter (gradient) of the regression line. Using the acquired slope parameter of the regression line for each pixel, all preprocessed ASAR WSM scenes were normalized to a reference incidence angle of 30° using the following equation:

$$\sigma^0(30^0) = \sigma^0(\theta^0) - b(\theta - 30^0) \quad (2.2)$$

The normalization of backscatter measurements ensures comparability of scenes for time-series analysis. Figure 2.5a,b illustrate the slope and the mean of normalized backscatter. In Figure 5c,d a single ASAR WSM scene from 1 March 2007 is depicted before and after the backscatter normalization to 30°. Since the incidence angle could have a significant influence on the backscatter sometimes even larger than the natural backscatter dynamics over time, the normalization of backscatter is essential for time-series analysis (Figure 2.6). The backscatter behavior with respect to incidence angle varies depending on surface characteristics. For example, the influence of incidence angle on backscatter is higher for bare soil (high gradient, steep regression line) than for densely vegetated areas (low gradient of regression line).

2.4.2. Time-Series Creation and Filtering

To generate ASAR WSM time-series composite for each day of year from multi-track and multi-year observations, some simplifying assumptions are needed to be made. First, we supposed that the backscatter changes over time exhibited by different rice-cropping schemes remained stable over the observation period. This entails that no changes in the cropping scheme, no change in land cover and no significant alterations in the growing seasons took place during the 2007 to 2011 period. Second, we presumed the distribution and amount of sample points to be sufficient to fulfill the criteria of the Nyquist–Shannon–Kotelnikov sampling theorem (Nyquist 1928, Shannon 1998). The average sampling of ASAR WSM observations is 1.5 to 2 measurements per week with a maximum two-week time

gap between observations in some limited periods of the year (see Figures 2.1 and 2.3). Therefore, it is supposed that the ASAR WSM weekly sampling (averaging 7-day intervals) is capturing any rice crop variations throughout the year as at least one measurement per week is occurring. Rice area extent in the Mekong Delta can be regarded as mostly stable based on our long-term in situ knowledge and previous studies also showing regular changes in cropping scheme affect only small areas at the fringes of irrigated triple-crop and rain-fed single-crop areas (Son et al. 2014).

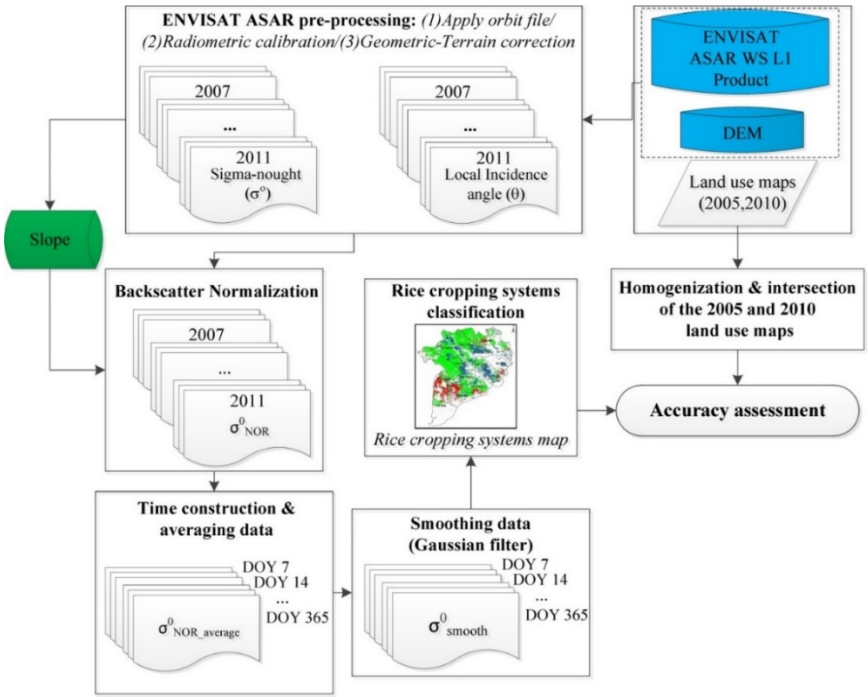

Figure 2.4. ENVISAT ASAR data analysis, rice classification, and validation steps.

To create a time series dense enough for rice mapping, we combined Envisat ASAR WSM data from multiple years into one dataset. We did this by considering only the day of acquisition (DOY) and disregarding the year that image was taken in. We created σ^{o}_{NOR} time series that represents the backscatter behavior over the year for the period of 2007 to 2011.

The number of observations in our study area ranges from 80 to 113 with a maximum time-gap of 16 days and a mean acquisition interval between 1.5 and 2.2 days. In the next step, we calculated the mean of backscatter over all acquisitions within 7-day intervals and created a single-year time series with 52 data points

denoted as $\sigma^{o}_{NOR\_average}$, which represents the average of backscatter for each week. Averaging was executed to tackle the temporal heterogeneity of the WSM acquisitions while at the same time creating a time series dense enough to capture phenological stages of the rice growth, like transplanting and heading. A 7-day interval was therefore chosen.

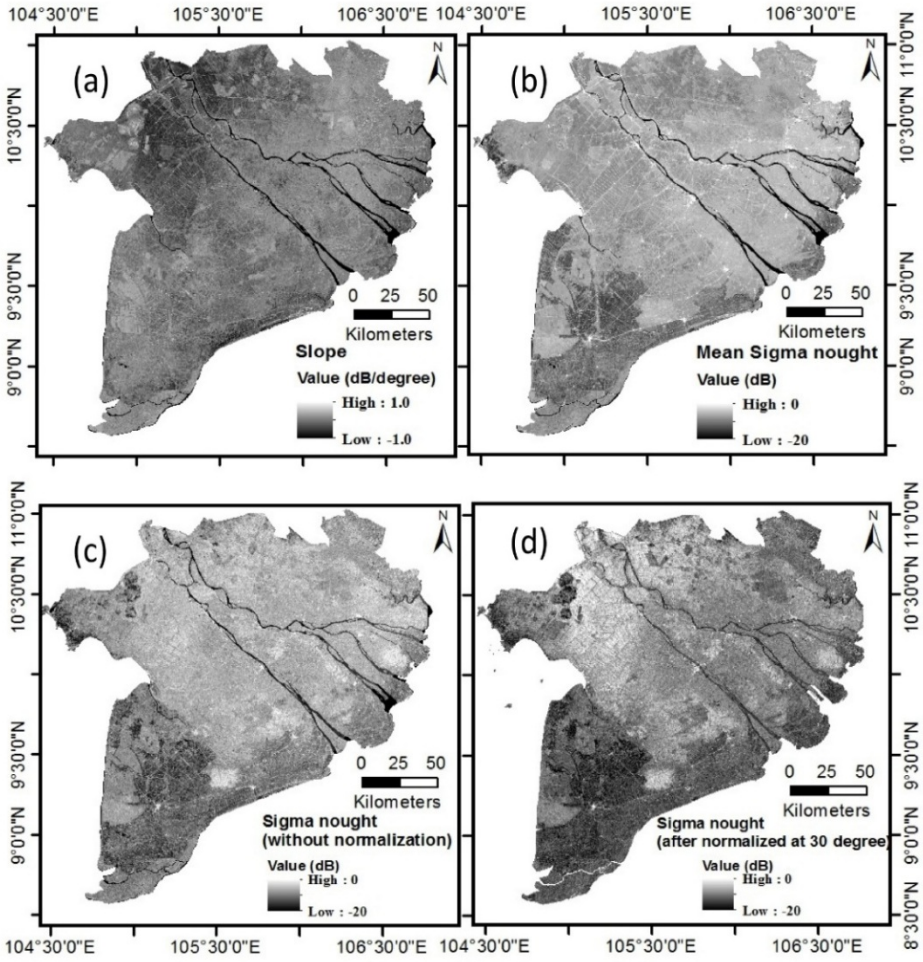

Figure 2.5. Slope parameter (a), mean backscatter without normalization (b), original backscatter without normalization (c) and backscatter normalized to 30° incidence angle (d) for the Envisat ASAR WSM scene from 1 March 2007.

The compositing of backscatter measurements has the advantage of reducing the random noise errors inherited in the ASAR WSM data from atmospheric attenuation and speckle noise. On the other hand, it has the disadvantage of introducing noise caused by land-use changes, shifts in the growing seasons, their start and end points, their length as well as changes in the cropping scheme, for

example a change from single-cropped rice to double-cropped rice or from double-cropped rice to triple-cropped rice, that could have happened over the five-year period. These kinds of errors are supposed to be of a random nature and therefore have already filtered in the $\sigma^o_{NOR\_average}$ time series, thereby resulting in a smoothed backscatter signal available for classification of different rice-cropping schemes. To smooth the $\sigma^o_{NOR\_average}$ time series, a Gaussian filter with standard deviation of 3 for the kernel was selected for temporal filtering as it shows satisfying coincidence with the reported number of rice crops, visible as distinct peaks, as well as their approximated heading dates compared to the reference data. An example of different standard deviation kernels is given in Figure 2.7.

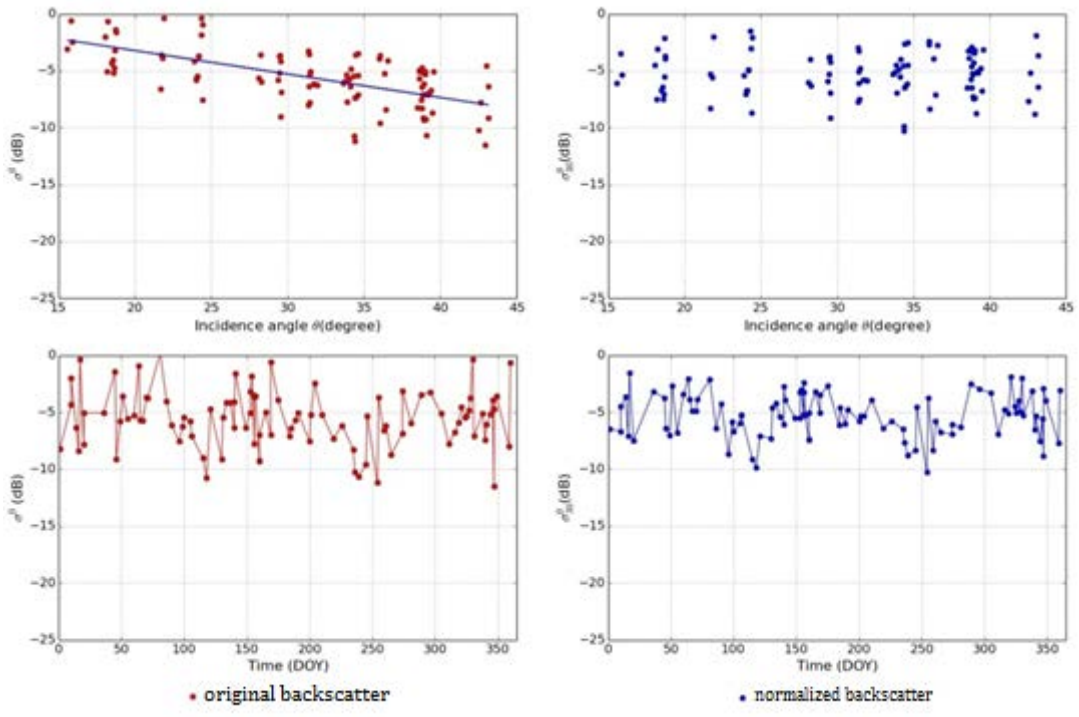

Figure 2.6. Time series of backscatter over rice-cropped area (backscatter vs. incidence angle, original backscatter and normalized backscatter).

2.4.3. Reference Dataset

The reference datasets used in this study are the land-use maps from 2005 and 2010 in the Mekong Delta. For simplification, we merged different legends from the land-use maps into single, double and triple cropped-rice classes as shown in Table 2.1. All remaining classes are considered non-rice-cropping areas.

Furthermore, both reclassified maps were intersected to derive quasi stable rice-cropping areas. In the resulted 2005–2010 map, the areas classified with the same cropping schemes were kept and all other areas were reclassified as non-rice (Figure 2.8).

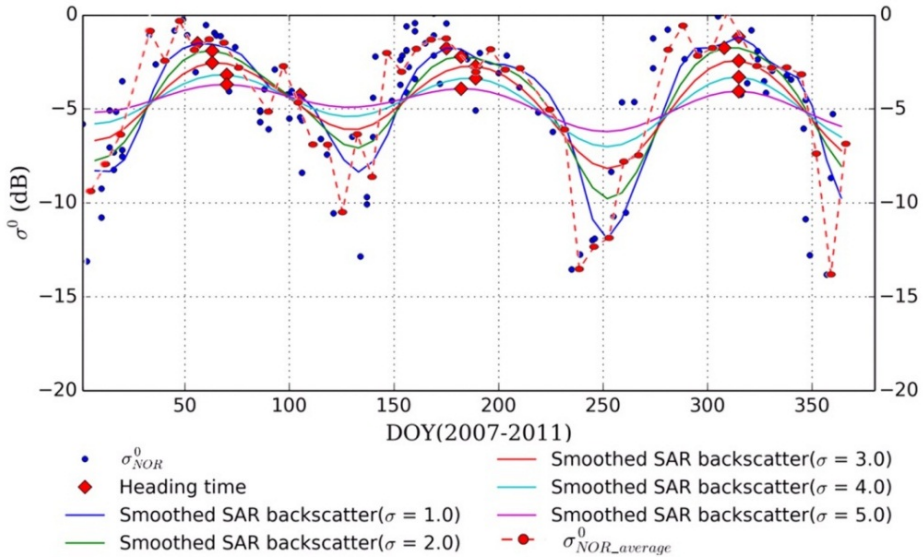

Figure 2.7. Gaussian window function with different standard deviations compared to the unfiltered, averaged time series and the non-averaged time series.

Table 2.1. Land-use map homogenization key.

Land-Use Map 2010	Merged Legend	Land-Use Map 2005
Triple-cropped rice	Triple-cropped rice	Triple-irrigated rice
Double-cropped rice + subsidiary Double-cropped rice (WS & SA) Double-cropped rice (SA & Main) Double-cropped rice (WS & Main)	Double-cropped rice	Double-irrigated rice Double rainfed rice
Single-cropped rice + subsidiary Single-cropped rice + shrimp Single-cropped rice + aquatic Single-cropped rice	Single-cropped rice	Single rainfed rice

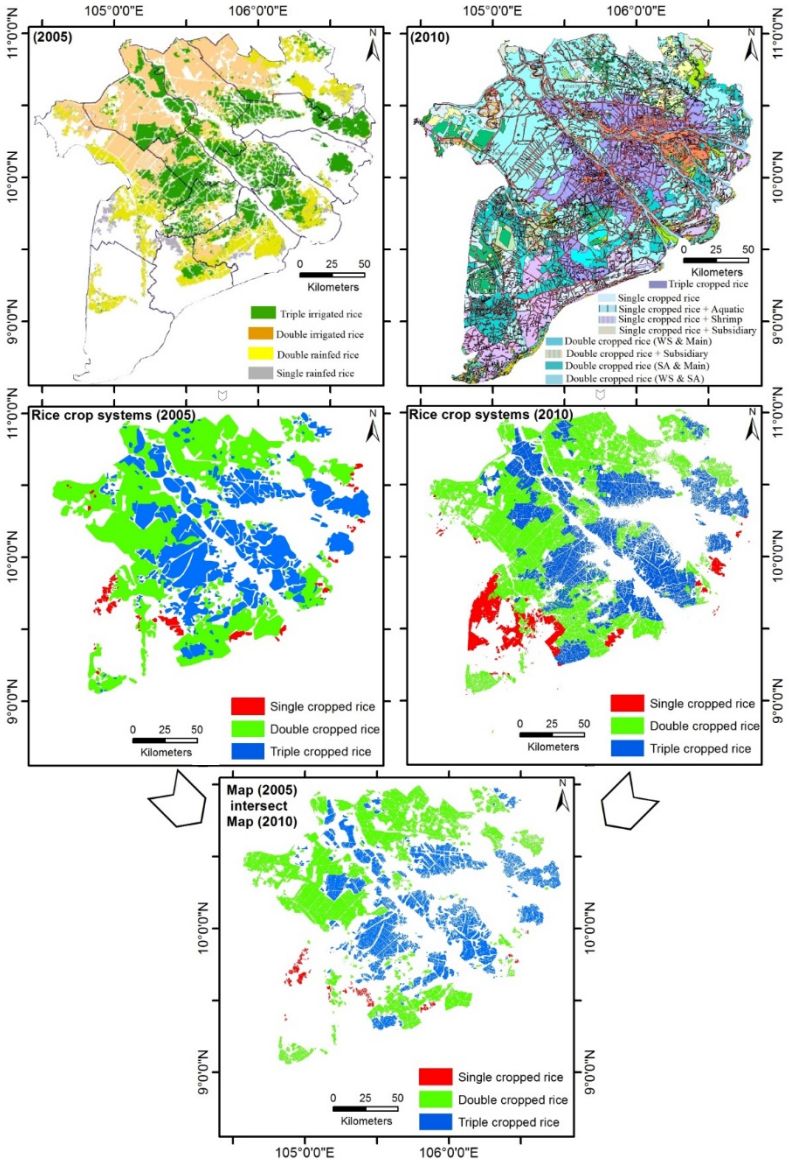

Figure 2.8. Homogenization and intersection of the 2005 and 2010 land-use maps.

2.4.4. Rice Crop Classification

A straightforward, knowledge-based decision-tree approach was used to discriminate different types of rice-cropping systems. This approach is based on the unique seasonal pattern of rice cropped in the magnitude of SAR backscatter coefficient throughout the growth cycle. Rice crops typically exhibit a temporally varying backscatter signal due to their phenological interaction with the microwave signal. For each location in the study area, the maximum and minimum of the σ^o_{smooth} and consequently the amplitude defined as maximum variation of σ^o_{smooth} are calculated. In addition, the local min, max, and variation of backscatter

for each time interval are calculated. Rice heading dates are distinct peaks in the σ^o_{smooth} time series and can be identified by a local maxima algorithm that detects all peaks within the one rice-growing cycle.

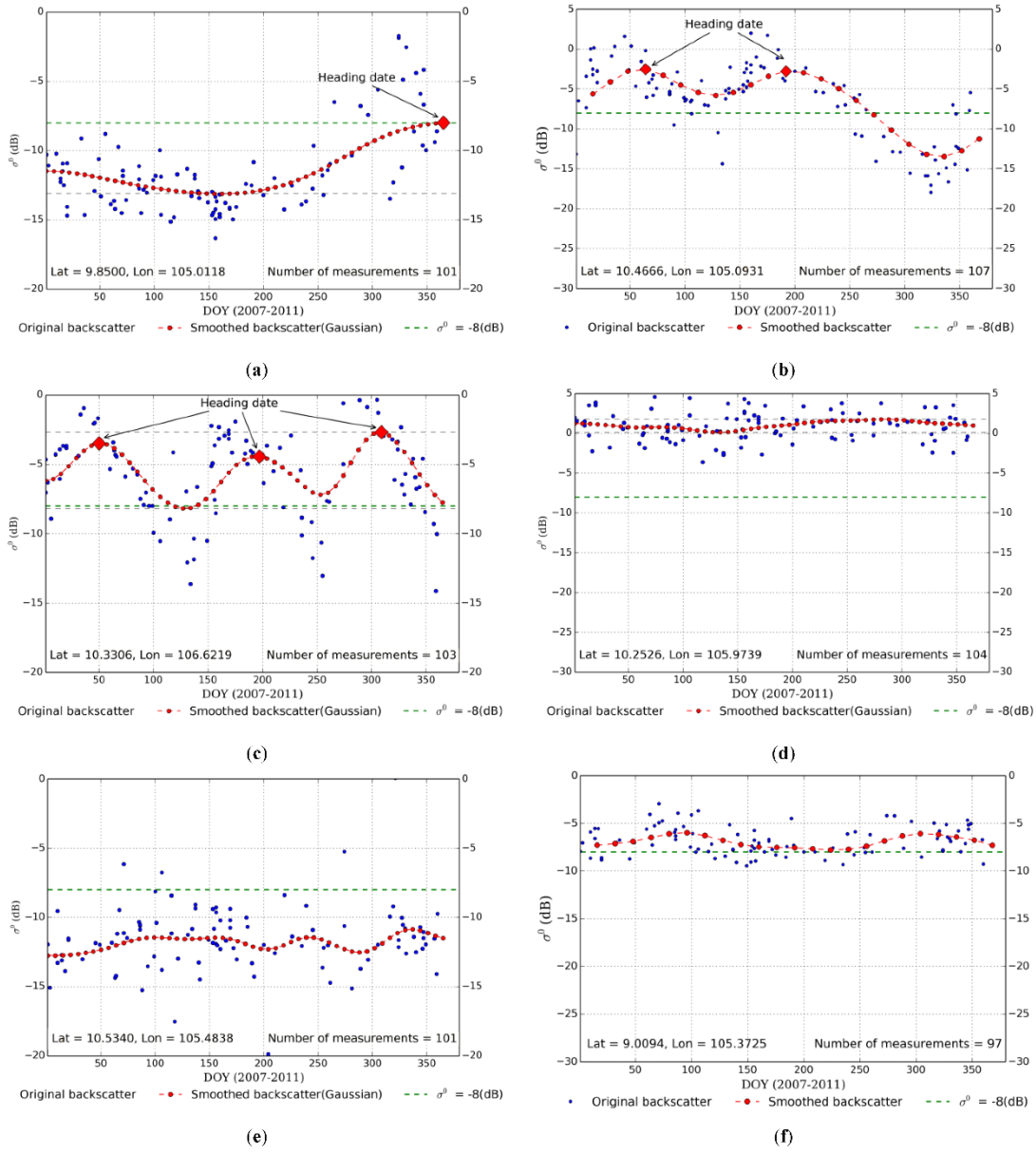

Figure 2.9. Normalized backscatter time series σ^o_{NOR} compared to the averaged, smoothed time series σ^o_{smooth} for six different land-cover types. (a) Single rice. (b) Double rice. (c) Triple rice. (d) Urban. (e) Water. (f) Mangrove forest.

Figure 2.9 shows results of the smoothing and backscatter peak detection from six different land-cover types. Additional conditions are applied for the peak detection since a distinct local maxima of the backscatter can also be found in time-series profile of the other land-cover classes as it is shown in Figure 2.9d–f. In order to

distinguish rice from other land-cover classes, three more static thresholds based on the σ^o_{smooth} values are empirically defined. The first threshold is set to −8dB for the local maxima, which has to be exceeded for a peak detection corresponding to the rice heading date. The second threshold is set for the minimum amplitude of the backscatter (difference between local minimum and maximum), which has to exceed 2.5dB. The third threshold is set for the temporal distance between the local maximums. The temporal distance between two local maximums has to be greater than the shortest possible rice-growing cycle which is about 90 days. If all three conditions are met, then the pixel is classified as rice; otherwise it is identified as a non-rice area. The number of detected local maxima in the σ^o_{smooth} time series determines the classified rice pixel as single, double or triple-cropped rice area, as can be seen in Figures 2.9a–c, respectively.

Backscatter is sensitive to roughness, vegetation and soil moisture. The latter two are fluctuating seasonally and therefore are well captured by SAR sensors. Moreover, the phenology patterns (translating and heading time) were well observed over rice-cropped sections in the study area. Therefore, for the next step, the smoothed backscatter time series are used for determination of key seasonality parameters over all rice-growing areas. Building on the methodology developed by Jönsson and Eklundh (Jonsson and Eklundh 2002), we defined following phenological parameters:

- Start of Season (SOS) as it can be identified from the inflection point in σ^o_{smooth} time series where the second derivative equals 0 and changes from negative to positive.
- End of Season (EOS) as inflection point in σ^o_{smooth} time series where the second derivative equals 0 and changes from positive to negative.
- Length of Season (LOS) as the difference between start and end of season.

This methodology was originally developed for multispectral vegetation indices, which in regard to time series over rice fields show a similar, albeit non-identical behavior as SAR backscatter and are therefore not directly comparable. Examples of single, double and triple rice-cropping schemes that have differing crop

calendars and rice varieties of unequal length and therefore different patterns in their seasonality parameters are given in Figure 2.10. Figure 2.10a,b show the influence of short- (b) and long- (a) duration rice varieties on backscatter values. Figure 2.10b is an example of a single-cropped rice + aquaculture field, which explains the prolonged flooding stage compared to Figure 2.10a.

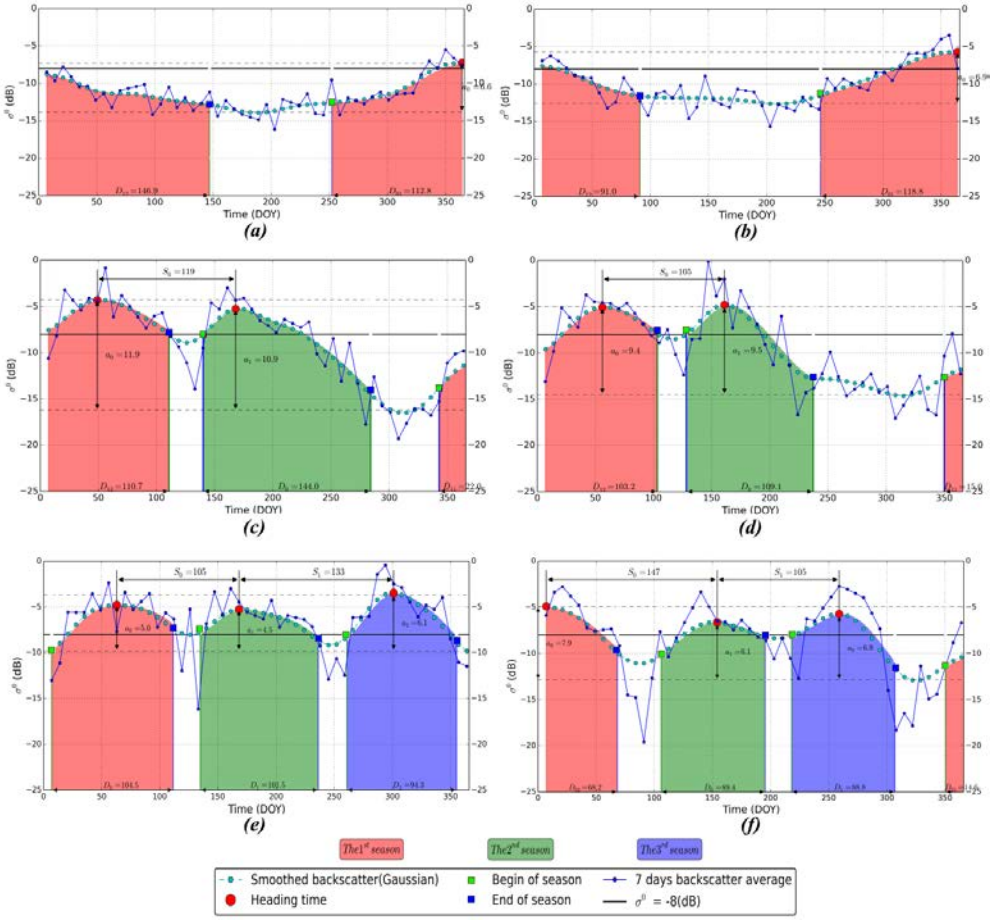

Figure 2.10. Retrieval of rice-growing season length for single, double and triple-cropped rice under different crop calendars.

2.5. Results

Time-series analysis of Envisat ASAR wide swath data from 2007 through 2011 resulted in a map of the rice-growing areas in the Mekong Delta and their respective cropping schemes shown in Figure 2.11. Double rice cropping is the dominant rice-cropping scheme in the Mekong Delta. Triple rice cropping is mainly practiced in the central part of the Mekong Delta in the direct vicinity of the Mekong and Bassac Rivers. The northern parts of the delta away from the rivers

are primarily double-cropped rice with small and scattered patches of single and triple cropping scheme. Towards the southern coastline of the Mekong Delta, rice fields are sparse, which is especially visible in the southern parts of the Ca Mau, Bac Lieu and Soc Trang provinces. A similar distribution, where rice area levels off toward the cost, is visible at the northwestern tip of the delta in the Kien Giang Province.

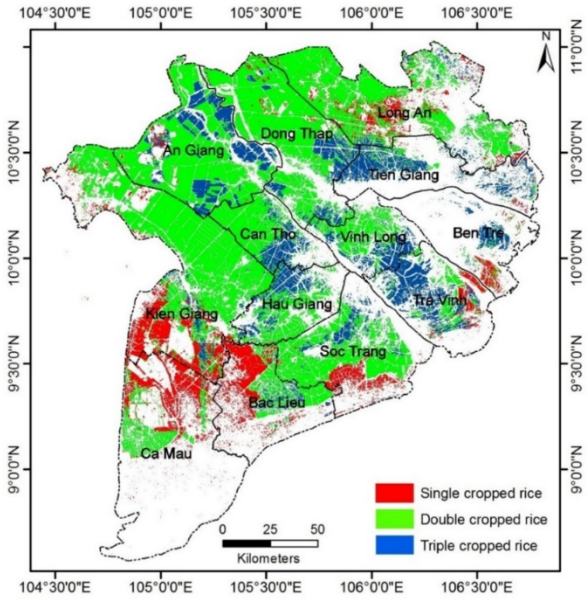

Figure 2.11. Rice crop map for the Mekong Delta derived from Envisat ASAR WSM data from 2007 to 2011.

Seasonality parameters extracted from the time series have been used to produce maps of the temporal distribution of the beginning of the first and second cropping season, end of second and last growing season, displayed in Figure 2.12, as well as the length of the first and second cropping season which are visible in Figure 2.13. Most areas that practice two rice crops per year start the first season around January and end the second season anywhere from August to November. Triple crop areas can be divided into two temporal patterns, where the first season either starts in December of the previous year or around April and March. The first group has the end of the third growing season in November or December and the second one around February and March. The majority of second growing seasons start in May and June. Areas with triple cropping and areas at the beginning of the first season in March and April have the start of the second season around August.

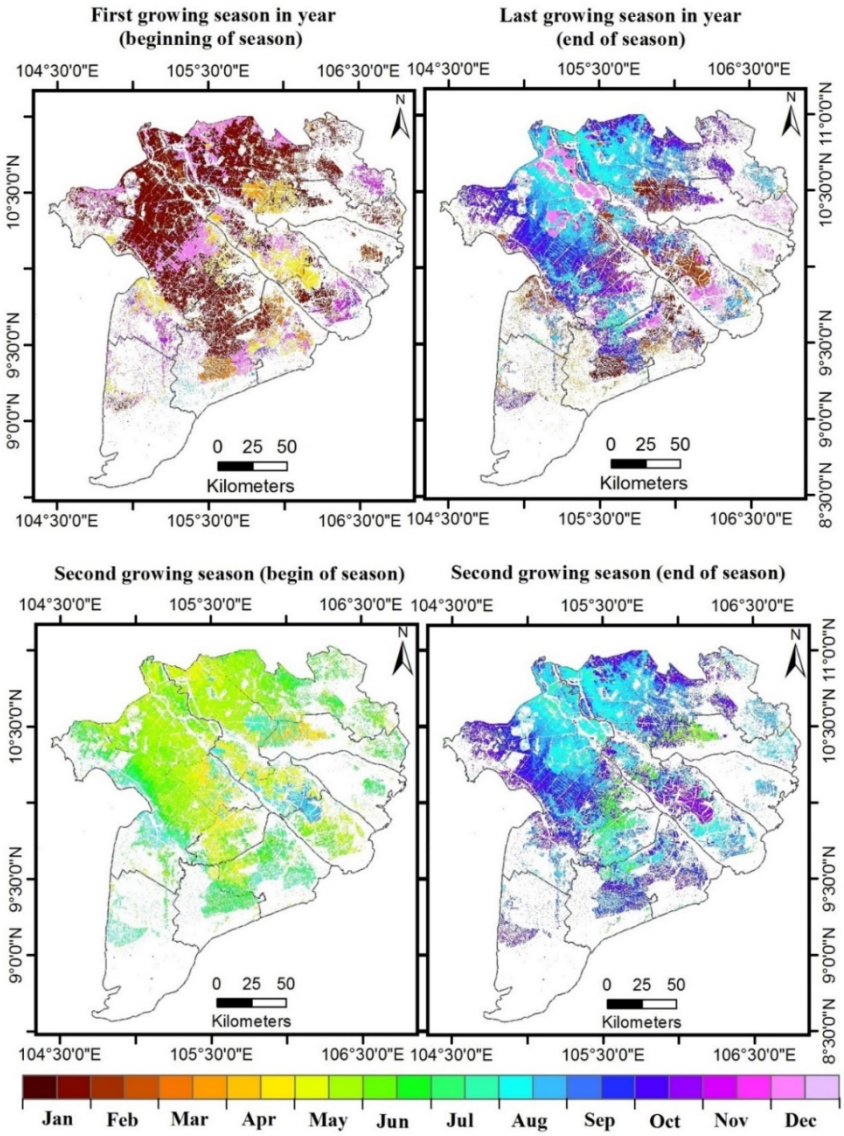

Figure 2.12. Growing season start and end dates in the Mekong Delta derived from Envisat ASAR WSM data from 2007 to 2011.

Length of the first and second growing season is depicted in Figure 2.13. Most double- and triple-cropped rice areas have a short first growing season below 80 days. For triple-crop schemes the second season is short as well, whereas double crop exhibits a longer second season. The length of the second season of double cropped areas can range from 80 to 140 days. The growing season from SAR point of view could be different than the growing season extracted from NDVI time series. The SAR sensor is sensitive to the vegetation structure and soil moisture rather than the greenness, which is the case with NDVI measurements. In general,

NDVI values start to increase earlier than observed in SAR measurements. This is why the SAR-detected growing season in the study region could go below 80 days. For determination of the SOS, EOS, and LOS, all observations from multi-years are considered since not enough measurements from single years are available to map the seasonal variations accurately. This is why the SOS and EOS might not represent the exact transplanting and harvest times in comparison to the values extracted from single-year NDVI time series.

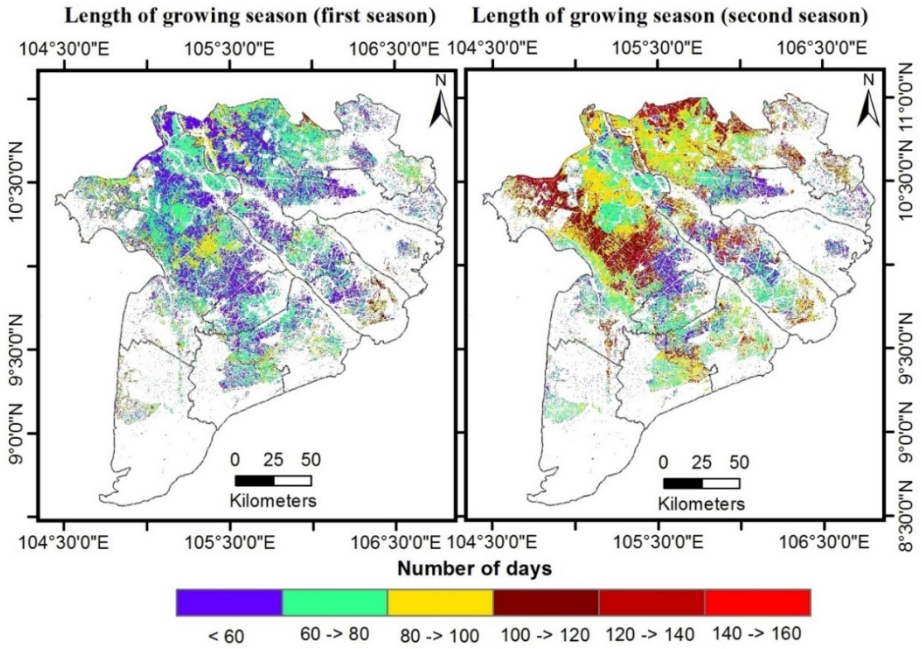

Figure 2.13. Length of first and second rice-growing season the Mekong Delta derived from Envisat ASAR WSM data from 2007 to 2011.

Accuracy of our classification has been assessed by comparing the classification results to the 2005 and 2010 land-use maps as well as their intersection. The minimum mapping units between the 2005 and 2010 land-cover datasets are not comparable (2010 MMU_{50k} = 4 ha and 2005 MMU_{650k} = 169 ha). Therefore, we extracted the sample points for each dataset by means of a regular grid with 500 m spacing where the sample point is extracted from the cell's center as depicted in Figure 14. Confusion matrices for all three reference datasets are presented in Table 2.2. We can report an overall classification accuracy of 85.3% (kappa coefficient 0.74) compared to the 2005–2010 intersection map, 77.2% (kappa coefficient 0.62) compared to the 2010 land-use map and 70.3% (kappa coefficient 0.52) compared to the 2005 land-use map.

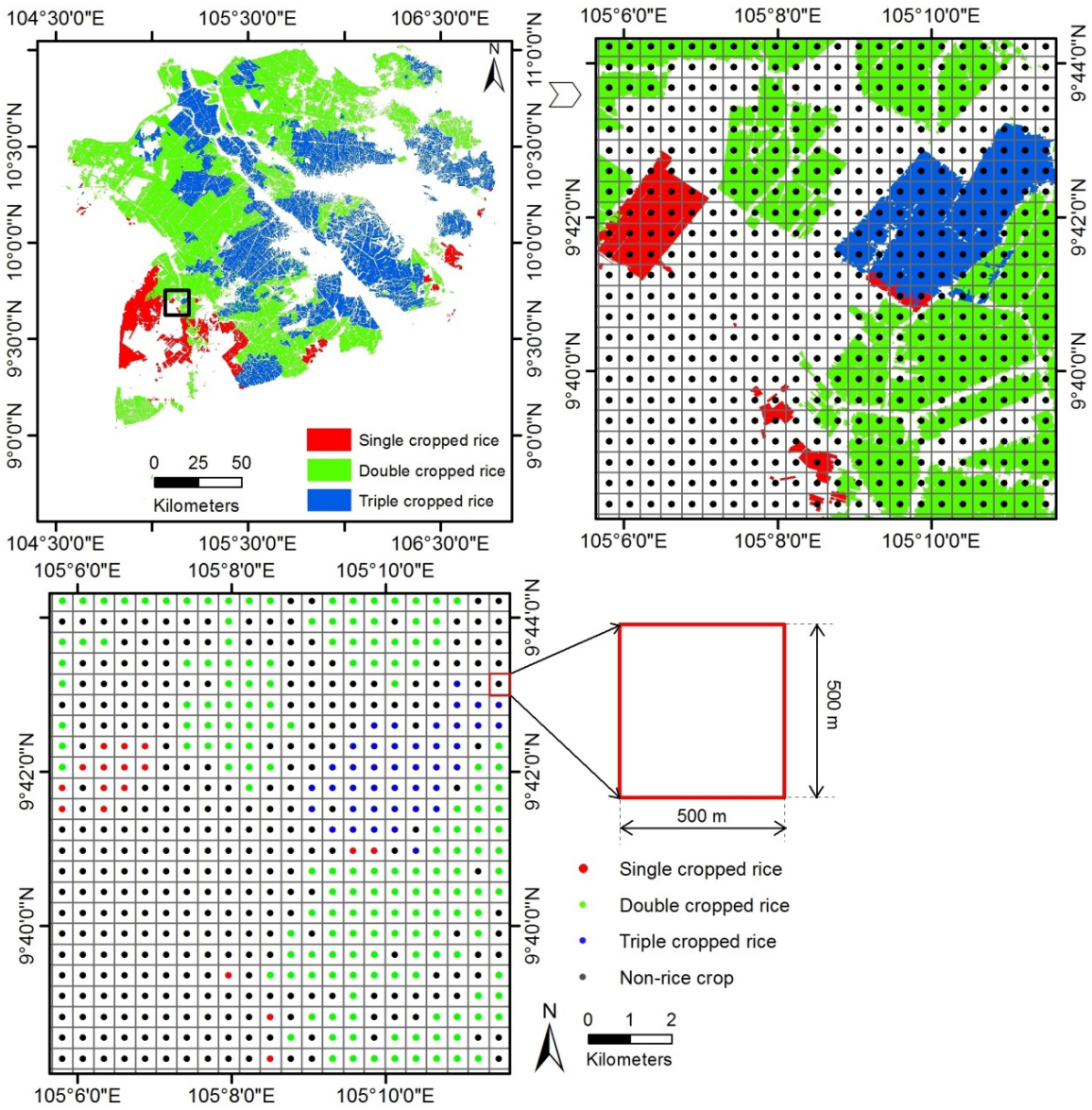

Figure 2.14. Sampling procedure with a regular 500 m grid from the 2010 land-use map.

Comparing the rice area from our classification with the rice acreage data (the mean values of the statistical yearly acreages over the 2007–2011 periods) provided by Vietnam's General Statistics Office yielded a correlation coefficient (R^2) of 0.98 with a root mean square error (RMSE) of 19,664 ha per province (Table 2.3).

Table 2.2. Confusion matrices of the accuracy assessment.

		Land use map 2005-2010 intersect					
	class	**SC**	**DC**	**TC**	**non-rice**	**total**	**user accuracy**
ASAR	**SC**	695	97	4	2561	3357	20.7%
	DC	20	21980	3544	2001	27545	79.8%
	TC	2	1290	12121	868	14281	84.9%
	non-rice	149	2905	3086	64474	70614	91.3%
	total	866	26272	18755	69904	115797	
	producer accuracy	80.3%	83.7%	64.6%	92.2%		
		Land use map 2010					
	class	**SC**	**DC**	**TC**	**non-rice**	**total**	**user accuracy**
ASAR	**SC**	2864	264	36	4371	7041	33.7%
	DC	252	30155	7261	6258	43926	68.7%
	TC	36	2643	15906	2972	21557	73.8%
	non-rice	934	6120	5558	75763	88735	85.7%
	total	3592	39182	28761	89364	160899	
	producer accuracy	66.0%	77.0%	55.3%	84.8%		
		Land use map 2005					
	class	**SC**	**DC**	**TC**	**non-rice**	**total**	**user accuracy**
ASAR	**SC**	1234	614	20	4199	6067	20.3%
	DC	234	29645	7639	6544	44062	67.3%
	TC	30	4213	14697	3346	22286	65.9%
	non-rice	714	10011	10712	68816	90253	76.3%
	total	2212	44483	28761	82905	162668	
	producer accuracy	55.9%	66.6%	44.4%	83.0%		

SC: Single-cropped rice; **DC**: Double-cropped rice; **TC**: Triple-cropped rice

2.6. Discussion

An annual SAR backscatter time series was reconstructed from Envisat ASAR data spanning five years with a novel method. The combination of acquisitions from multiple years was necessary since the inclusion of multiple tracks alone does not meet the temporal density required for reliable time-series analysis. Inclusion of scenes with partial coverage increased the temporal coverage with the drawback of unequal spatial distribution. This temporal and spatial heterogeneous dataset required a robust approach to combination and filtering in order to create a time-series representative for the study period. Homogenization of the ASAR wide swath acquisitions was executed by averaging the available data over the temporal

domain, where the averaged value is calculated from all available observations for each pixel over 7 (see Figure 2.4) and normalizing them to a common incidence angle. Incidence angle normalization was performed following an approach described by Pathe et al. (Wagner et al. 1999). In their study, the authors assumed that the influence of vegetation growth and seasonality on backscatter is smaller than that of soil moisture given that the linear model used to normalize the incidence angle is fitted to enough scenes. We transfer this approach to rice areas that are proven to have a high influence on backscatter. We postulate that the influence of rice growth on backscatter change in a time series is the main contributing factor; rice areas and growth seasons in the Mekong Delta are temporally stable enough to employ this normalization approach. Our results show that these assumptions have been correct and the incidence angle normalization can be used to combine multiple Envisat ASAR WSM tracks into a single time series. This novel approach allowed us to include a greater number of SAR scenes than any of the previous studies for the MKD.

Our algorithm produced a time series that represents the smoothed average of the SAR backscatter over five years, thus enabling us to evaluate the dominant rice-growing areas, cropping schemes and seasonality parameters for our study period. Any change in rice crop patterns and growing seasons happening in the 2007 to 2011 period is likely to be a source of error when we compare our classification to reference data representing a single year and we acknowledge that errors caused by dynamic shifts in rice-cropping patterns and seasonality will be present in our results. This is visible by comparing the users' accuracies for the 2010 and 2005 reference with the quasi stable areas of the 2005–2010 intersection. User accuracy compared to the 2005 land-use map is 66.6% for double rice but 83.7% when regarding areas that are double rice in the 2005–2010 intersection. For all classes, the user accuracy is higher when we compare our classification to the quasi stable areas of the 2005–2010 intersection reference. On the one hand, this highlights a limitation in our method which relies on temporal averaging and smoothing to create an ASAR time series. On the other hand, it also underlines the temporal dynamics in rice-cropping schemes and other land-cover changes in the MKD.

Table 2.3. Average planted area of rice by province (in ha) for all seasons in five-year period (2007–2011) from the statistical database and from the WSM data.

Province name	WSM data (× 103 ha)	Statistical Database (× 10^3 ha)	Δ (× 10^3 ha)	Δ^2 (× 10^6 ha)
LongAn	507.4	489.6	17.8	316.84
TienGiang	210.4	247.1	−36.7	1346.89
BenTre	68.2	81.5	−13.3	176.89
TraVinh	240.5	237.4	3.1	9.61
VinhLong	198.2	184.2	14.0	196.00
DongThap	538.0	468.5	35.4	1253.16
AnGiang	633.9	610.3	23.6	556.96
KienGiang	722.6	694.7	27.9	778.41
CanTho	233.3	228.1	5.2	27.04
HauGiang	210.0	214.0	−4.0	16.00
SocTrang	351.9	355.8	−3.9	15.21
BacLieu	187.9	171.2	16.7	278.89
CaMau	146.6	139.2	7.4	54.76

Most classification errors can be attributed to this dynamic but cannot be completely assessed due to the lack of a reference dataset covering the complete 2007 to 2011 period. We suspect that these dynamic changes are also one of the error sources contributing to the low producer accuracy of the single-cropped class compared to the 2005–2010 intersection. Single-cropped, rain-fed rice is increasingly diminished in favor of more profitable shrimp and fish farming (Jonsson and Eklundh 2002, Nguyen et al. 2012, Son et al. 2014) and could thusly be misclassified when such a change occurred during our study period. In addition, this cropping scheme is less widely distributed and spatially homogeneous than double or triple crop rice and might therefore be underrepresented in the 2005 land-use map which is based on moderate resolution data. Triple-cropped rice shows relatively low user accuracy compared to the 2005–2010 intersection. We suspect the error source for this in our time-series creation methodology. If an area is triple cropped throughout the study period but with slight shifts in heading and sowing dates, our temporal averaging and smoothing approach is unlikely to produce the discernible heading dates necessary for the decision-tree classifier to detect rice areas. We found good agreement in the spatial distribution of single,

double and triple rice-cropping schemes compared to previous studies in the Mekong Delta that reported cropping scheme maps with accuracies similar to our product (Xiao et al. 2006, Bouvet et al. 2009, Son et al. 2014, Jonsson and Eklundh 2002, Nguyen et al. 2012). The major driving force behind a farmer's choice of cropping scheme is the availability and management of water (Nguyen et al. 2012). The central parts of the delta are close to two large rivers and have a dense system of dykes and channels that allow flood management. Kuenzer et al. (Kuenzer et al. 2013) already pointed out that the level of flood management coincides highly with the employed rice-cropping scheme. This abundance of water combined with the ability to manage the flooding enables the cultivation of two or three rice crops per year. Son et al. (Son et al. 2014) found that triple cropping increased by about 12% at the expense of double cropping under irrigated conditions for the 2007 to 2011 period. The method we employed has limited ability to show these changes since it detects the dominant cropping scheme over the studied time period. We therefore have to assume that some classification errors in the central Mekong Delta between double- and triple-cropping occurred. These, however, do not influence the accuracy of total rice area, which has been reported as stable over time (Son et al. 2014). Moreover, the rice area of our product correlates highly with governmental statistics at the provincial level. Away from the rivers, the flooding is less managed and rice tends to be double cropped under rain-fed conditions. Triple cropping is not employed in these regions due to a lack of water during the dry season. Rain-fed single cropping is mostly practiced in coastal areas under less than ideal growing conditions induced by salinity intrusion. These areas experience a shift away from rice towards more profitable shrimp and combined rice and shrimp farming (Son et al. 2014) (Jonsson and Eklundh 2002, Nguyen et al. 2012). Our methodology is unsatisfactory in detecting changes in land cover and we can only report the dominant land cover. We therefore have to assume these changes to be a source of commission and omission errors between classes as well as between rice and non-rice areas.

Length of flooding influences whether double cropping is performed with two short or a short followed by a long season, visible from the length of the second

season in Figure 2.14. It is likely that the short-long double-cropping areas grow different rice varieties each year for the second season with different growth period lengths depending on water availability, pest control and market prices. In unfavorable conditions, farmers are more likely to plant resilient rice varieties with longer growing periods (Nguyen et al. 2012). These diverse cropping practices have likely been averaged out by our algorithm. Classification of growing season length and the respective start and end points is most accurate for areas with stable cropping practices and otherwise shows the average for 2007 through 2011. Triple cropping is executed with three short growing seasons in the Winter–Spring, Summer–Autumn and Autumn–Winter periods in order to manage three whole crops throughout a year. Our classification shows significant differences in the beginning of the first season for triple-cropped areas. This, to some extent, might be attributed to our algorithm. Depending on the heading date, either the Winter–Spring or Spring–Summer crop is detected as the first crop of the year. Nonetheless, this reveals that even under the same cropping scheme and comparable environmental conditions, a shift of more than a month for the heading dates is possible. This variation is also exhibited by single- and double-cropping rice areas, proving to be one of the major challenges of rice classification in MRD.

Mixed pixel effects caused by the spatial resolution of wide swath mode data are a source for commission errors. While single rice fields usually have a size of 1–2 ha they tend to be aggregated to larger rice area clusters in our study area. Fields inside these clusters are bound by small dykes, dams, roads, non-rice vegetation and other land cover smaller than the geometric resolution of our SAR data. Since these elements cannot be detected in ASAR images, they will lead to an overestimation of the total rice area by virtue of commission errors. A reverse effect of omission errors does not hold true since there are no small rice fields located inside larger areas of other land cover. This effect is likely to be small or cancelled out by omission or other error sources since the comparison of our estimated rice area with official statistics showed good correlation, albeit with a small overestimation of rice area.

2.7. Conclusions

Our study presents a novel approach to rice mapping by combining multi-year and multi-track SAR wide swath acquisitions into a normalized time series which can be used to observe the temporal backscatter dynamics over paddy rice fields. Effects of differing incidence angles and temporal density of acquisitions have been tackled by temporal averaging and incidence angle normalization based on statistical methods. Classification was performed with a rice crop phenology decision-tree classifier based on previous studies. This novel approach to combining Envisat ASAR WSM data led to a significant increase in temporal density by using all available observations compared to previous studies that employed narrow swath multi-polarization data or only detected the temporal change within single tracks.

We used the method to map rice areas and cropping schemes in the Mekong Delta for the 2005 to 2011 period based on all available ASAR WSM acquisitions. Compared to 2005 and 2010 land-use maps, we can report an overall accuracy of 85.3% with a kappa coefficient of 0.74. Our data is highly correlated with official rice area statistics (R^2 of 0.98). A disadvantage of our method is that no yearly rice maps of the Mekong Delta can be produced based on Envisat ASAR data which would allow the detection of dynamic changes in rice area and seasonality. This is less a limitation of the method, however, and more a reflection of a lack in the availability of suitable SAR data. Sentinel-1 has the ability to cover our study area with a repeat cycle of 12 days and could be used for timely rice mapping and seasonality detection in the Mekong Delta. Our method of backscatter time-series creation from multiple-tracks with incidence angle normalization to enhance temporal and spatial coverage should be transferable to Sentinel-1 data. We tested this approach in the Mekong Delta but it should be applicable to paddy rice areas worldwide demonstrating a distinct temporal backscatter change. Previous studies and theoretical models have shown that this holds true for all rice fields that are flooded before direct seeding or transplantation of rice seedlings.

CHAPTER 3

MAPPING RICE EXTENT AND CROPPING SCHEME IN THE MEKONG DELTA USING SENTINEL-1A DATA

Synthetic Aperture Radar (SAR)-based multi-temporal backscatter analysing is a common approach that has been widely used for rice mapping. Co-polarized C-band microwave backscatter (HH or VV) and the co-polarization ratio (HH/VV) are the most commonly used data sets for rice mapping due to their high data availability while the utilization of cross-polarized backscatter (HV or VH) has received less attention. In this study, Sentinel 1A time series - acquired in the dual-polarized (VV/VH) Interferometric Wide (IW) swath mode during the spring growing season (October, 2015 to March, 2016) in the Mekong Delta - were used to analyse the relationship between the growing cycle of rice plants and the temporal variation of SAR backscatter at different polarizations. Results show that VH backscatter is more sensitive to rice growth than VV backscatter. Several vegetation phenological parameters including beginning date, heading date and the length of the growing season were extracted from the VH backscatter time series. A decision tree approach was applied to delineate rice-cultivated areas based on seasonal phenological parameters. The classification result was validated against a 2015 land use map. The overall classification accuracy is 87.2% ($\kappa = 0.71$). In addition, the SAR-derived rice area was compared against ground statistical data at the provincial level ($R^2 = 0.98$).

3.1. Introduction

In 2015, Vietnam was the world's sixth-largest rice producer and the third-largest rice exporter (after Thailand and India) with the Mekong Delta being the main cultivation area. (Agriculture 2016). However, in recent years, rice production systems of the region have become increasingly threatened by the impact of climate change (Masutomi et al. 2009) and human activities (Santasombat 2015). Therefore, systematic rice crop mapping and monitoring in the Mekong Delta plays an important role for sustainable development, and economical and ecological planning. Traditionally, two main approaches are being used to generate rice cropland layers for these purposes: (1) through manual harmonization from cadastral maps, and (2) through manual digitization based on visual interpretation of high-resolution optical/near-infrared satellite images. However, these methods are very time-consuming and expensive especially since land use maps in this region shall be updated every 5 years.

Recently, Synthetic Aperture Radar (SAR)-based techniques have been recognized as very attractive alternative for mapping and monitoring rice crop dynamics due to the independency of radar signals to cloud coverage and illumination conditions. Moreover, SAR data availability has increased tremendously since the launch of Sentinel-1A on April 3rd 2014, which is the first operational SAR mission, operated within the European Commission's Copernicus program (Potin et al. 2012). It is designed for continuous near real-time (NRT) land monitoring, providing dual-polarized (VV/VH) SAR images over entire Europe (acquired in the Interferometric Wide swath (IW) mode) every four days and globally at least every 12 days. Furthermore, free, full and open data policy adopted by the Copernicus programme (Sentinel-1A is one of these data products) will make this valuable resource accessible to the broader science community, accelerating progress in geophysical research generally and paddy rice cropland mapping in particularly. These utilizing allow an efficient mapping and monitoring of rice crops over large areas at regular and frequent intervals.

Several researches have been carried out for mapping and monitoring rice areas using SAR backscatter (for a recent review see (Kuenzer and Knauer 2013, Mosleh

et al. 2015)). Among those studies, co-polarized (HH) backscatter and co-polarization ratio (HH/VV) images were the most commonly used data sets showing high correlations with the rice growing cycle (Bouvet et al. 2009, Lam-Dao 2009). The utilization of cross-polarized backscatter (HV or VH) has received less attention (Fan et al. 2011, Yang et al. 2012), likely due to the limited availability of such acquisitions. The potential of dense C-band SAR backscatter time series for mapping rice seasonality has been investigated by (Nguyen et al. 2015, Nguyen et al. 2015). The high temporal resolution of Sentinel-1 observations is expected to further improve the classification accuracy for such SAR-based multi-temporal rice crop monitoring methods. The goal of this study is to: (1) analyse temporal variations of backscatter and rice growth at different polarizations, and (2) classify rice field extents and crop growth seasonality in the Mekong Delta by based on Sentinel-1A data.

3.2. Data sets and study area

3.2.1. Study area

Study area is the Mekong Delta, which covers an area of about 40,000 km^2 between 8.5°–11.5°N and 104.5°–106.8°E containing 12 provinces and a city in southern Vietnam (Figure 3.1).

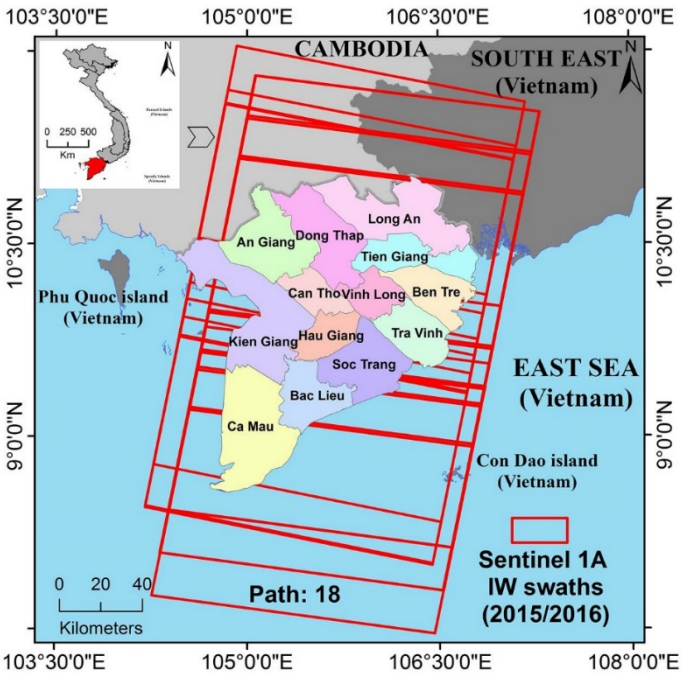

Figure 3.1. Study area and spatial extent of the used Sentinel-1A scenes.

Rice is grown in three distinct cropping seasons called "Đông-Xuân" ("Spring") from October/November to March/April, "Hè-Thu" ("Autumn") from March/April to August/September, "Thu-Đông" ("Winter") in inland areas from July/August to November/December and "Mùa" ("Main wet season") in coastal areas from June/July to January resulting in one to three rice harvests per year (Figure 3.2).

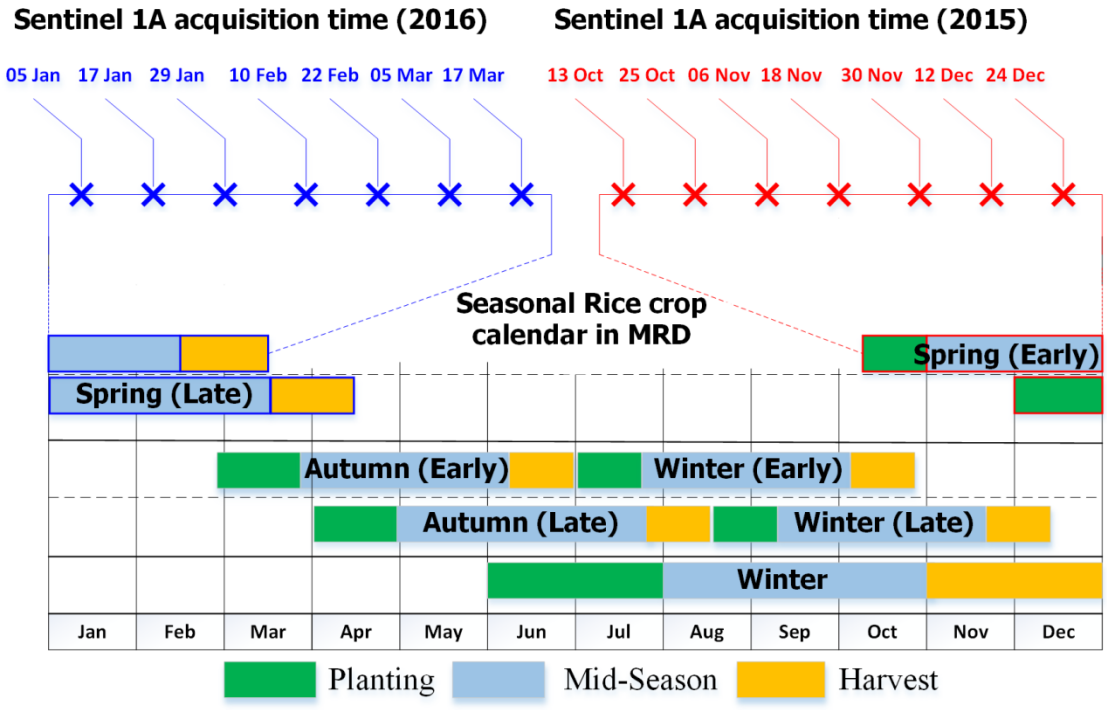

Figure 3.2. Sentinel-1A acquisition dates and seasonal rice crop calendar in the Mekong Delta (source: Ministry of Agricultural & Rural Development, Vietnam, 2015).

3.2.2. Sentinel-1A data

The Sentinel-1A IW Level 1 (L1) GRDH (ground-range detected, high resolution) product, was used in this study. Analysis are based on acquisitions during the "Spring" 2015/2016 season (from October, 2015 to March, 2016), which cover the entire Mekong Delta area (Figure 1 and Figure 2). L1 data was pre-processed using ESA's open source "Sentinel-1 Toolbox", including orbit correction, geocoding, radiometric calibration and resampling. The geocoding is based on Range Doppler Terrain Correction using the Shuttle Radar Topography Mission

(SRTM)-based 1 arc-second Digital Elevation Model (DEM) and Precise Orbit files (POD) provided by ESA from Array's servers (https://qc.sentinel1.eo.esa.int).

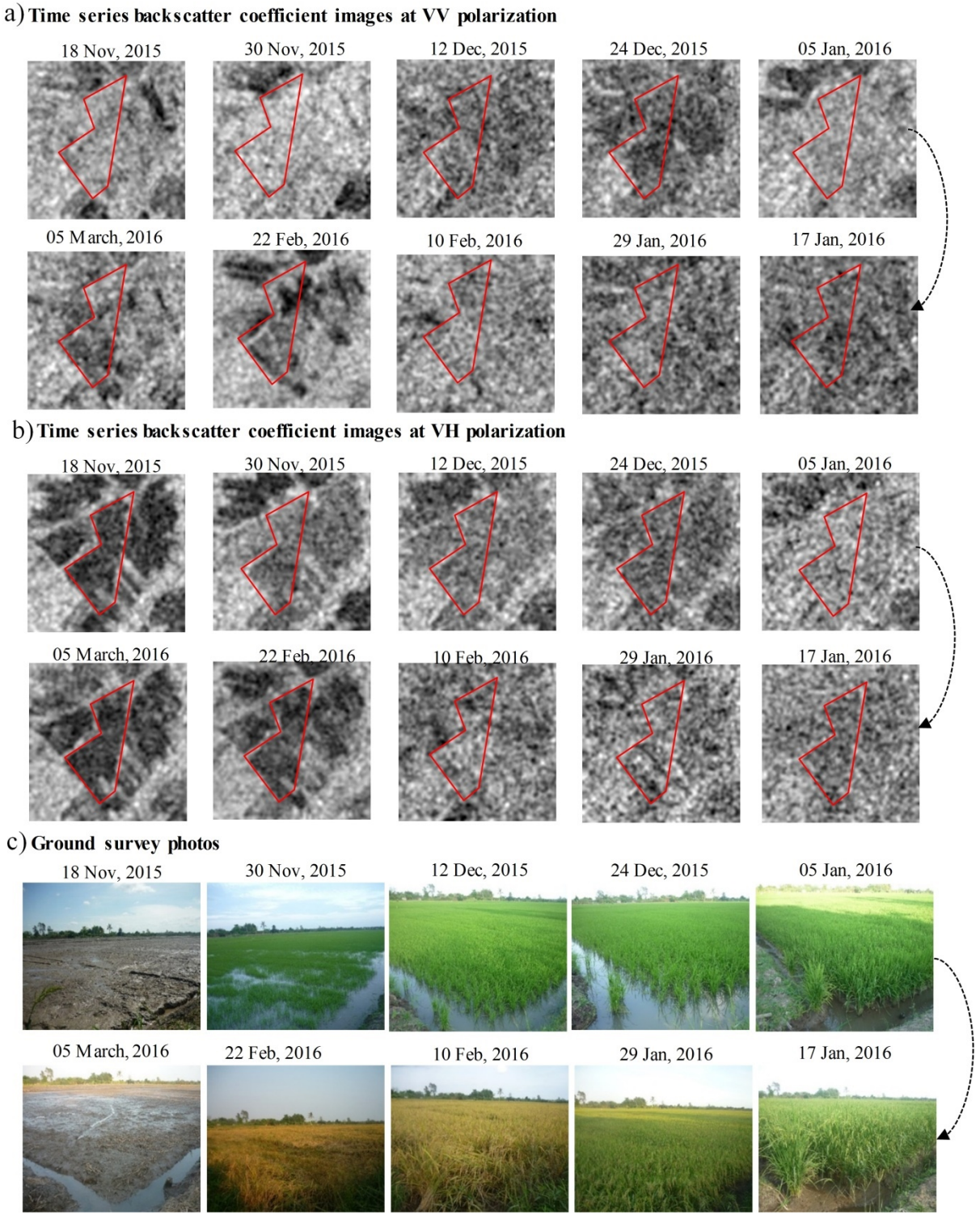

Figure 3.3. Backscatter images at VV (top) and VH (middle) polarizations, and survey photos (bottom) acquired at 10 different.

3.2.3. Reference data

Optical images were acquired during a field survey from November 18th 2015 to March 15th 2016 for monitoring different phenology stages and water coverage conditions within the rice growing season.

Four land use maps of the year 2015 for the administrative units at the provincial-level (An Giang, Can Tho) have been provided by the General Department of Land Administration of Vietnam. In addition, paddy rice cultivated area data for the study season were also provided by the Center for Informatics and Statistics (CIS) of the Ministry of Agriculture and Rural Development in Vietnam.

3.3. Data analysis

Multi-temporal backscatter observations at different polarizations have been analyzed to: (1) Investigate the backscattering characteristics of rice at different polarizations. (2) Derive rice phenological parameters including the Date of the Start of season (DoS), the Date of Maximum backscatter (DoM), and the Length of Season (LoS). (3) Delineate rice cultivated areas.

3.3.1. Polarization analysis

VV and VH polarized backscattering time series over selected rice fields are shown in Figure 3.3 together with optical ground images. After sowing (November 18th 2015) one can see, as expected from bare soil surfaces, much lower backscattering at VH polarization than at VV polarization.

The temporal evolution of the VV and VH backscattering coefficients is shown in Figure 3.4. Backscatter at VV polarization is generally larger than at VH polarization and the backscattering coefficients at both polarizations gradually increase during the growing period until the end of the reproductive state at February 10th, followed by a backscattering decrease in the maturation state. VV polarized backscatter reaches a maximum on December 12th (approximately 30 days after sowing) with a strong subsequent depression on January 5th, whereas VH polarized backscatter reaches its maximum on January 17th (approximately 70 days after sowing) without such distinct depression. As rice plant height increases, the observed response is stronger for vertical than for horizontal polarization, due

to longer propagation paths inside the vegetation volume and According to the ground surveying photos there was no longer standing water in the field from January 5th onwards, and this is the mechanism driving the depression in VV backscatter due to the lack of double-bounce backscattering effects. According to the figure 4, the monotonic rice growth cycle is better represented in the VH backscatter time series than in the VV time series. In particular, the presence of the local maximum on Dec 12th and the depression on Jan 5th would not allow for a derivation of the pheneological parameters (see in Sec. 3.2). We therefore conclude that the cross-polarized VH signal seems to be better suited for studying rice growth than the co-polarized VV signal.

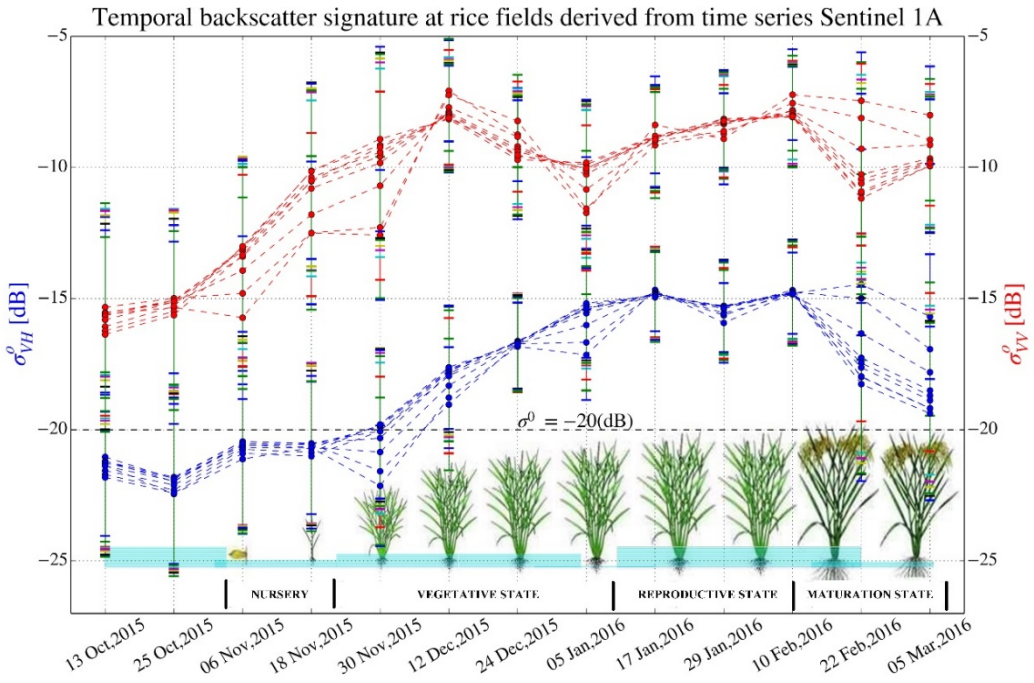

Figure 3.4. Temporal evolution of the VV and VH polarized backscatter over selected rice fields.

3.3.2. Derivation of rice phenological parameters

Following results were obtained from analyzing temporal variation of backscatter and rice growth in the previous section, first order statistics parameters derived from time series VH polarization backscatter data were computed, including the dynamic range, the mean and the standard deviation, of the time series (Figure 3.5).

In a first step, potential rice pixels were selected based on a threshold for the dynamic range of the backscatter (i.e., the threshold above 8.5 dB based on experiment data analysis was performed). The potential rice pixels were denoted $\sigma^o_{VH_{potential}}$. A Gaussian filter was then applied to the time series at the selected pixels. For the remainder of the paper, the resulting smoothed backscatter will be denoted as $\sigma^o_{VH_{potential\_smoothed}}$. Subsequently, rice phenological parameters were defined as follows (Jonsson and Eklundh 2002) and these parameters were derived from $\sigma^o_{VH_{potential\_smoothed}}$ pixel only:

- Date of the Start of season (DoS): The point in $\sigma^o_{VH_{potential\_smoothed}}$ where the second derivative changes from zero or negative to positive.
- Date of Maximum backscatter (DoM): The point where $\sigma^o_{VH_{potential\_smoothed}}$ reaches its maximum
- Length of Season (LoS): The difference between DoM and DoS.

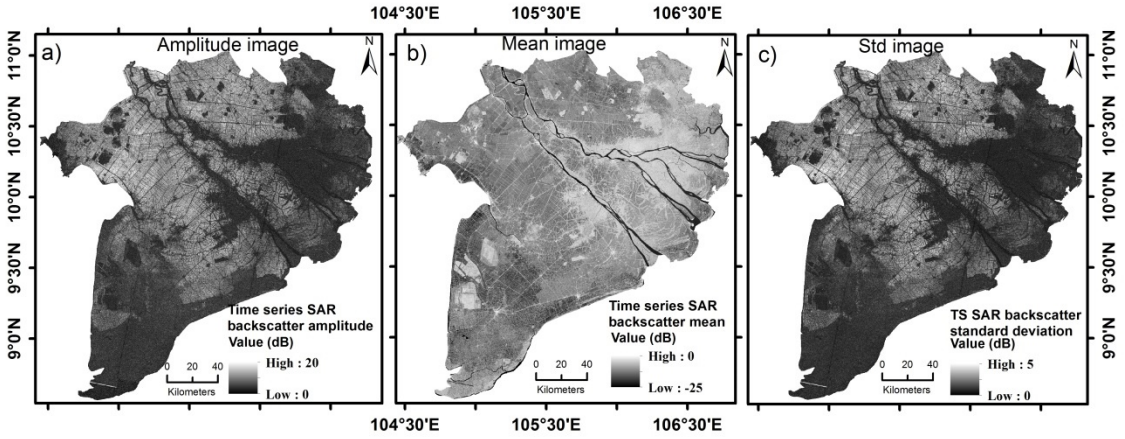

Figure 3.5. Backscatter amplitude (a), mean backscatter (b), and backscatter standard deviation (c) of the Sentinel-1A acquisitions from October 23rd, 2015 to March 17th, 2016.

3.3.3. Delineation of rice cultivation area

A decision tree approach was used to classify rice cultivated areas (Nguyen et al. 2015). In order to distinguish rice from other land cover classes, three static thresholds for $\sigma^o_{VH_{potential_smoothed}}$were empirically derived from the time series as: (1) –larger than 20 dB for the local maxima, (2) larger than 2.5 dB for the

minimum amplitude of the backscatter (i.e., the difference between the local minimum and maximum), and (3) larger than or equal 50 days for the LoS, which represents the shortest possible rice growing cycle (Figure 3.6). If all three conditions are met then the pixel is classified as rice.

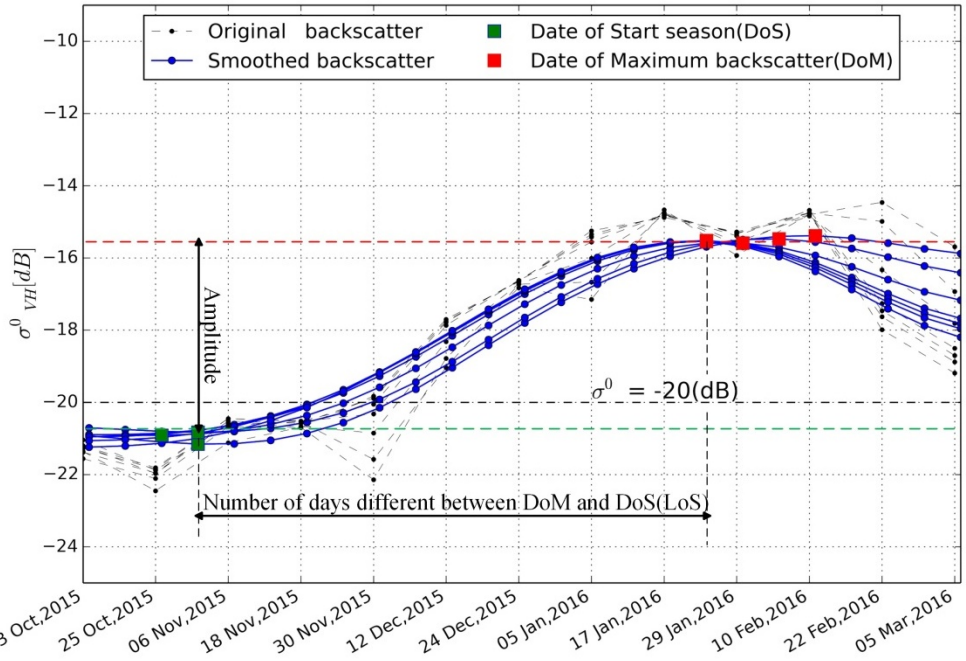

Figure 3.6. Empirical threshold derivation for rice classification.

3.4. Results and discussion

A map of the rice cultivated area within the Mekong Delta, delineated using Sentinel-1A VH data of the spring season 2015/2016, is shown in Figure 3.7d. We found good agreement in the spatial distribution of rice crop extent in the upstream and central parts of the delta when compared to the rice cropland layer from the reference land use map. In these parts of the delta, rice cultivation takes place mainly in areas close to the Bassac River which have dense irrigation networks. Away from the rivers, scattered and small rice fields were observed in the northern parts and coastal areas where rain-fed rice is mostly grown under less optimal growing conditions induced by salinity intrusion. In addition, a strong El Niño event has suppressed rainfall over south-eastern Asia during 2015 and early 2016, resulting in very low water availability for a long period of time, to that effect, very low amounts of water in a long period of time in the rice fields have

been observed. Moreover, a 12-day revisit time of Sentinel 1A property lead to lack of observations at the flood stage of rice fields which might lead to an increased uncertainty in the delineation of rice cultivated areas. These issues might be considered as a source of omission errors, which is especially visible in the southern and eastern parts of the Kien Giang, Soc Trang, and Long An provinces (Figure 3.8).

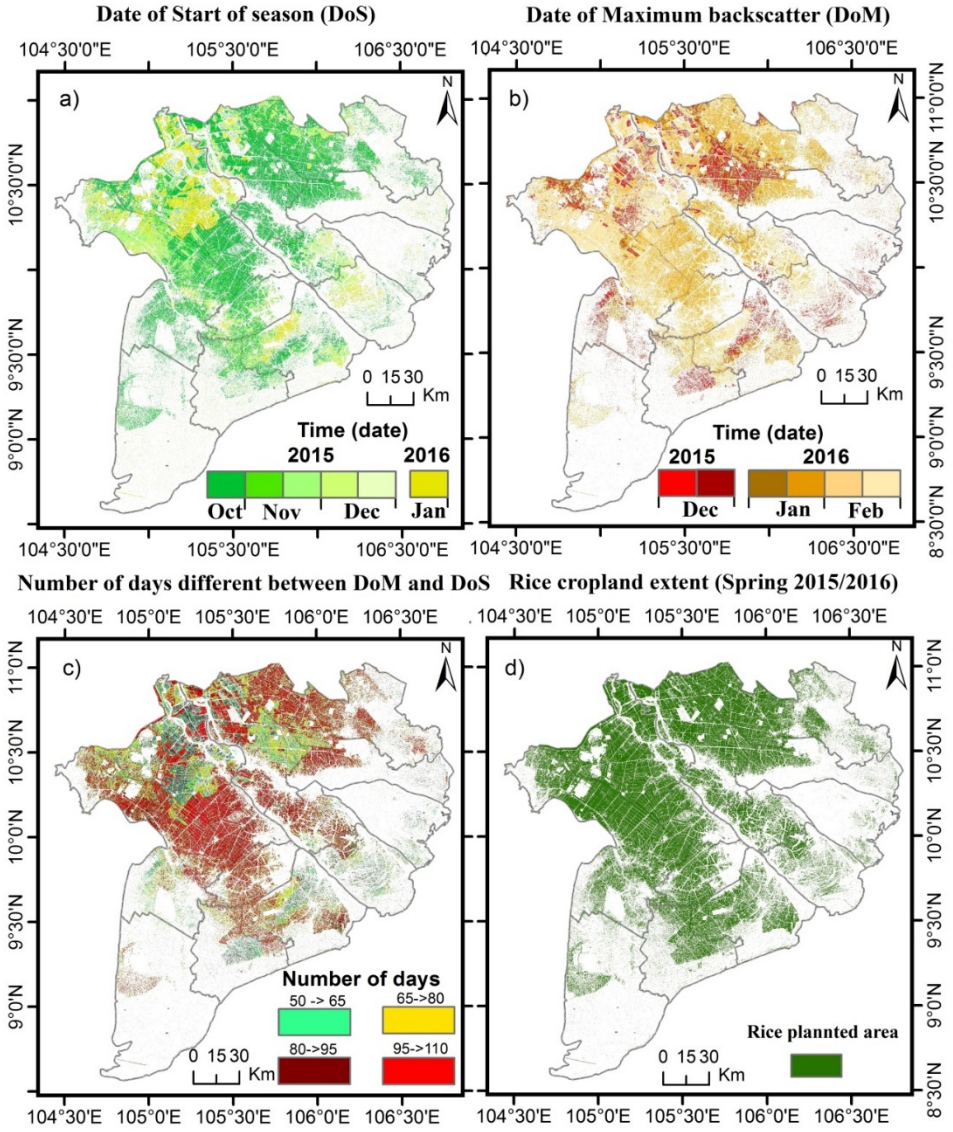

Figure 3.7. Rice phenological parameters in the Mekong Delta region derived from Sentinel 1A VH time series during the Spring 2015/2016 season.

The classification accuracy has been assessed relative to the 2015 land use map. The therefore generated confusion matrix is presented in Table 3.1. The overall

classification accuracy is 87.2% (κ = 0.71). Mixed pixel effects including the contribution of small dykes, dams, roads, non-rice vegetation and other land cover features within the Sentinel-1A footprints might be one source for commission errors. In addition, a lack of SAR acquisitions or drought events during flooded stages might also cause rice-covered areas not to be captured as such. Figure 8 further shows the areal rice cultivation extent obtained from the reference statistics compared to the cultivated area retrieved from the Sentinel-1A acquisitions for all provinces. One can see that the estimation accuracy in coastal provinces is significantly worse than in inland provinces. This further confirms that flooded conditions are the most important factor when trying to distinguish between rice- and non-rice fields.

Table 3.1. Confusion matrix for the rice classification.

		Land use map 2015			
		Non-rice	Rice	total	user accuracy
Sentinel-1A based	Non-Rice	40443	11445	51888	77.9%
	Rice	8939	98016	106955	91.6%
	total	49382	109461	158843	
	producer accuracy	81.9%	89.5%		

The derived plant phenological parameters for the delineated rice cultivated areas are shown in Figure 3.7. Most regions start the cultivation of rice (DoS) around October/November (Early Spring season) or December/January (Late Spring season) (Figure 3.7a). The DoS depends mainly on water availability. In the coastal regions, a very large number of rice pixels have been omitted because there were no SAR-observations available during the flooded period (Figure 7a). The DoM typically reaches from December, 2015 to January/February, 2016 (Figure 3.7b) and the LoS ranges from 50 to 110 days (Figure 3.7c). These results are in good agreement with the crop calendar presented in Figure 3.2.

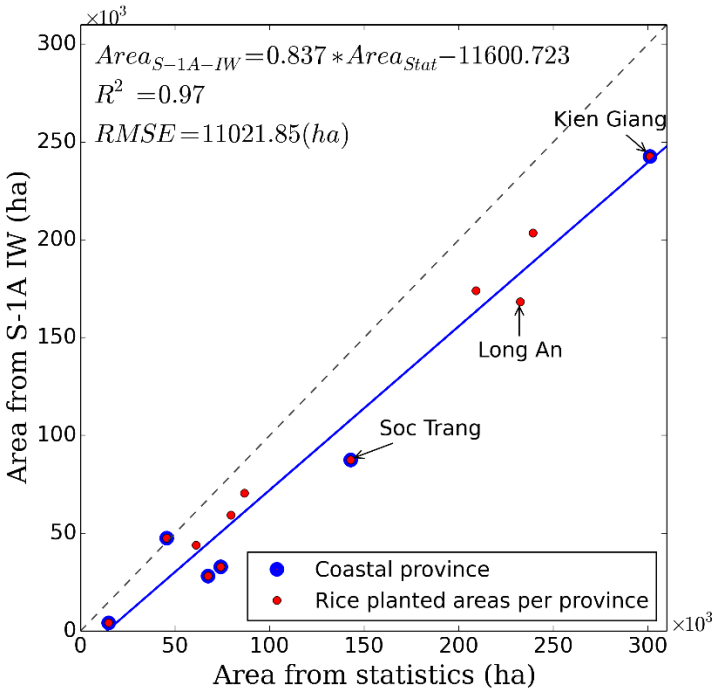

Figure 3.8. Retrieved rice cultivated areas per province (in ha) for Spring 2015/2016 season vs. statistical rice cultivated areas. The blue line represents the linear regression between the two datasets.

3.5. Conclusion

This study demonstrates the potential of Sentinel-1A VH imagery for mapping regional rice cultivation extent and rice phenological parameters. VH polarized backscatter has been shown to be more sensitive to rice growing behaviour than VV polarized backscatter.

A decision tree approach has been used to map rice cultivated areas in the Mekong Delta region during the 2015/2016 Spring season with a classification accuracy of 85.3% (with respect to a reference land use map) and a kappa coefficient of κ = 0.74. The estimated extent of the delineated rice cultivated areas is well correlated with official rice area statistics (R^2 = 0.98). Finally, flooded events were shown to be the most important feature to distinguish between rice- and non-rice fields. This study is, to our best knowledge, the first Sentinel-1A based analysis for mapping rice cultivated area and for estimating rice phenological parameters at a regional scale.

CHAPTER 4

EUROPEAN RICE CROPLAND MAPPING WITH SENTINEL-1A DATA: THE MEDITERRANEAN REGION

Rice farming is one of the most important activities in the agriculture sector, producing staple food for the majority of the world's growing population. Accurate and up-to-date assessment of the spatial distribution of rice cultivated area is a key information requirement of all stakeholders including policy makers, rice farmers and consumers. Timely assessment with high precision is e.g. crucial for water resource management, market prices control and during humanitarian food crisis. Recently, two Sentinel-1 (S-1) satellites carrying a C-band Synthetic Aperture Radar (SAR) sensor were launched by the European Space Agency (ESA) within the homework of the Copernicus program. The advanced data acquisition capabilities of S-1 provide a unique opportunity to monitor different land cover types at high spatial (20 m) and temporal (twice-weekly to biweekly) resolution. The objective of this research is to evaluate the applicability of an existing phenology-based classification method for continental-scale rice cropland mapping using S-1 backscatter time series. In this study, the S-1 images were collected during the rice growing season of 2015 covering eight selected European test sites situated in six Mediterranean countries. Due to the better rice classification capabilities of SAR cross-polarized measurement as compared to co-polarized data, S-1 cross-polarized (VH) data were used. Phenological parameters derived from the S-1 VH backscatter time series were used as an input to a knowledge-based decision-rule classifier in order to classify the input data into rice and non-rice areas. The classification results were evaluated using multiple regions of interest (ROIs) drawn from high-resolution optical remote sensing (SPOT 5) data and the European CORINE land cover (CLC 2012) product. An overall accuracy exceeds 70% for all eight study sites was achieved. The S-1 based classification maps reveal much more details compared to the rice field class contained in the CLC 2012 product. These findings demonstrate the potential and feasibility of using S-1 VH

data to develop an operational rice crop monitoring framework at continental scale.

4.1. Introduction

Europe is the fourth largest importer of rice in the world (Figure 4.1a). Over the last five years, Europe's annual rice imports were on average about 1000 million tons (milled basis), ranging between 873 million tons in 2011 to 1190 million tons in 2015 (FAO 2015). Meanwhile, the size of rice cultivated areas has either reduced or remained stable around 420,000 hectares (Figure 4.1b). Information about how the area of rice croplands varies from year to year is an important piece of information for the European economy being relevant for: risk management for the insurance industry (van der Sandeg et al. 2003), environmental reporting, contributions to greenhouse gases (Koellner and Scholz 2006), life cycle inventory (Roy et al. 2009, Koellner, Baan et al. 2012), life cycle assessment (Blengini and Busto 2009, Roy et al. 2009), water cycle analysis (Weng et al. 2007), crop forecasting (Genovese et al. 2001), and others.

According to the FAO Technical Guidelines, the standard procedure to derive rice cropland layers is to manually digitize optical (near-infrared) satellite imagery (EEA 2007, EEA 2012). This process provides a data product with an internal and external quality assurance. However, the process is time-consuming, expensive, labor-intensive and best suited for small scale applications, whereas over large regions classification results may not always be directly comparable because the results achieved by different experts may differ. One rice cropland layer produced in this way is part of the CORINE land cover (CLC) product that has a resolution of 100 meters and will be updated after every 4~6 years. This does not meet the requirements of many users who prefer having annual rice cropland maps with higher spatial resolution (e.g., 20 meters).

Day-night and weather independent data acquisition capabilities of SAR sensors have made them attractive for monitoring land surface dynamics. With the launch of Sentinel-1A/B (a C-band space-borne SAR sensor), data with much improved spatio-temporal sampling characterizations have become available (over Europe 20m spatial resolution images are acquired every three days). Furthermore, the

free and open data policy adopted by the Copernicus programme will make the data accessible to a large user community, and will help accelerating the progress in geophysical research in general and paddy rice cropland mapping in specific.

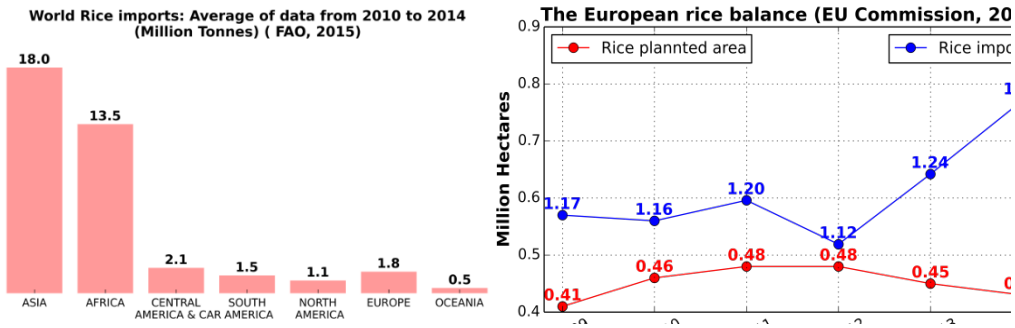

(a) (b)

Figure 4.1. (a) Global rice imports - average of data for 2010 to 2014 (FAO, 2015); (b) the EU rice balance for 2008 to 2013 (Europe Commission, 2015).

There is a long history of rice cropland area mapping with SAR sensor imagery (Kurosu et al. 1995, Le Toan, Ribbes et al. 1997, Bouvet et al. 2009, Bouvet and Le Toan 2011, Nguyen et al. 2015). Multi-temporal SAR data can be used to retrieve the rice growing cycle based on the temporal variations in the SAR backscatter (σ°[dB]) signal (Kurosu et al. 1995, Choudhury and Chakraborty 2006, Nguyen et al. 2015). The annual variation in σ°[dB] from rice fields is higher than any other agricultural crop (Toan et al. 1997). In this particular application domain, a substantial number of studies have already been reported in the literature. Most of them used medium resolution SAR data over test sites mostly located in India (Panigrahy et al. 1999), Bangladesh (Panigrahy et al. 2012), Thailand (Kaojarern et al. 2002), China (Li et al. 2005, Chen et al. 2007, Yu et al. 2010), Vietnam (Liew et al. 1998, Bouvet et al. 2009, Bouvet and Le Toan 2011, Nguyen et al. 2015) and also a few in Europe (Özküralpli and Sunar 2007, Lopez-Sanchez et al. 2011). High spatial resolution SAR data (≤ 20m) have been investigated over a fewer study sites because of the difficulty of collecting dense and long-enough image time series (Rosenqvist 1999, Chakraborty and Panigrahy 2000, Tan et al. 2004, Zhang et al. 2009).

Time series analysis of SAR backscatter values is the most common data analysis approach used for paddy rice identification. Both single and multi-polarization SAR data have been used for rice monitoring and the discrimination of different growth stages (Bouvet et al. 2009, Lam-Dao 2009). In this approach, C-band SAR sensor have been the most attractive data source for rice mapping at regional or continental scale because data from other SAR sensors is hampered either by limited spatial coverage (e.g., TerraSAR-X) or longer revisit time (e.g., ALOS PALSAR).

Several investigations (Bouvet et al. 2009, Lam-Dao 2009) demonstrated that the C-band like-polarized ratio (HH/VV) is a useful parameter for mapping and monitoring rice cropland. Wu et al. (2011) reported that the HH/VV ratio was best for discriminating rice from bananas, forest, and water (Fan et al. 2011). However, Schmitt and Brisco (2013) reported that the HH/VV combination produced a significantly lower accuracy than the combination of HH/HV and VV/VH (Schmitt and Brisco 2013). The backscatter coefficients of cross-polarized data have a significant correlation with the development of rice plants (Fan et al. 2011, Yang et al. 2012). Schmitt and Brisco (2013) also found that the cross-polarized data gave the best relationship with rice age after transplantation. Due to the improved spatio-temporal resolution and ability to acquire data in different polarizations (VV, VH), S-1 is expected to improve the accuracy of rice cropland monitoring and mapping applications.

Literature review suggests that most of the studies have been limited to map paddy rice from C-band SAR data either by using single polarization (HH) or a combination of different polarizations (HH/VV, HH/HV or VV/VH). However, only a few of them have investigated dense VH backscatter time series in order to have a better understanding of the SAR response to growth stages of the rice fields. Furthermore, to our knowledge, no work using real S-1 data for paddy rice mapping in the Mediterranean region has been published yet.

The goal of this research is to evaluate the potential and transferability of a phenology-based classification strategy developed by Nguyen et al. (2016) (Nguyen et al. 2016) over a regional test site in the Mekong delta to a continental

scale (Mediterranean region). To achieve this objective we used a dense time series stack of S-1 backscatter data as input to map rice paddy area at fine spatial scale over eight study sites in six European countries.

4.2. Study area and Materials

4.2.1. Study sites characteristics

In the European Union (EU) the total area of cultivated rice is about 430,000 hectares. The growing areas are mostly located in the Mediterranean countries (FAO 2015) (Figure 4.2), where the summer seasons are warm and dry.

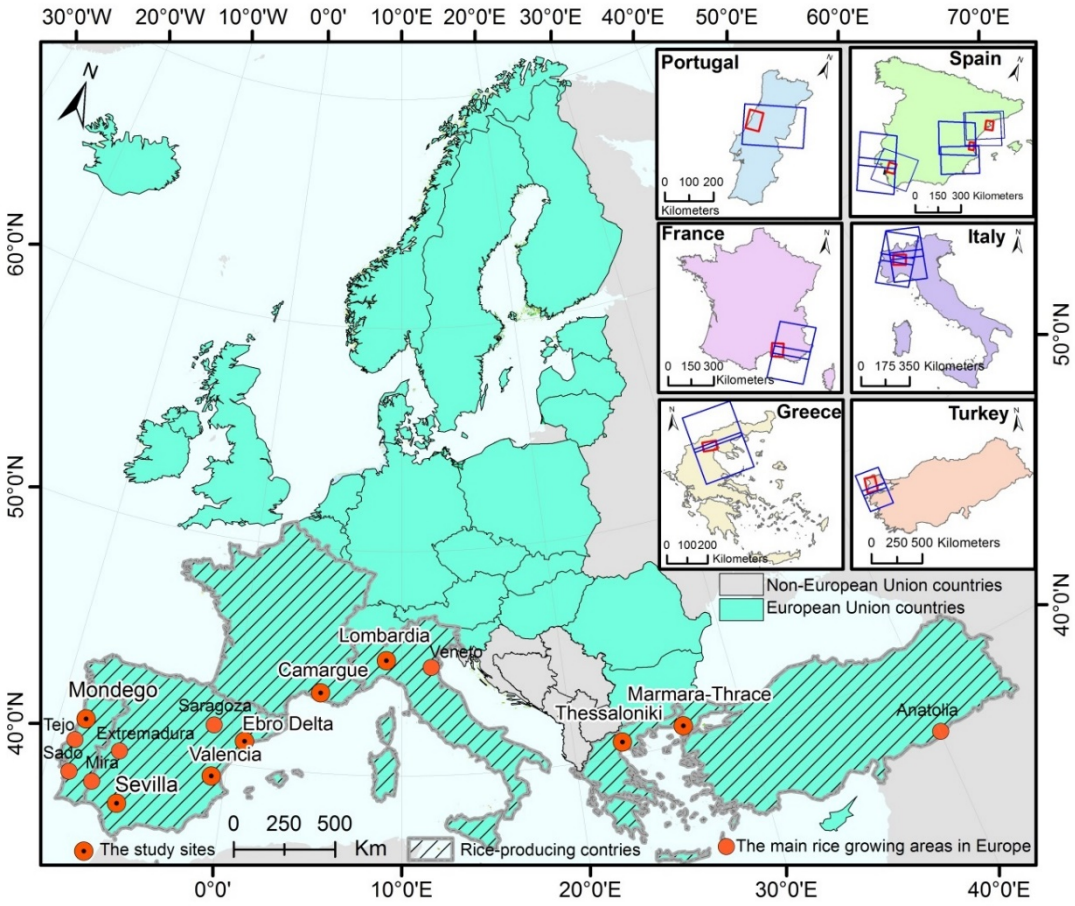

Figure 4.2. Study sites (red) and spatial extent of the used S-1 scenes (blue).

The normal growing season is either from April/May to September/October or from May to October/November depending on the temperature. Italy and Spain are the top rice producer EU member countries followed by Greece, Portugal and France (European Commission 2015).

Rice varieties grown in Europe mostly belong to the Japonica (70%) and Indica (30%) species group. The recent evolution of Japonica and Indica areas (in hectares) in the EU member States is shown in Figure 4.3. Rice is mostly grown in congregated areas such as in the Po valley in Italy, the Rhône delta in France, and the Thessaloniki area in Greece. In Spain, rice cultivation is more scattered; rice growing areas are found in the Aragon region, the Guadalquivir valley, the Ebro delta and Valencia Albufera (Ferrero and Tinarelli 2007). In Portugal, rice cultivation area is concentrated mainly in three regions: the Tagus and Sorraia valleys, the Mondego, and the Sado and Caia river valleys (Calha et al. 1999, Silva et al. 2006). In Turkey, the most productive regions are Thrace and Marmara, which are producing 10-15 percent of the total national rice production.

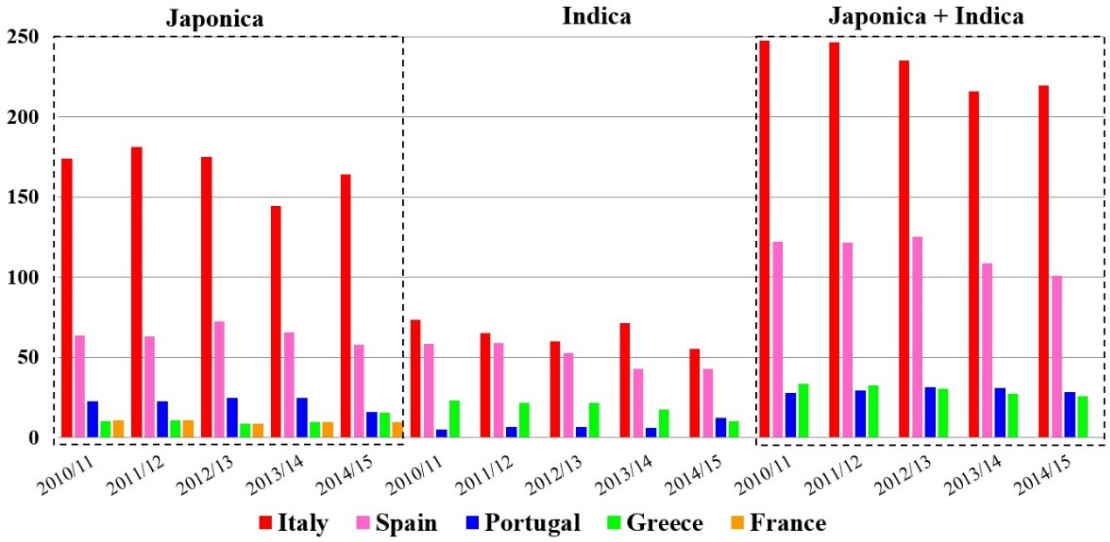

Figure 4.3. Rice varieties areas in the EU member states (European Commission 2015).

Rice planting in Europe involves direct seeding into flooded soil (water seeding) or dry soil (dry seeding). With both the farming methods, the floodwater is maintained until the harvest season. Water is drained several times from the field prior to harvesting so that the fields can be dried and harvesting equipment can pass through. Fields are also drained for early foliar herbicide treatments, then re-flooded within few days. The drainage period allows certain weed species to germinate in the aerobic environment (Figure 4.4).

4.2.2. Materials

4.2.2.1. Sentinel 1A data

For this study, we accessed archived Interferometric Wide Swath (IW) mode S-1 data acquired during the rice crop growing cycle in 2015, from April to early November to completely cover every test site. The S-1A SAR IW mode acquisitions come from eight different tracks, whereas each test site is covered by the same track (Figure 4.2). The details for each test site regarding data acquisition, location, date, path and range of incidence angle are shown in Figure 4.4. All the images were obtained from ESA as standard Level 1 GRD (ground-range detected) high resolution images. Only the S-1 IW acquisitions with VH polarization were selected for rice cropland classification.

2.2.2. Optical data and Ancillary data

For the study sites in France, and Italy, multi-temporal Spot 5 (10m spatial resolution) for the year 2015 were downloaded from the SPOT website (https://spot-take5.org/client/#/products/SPOT5). These optical datasets were used to produce reference classification maps for validating the S-1 rice maps. Rice cropland area—a vector dataset with a minimum mapping unit (MMU) of 1 hectare—over Seville in Spain for the year 2015 has been obtained from the Institute of Statistics and Cartography of Andalusia's website http://www.juntadeandalucia.es/institutodeestadisticaycartografia/sima/htm/sm41902.htm. Two others vector dataset of rice cropland area—over Valencia in Spain and Marmma- Thrace in Greece for the year 2015 were retrieved from the ERMES (An Earth Observation Model Based Rice Information Service)'s website http://ermes.dlsi.uji.es/prototype/geoportal/index.html. Google Earth imagery and Sentinel-2 (https://s2maps.eu) optical data were used to produce reference data for the rest of study areas. In addition to this, the European CORINE land cover (CLC 2012) product was also used for comparing classification results across all European test sites in a consistent manner. The data set is not as detailed and accurate as the other two datasets. However, it is the only available reference datasets covering all our study regions. Figure 4.5 shows the land cover composition over the eight selected test sites in 2012. Rice cropland is the most

common land cover in Lombardia, Italy with 33.6%, followed in Ebro, Spain (18.8%) in Valencia, Spain (12.4%), and only 2.3% of rice cropland in Mondego, Portugal. Inland water makes up over 10% of the total land covers in Camargue, France and below 1.5% for the others. It is the same for wetland class, e.g. 7% in Camargue, France and below 2% for the others.

	APR	MAY	JUN	JUL	AUG	SEP	OCT	NOV	Pass	LIA (degree)
Valencia (SPAIN)	10 22	04 16 28	09	03 15 27	08 20	01 13 25	07 31	12	Descending	45.5 -> 46.5
	11 23	05 17 29	10	04 16 28	09 21	02 14 26	08	01 13	Ascending	43.5 -> 44.5
Seville (SPAIN)	01 13	07 19 31	12 24	06 30	11 23	16 28	10 22	15	Descending	43.5 -> 44.5
	02 26	08 20	01 13 25	07 19 31	12 24	17 29	11 23	16	Ascending	43.5 -> 44.5
Ebro delta (SPAIN)	01 13	07 19 31	12 24	06 30	11 23	16 28	10 22	15	Descending	39.5 -> 40.5
	02 26	08 20	01 13 25	07 19 31	12 24	17 29	11 23	16	Ascending	40.5 -> 41.5
Camargue (FRANCE)	01 13 25	07 31	12 24	06 18 30	11 23	04 16 28	10	03	Descending	43 -> 45
Lombardia (ITALY)	04 16 28	10 22	03 15 27	09 21	02 14 26	07 19	01 13 25	06	Ascending	33 -> 45
Thessaloniki (GREECE)	10 22	04 16 28	09 21	03 15 27	08 20	01 13 25	07 31	12	Ascending	36 -> 46
Marmma-Thrace (TURKEY)	06 18 30	05 17 29	10 22	16 28		02 14 26	08	02 14	Ascending	33.5 -> 36.5
Mondego (PORTUGAL)	18 30	12 24	05 17	11 23	04 16	09 21	15 27		Ascending	35 -> 37
JULIAN DAY	91 -> 120	121 -> 151	152 -> 180	181 -> 211	212 -> 242	243 - > 272	273 -> 303	304-> 334		

Planting Mid-Season Harvest L1 GRD-HD data available LIA: Local Incidence Angle

Figure 4.4. Growing season of paddy rice crop and the available S-1A SAR scenes over eight selected test sites.

4.3. Methodology

The time series algorithm used in this study was introduced by Nguyen et al. (Nguyen et al. 2016). It consists of six steps as illustrated in Figure 4.6: (1) S-1A pre-processing, (2) segmentation (image thresholding) to extract the potential rice areas (σ° → σ°potential), (3) time-series smoothing with a Gaussian moving window filter (σ°potential → σ°potential_smooth), (4) vegetation phenology

parameters extraction (σ°potential_smooth → DoS (Date of Start Season), DoM (Date of Maximum backscatter), LoS (Length of Season)), (5) classification using a knowledge-based decision-tree approach, and (6) accuracy assessment based on reference data.

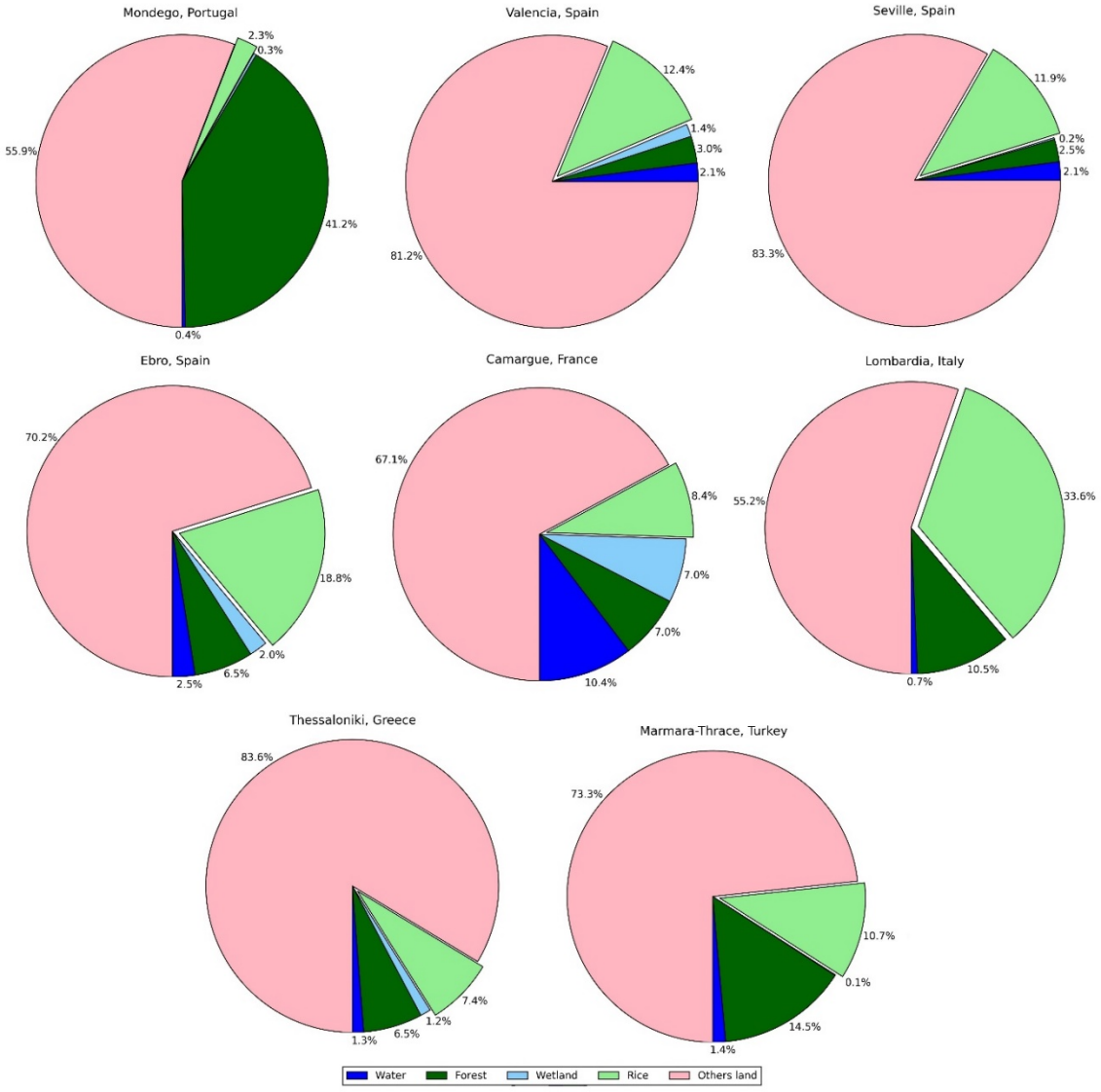

Figure 4.5. Relative contribution of harmonized of land-cover categories in eight selected test sites.

4.3.1. Pre-processing

All the selected S-1 SAR IW images were pre-processed (orbit correction, radiometric calibration, resampling and geocoding) using ESA's Sentinel-1 Toolbox. The geocoding step involved a Range Doppler Terrain correction

algorithm that uses the elevation data from the 1 arc-second DEM product from the Shuttle Radar Topography Mission (SRTM) and POD orbit state vectors provided by ESA. Notice that precise orbits files (POD) are produced few weeks after the acquisition and they are automatically downloaded from https://qc.sentinel1.eo.esa.int. In this process, data are resampled and geo-coded to a grid of 10m spacing preserving the 20m spatial resolution.

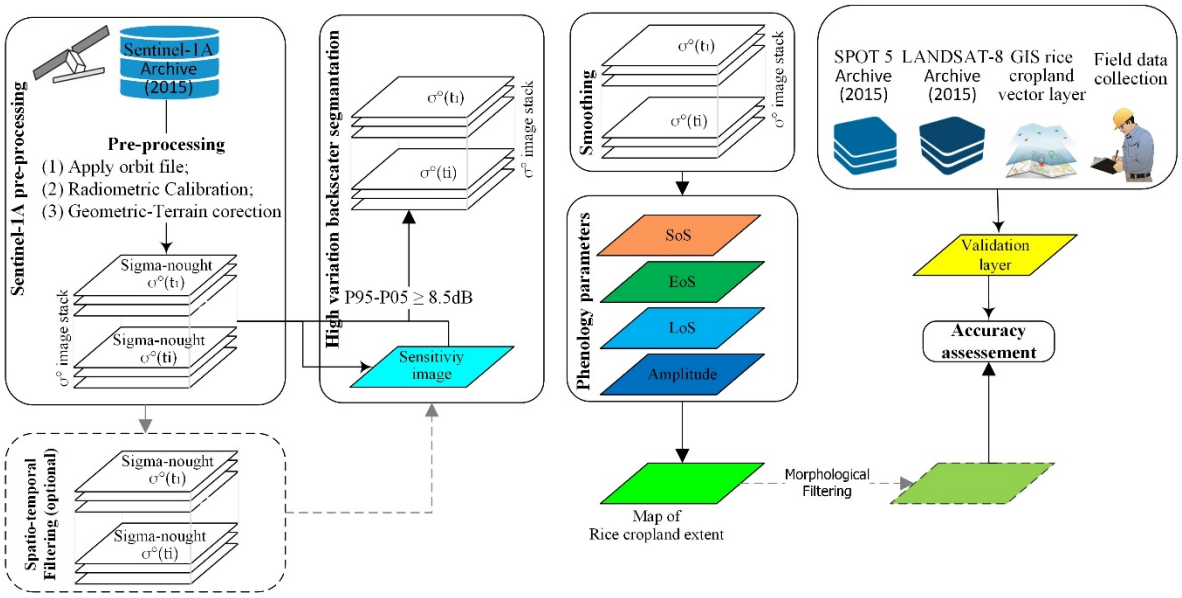

Figure 4.6. Systematic workflow of S-1 SAR (VH polarization) data processing, rice area classification and validation.

4.3.2. Identification of potential rice pixels

For the identification of potential rice growing areas, our approach is to threshold the dynamic range backscatter image to identify image pixels that change more than the defined threshold value (dB). Threshold value selection depends on the nature and expected changes in the magnitude of VH backscatter and the SAR geometry (e.g., incidence angle). A generalized threshold for the rice fields can only be determined if the optimum SAR data acquisition is guaranteed (e.g., SAR observations are available in the flooded and vegetative stages). Otherwise, the threshold must be optimized considering the data acquisition and the constraints of local crop calendar. S-1A provides at least one acquisition after every 12 days over the selected study sites (see Figure 4.4); after the launch of S-1B the temporal sampling was reduced to 5-6 days. Based on the visual interpretation of optical

imagery for the selected period and expert knowledge acquired from the ancillary data, a threshold of 8.5 dB was used to extract the potential rice pixels referred to as $\sigma^{o}_{VH\_potential}$.

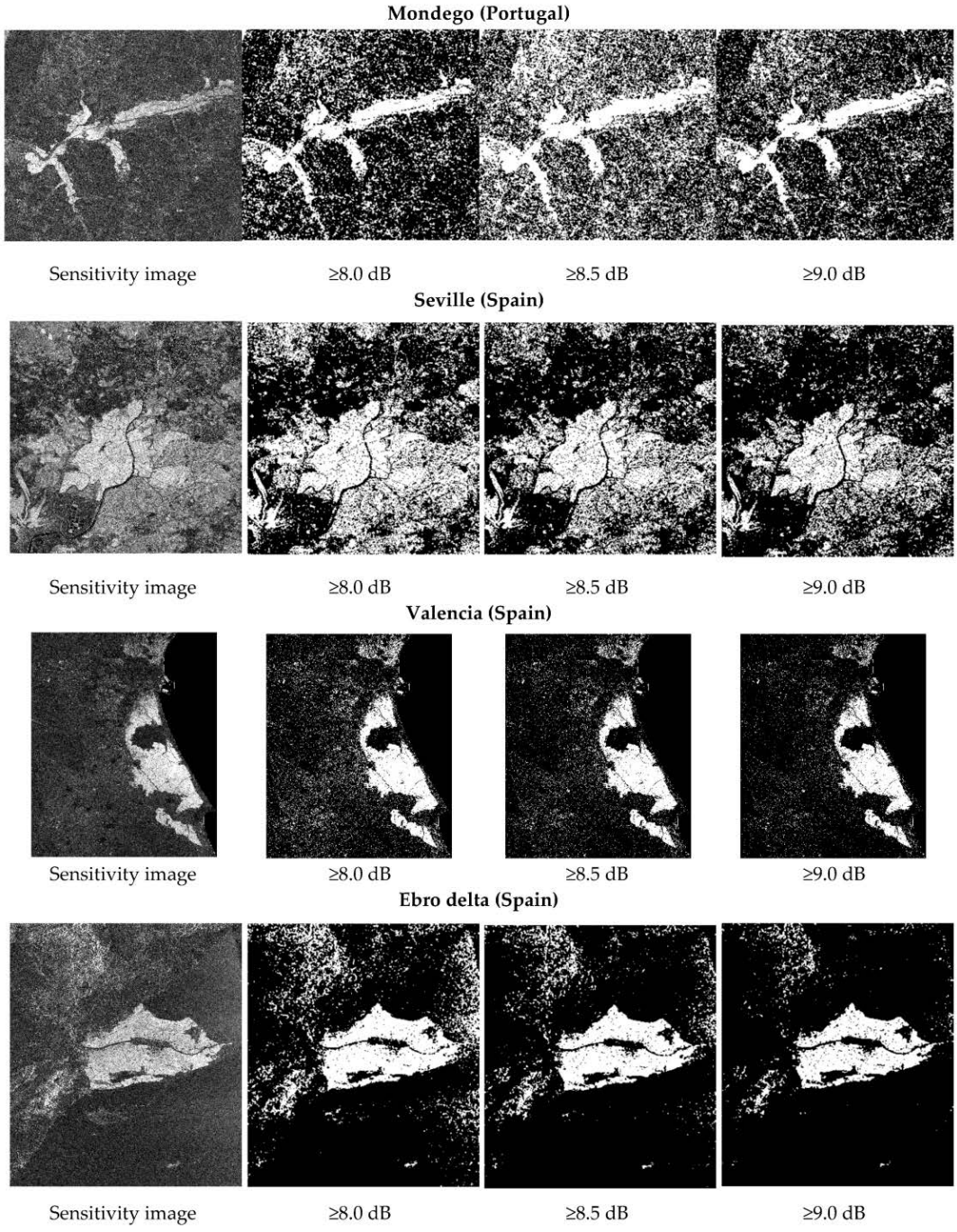

Figure 4.7. Sensitivity images and potential rice cropland area extent results using different thresholds.

Figure 4.7 (first column) shows sensitivity images based on dry reference (P05) and wet reference (P95) images for all study areas, and the results of applying thresholds of 8, 8.5 and 9dB to these images are illustrated in following columns of the figure. The CLC 2012 map is used to indicate the compartment boundaries, and pixels exhibiting change below and upper the threshold (8.5 dB) are classified as potential rice cropland areas. Combining Figure 4.6 with Figure 4.7 suggests a threshold on sensitivity of 8.5 dB to extract the potential rice cropland pixels. Lowering the threshold to 8.0 dB increases area outside the potential rice cropland areas in all the study sites leads to computation time increases. Raising the threshold to 9.0dB decreases the potential rice cropland areas may leads to numerous rice pixels are omitted. Thus 8.5 dB seems the better choice as long as we accept that physically, processing time, as well as classification precision. With this threshold, the majority of the rice cultivated areas are correctly picked out in all data sets. From the basic concept of the approach, it is clear that classification error will occur for the rice pixels whose variation is less than the selected threshold. Different of farming activities during the growing season (rice varieties, water level in the fields, density of rice plants in the fields), SAR acquisitions period may give rise to this type of misclassification.

4.3.3. Time series filtering

Filtering the backscatter time series has the purpose of reducing the short-term influence of environmental conditions and noise inherent in the S-1 data due to speckle and other noise-like influences. The processed output is a smoothed backscatter signal ($\sigma^o_{VH_{potential\_smooth}}$), which will be used for the extraction of different phenological stages of rice (e.g., a start of the season, heading time, and length of season). For the temporal filtering of the $\sigma^o_{VH\_potential}$ time series a Gaussian smoothing filter (with the standard deviation of 3 dB for the kernel) was used. A detailed investigation on the selection of kernels with different standard deviation was already reported by Nguyen et al, 2015 (Nguyen et al. 2015). Moreover, in order to discriminate the rice pixels from the other land cover classes we have empirically defined a list of three more static thresholds based on the $\sigma^o_{VH_{potential\_smooth}}$ values.

4.3.4. Extraction of vegetation phenology parameters

For this step, we calculated three phenological indicators, namely, date of beginning of season (DoS), date of maximum backscatter (DoM), and Length of the season (LoS). This allows to delineating the areas as "rice paddy", and all other areas were placed in a generalized "non- rice" class. These parameters were introduced by (Nguyen et al. 2016), summarized in the table below (Table 4.1).

Table 4.1. Phenological parameters for the rule-based classification.

Parameters	Definition & Explanation
DoS	During the growing season, the date of the beginning of season is defined as the first local minima in $\sigma^{o}_{VH_{potentia\_smooth}}$ time-series.
DoM	During the growing season, the date when backscatter reaches a maximum value is defined as the local maxima in $\sigma^{o}_{VH_{potentia\_smooth}}$ time-series. And this date must come after the date of the beginning of season, where it reaches its local minimum backscatter value
LoS	The length of the season is defined as the number of days difference between DoM and DoS.

The first threshold is set to exceed -19 dB for the local maxima (for a peak detection corresponding to rice heading date). This threshold was set based on the analysis of rice crop phenology to eliminate unrealistic peaks that were equal to or lower than -19 dB (Figure 4.8). The second threshold is set to the minimum value of the backscatter (the difference between local minima and maxima), which has to exceed 3.0 dB. Date of beginning of season (blue dot) and date of maximum backscatter (red dot) are depicted in Figure 4.9. All areas that practice rice crops start the growing season between May–June where the lowest backscatter is observed. Rice flowering period then comes after more than one and a haft month (July-August) where S-1 respond signal in the temporal signature reaches the peak. These results are in good agreement with the crop calendar presented in Figure 4.4. In addition, considering a rice cycle of irrigated rice cropping systems in the region from 100–120 days, the last one threshold is set for the temporal distance between the date of beginning of season and the date when maximum backscatter value is recorded. This temporal distance has to be greater than the shortest

possible rice growing cycle and smaller than the longest possible rice growing cycle, which is about 50 and 120 days respectively. If all three conditions are met then the pixel is classified as rice, otherwise as non-rice area.

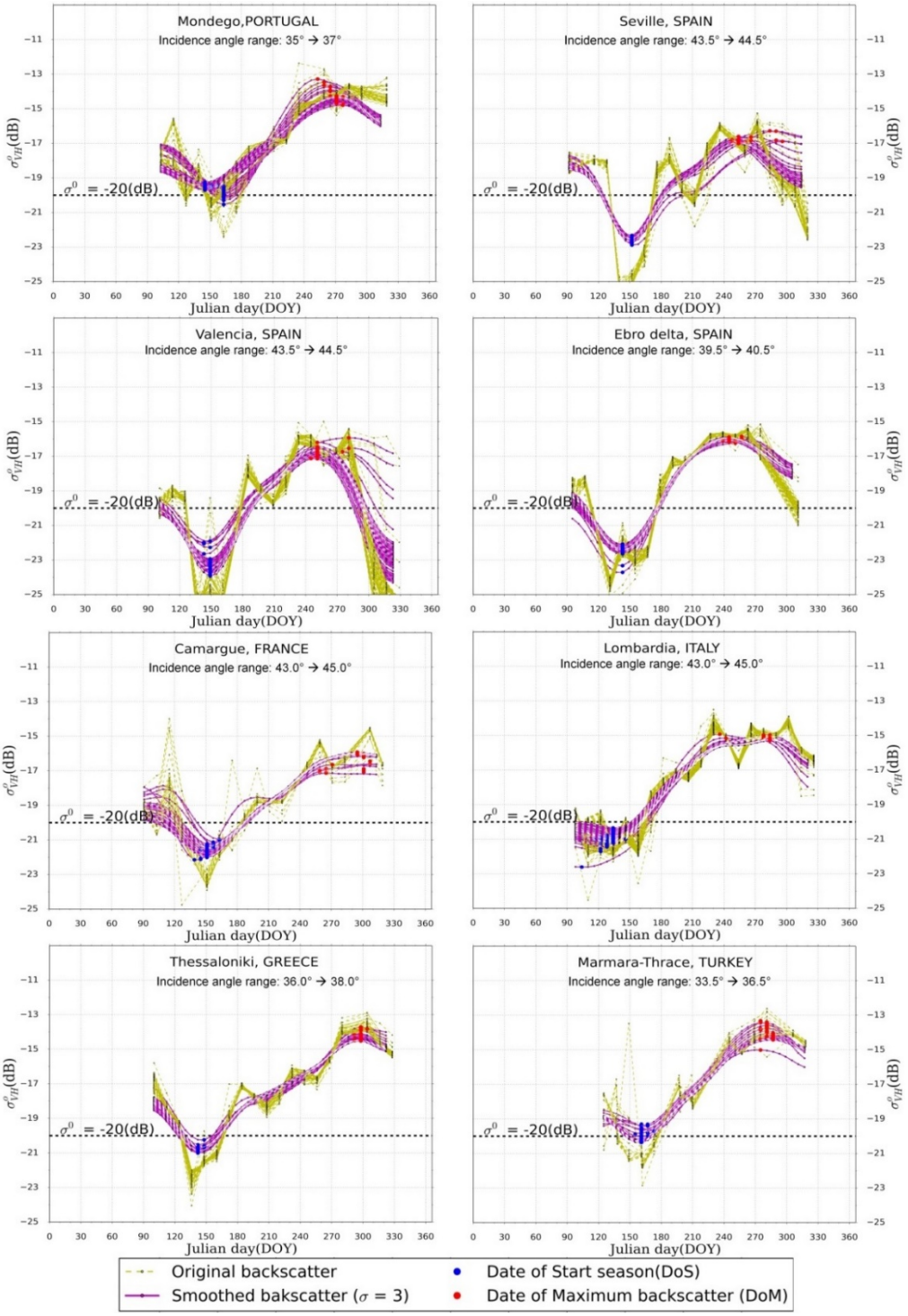

Figure 4.8. Temporal evolution of the backscattering coefficients derived from VH polarization (where, $\sigma^o_{VH} = -20\ [dB]$ is base line.

4.3.5. Rice paddy identification

Due to the high temporal variability in the SAR backscatter signal across the different study sites, the raw output from the thresholding of phenological profiles contained some noisy pixels. This implies that most fields were not fully classified as rice and non-rice class at the pixel level. Therefore, we constrained the minimum mapping unit to the average farm size in the Mediterranean region, which is 1/4 hectares. This means that no polygon was composed of fewer than 25 S-1 pixels (20m spatial resolution, 10m pixel spacing). We implemented this through a post-classification processing step, whereas a majority/minority analysis with the window size of 5×5 pixels was applied to remove the small pixel groups in order to obtain refined classification results.

4.3.6. Accuracy assessment

For validation and evaluation of classification results, standard accuracy assessment measures were used i.e., kappa coefficient, overall accuracy, omission error, and commission error. Rice cropland vector layer 2015 for study site in Spain (Seville), rice cropland maps created through interpretation of SPOT-5 data for three study sites in Spain (Valencia), Italy, and France; rice cropland raster layers 2006 from CLC 2006 for Marmara-Thrace, Turkey; and rice cropland raster layers from CLC 2012 for all study sites were used.

4.4. Results and Discussion

4.4.1. Temporal rice backscatter signature from Sentinel-1 SAR data

Seasonal VH time series are shown in Figure 4.8 (a-h), for Mondego (Portugal), Seville (Spain), Valencia (Spain), Ebro delta (Spain), Camargue (France), Lombaria (Italy), Thessaloniki (Greece) and Marmma-Thrace (Turkey) respectively. In addition to this, Figure 4.8 (a-h) also shows the results of smooth backscatter profiles (magenta color), the date of maximum and minimum backscatter values for the selected rice fields are represented by the red and blue dots respectively. To complement this analysis, Figure 4.9 shows the VH backscattering coefficients and false color composites of the study sites.

Figure 4.8 (column 4) shows the color composites, which are created by using the multi-temporal SAR acquisitions in order to highlight the temporal characteristics

within the rice fields. The red, blue, and green colors in these figures correspond to the images acquired during the flooded/seeding (April/May), heading (August/September) and post harvested (October/November) period respectively. The blue and dark green color regions in these figures (Fig. 4.9, column 4) indicate the rice cropland areas. At the beginning of the growing season (April-May) the σ^o_{VH} values from the rice fields were very low due to flooding after sowing. Thus, in the early stage of rice crop growth the fields appeared as dark areas in SAR images. This condition corresponds to those scenes that were acquired during the months April and May (see black areas in Figure 4.9, the first column). In general, during this period the rice fields show low backscatter values e.g., less than -20dB (for reference see Figure 4.8). However, there are several conditions related to the soil preparation and wind speed/direction that must also be considered. Some rice fields require a special tillage, such as furrows, or the presence of low water level in the field for a shorter period due to the diversity in farming activities among different parts of the region. If these furrows are shallow and under light wind conditions, the surface is smooth irrespective of the furrow direction. However if the furrows are deep, the furrow direction becomes an important factor regarding SAR image acquisition geometry. In case that the deep furrows are nearly parallel to the radar viewing direction, the surface seems smooth in radar image. On the other hand, if the deep furrows are perpendicular to the radar viewing direction, the surface becomes strongly rough, and the signal backscatter becomes very strong. These results are in accordance with Brisco et al. (1991) when evaluating the effect of tillage row direction in relation to the radar's look direction using radar backscattering coefficient from three different radar frequencies (Brisco et al. 1991). These types of influences on the radar signal can be considered as one of the scenarios that affected to the backscatter values in the cases of Marmma-Thrace (Turkey) and Lombaria (Italy) as shown in Figure 4.8.

In the second stage (i.e., vegetative stage), backscatter value increases as the vegetation grows (e.g., plant size increases), and eventually the SAR images show no significant difference between rice fields and other agricultural fields or vegetated areas (see bright areas in Figure 4.9, second column). One month to 45

days after the start date of the growing season it reaches the first peak in June/July. Specifically, a simple visual inspection to the σ^o_{VH} images which were acquired at the end of July (where DoY is around 210, Figure 4.8 (a-h)) reveals that the backscatter value has dropped suddenly, despites the fact that vegetation is fully developed. This anomaly is observed for all study sites, except Mondego (Portugal) and Lombaria (Italy). It is clearly illustrated in the case of Seville (Spain) and Valencia (Spain) in the Figure 4.8. The scale of these changes is quite different for different study sites due to different agricultural practices. Like in other European regions, rice crop in Seville and Valencia (Spain) begins in mid-April with the deep placement of fertilizers under dry conditions. Flooding starts during the first week of May and then the seeds are sown. At the end of June there is a short dry period of ten days (Rodríguez Díaz, Weatherhead et al. 2007). Furthermore, this period is characterized by the increase of the rice plant height and the number and size of tillers that lead to make free space among narrowed or blocked rice stems. As a result, the absence of water from the rice fields will minimize the double bounce effect of SAR signals and this explains the decrease in backscattering values at this stage. For the other regions, throughout the rice cultivation period, water is commonly kept at a depth of 4 to 8 cm, and drained away 2 to 3 times during the growing season to improve the crop rooting, reduce the algae growth and to allow application of herbicides. For the reproductive stage (August/September), backscatter values continuously keep increasing until they achieve the maximum value in September. During this period the values of backscattering coefficient vary between the range of -17dB and -13dB, which might get influenced by the variations in incidence angle, water level in the fields, cultivation activities or the rice varieties. However, during the ripening phase a slight decrease in SAR backscatter signal is observed. One potential reason for this could be due to the fact that the plants will dry before the harvesting. Normally the rice fields are drained towards the end of August to allow harvesting (IRC, 2014).

After harvest, the fields can have diverse conditions, either bare and dry fields or covered with weeds in wet conditions. Fields may also be flooded due to local farming activities, e.g., in some areas fields are flooded again until January for duck

hunting (Rodríguez Díaz, Weatherhead et al. 2007). This event is clearly visible at the study sites in Spain (Fig. 4.8 (b-d) and Fig. 4.9). However, the levels of change are quite different among the study sites due to the differences in farming activities. Meanwhile, in other regions, some small crops or weeds cover is possible right after the rice crop is cultivated. The radar backscatter is thus variable and in most cases can have high backscatter values. Moreover, as a result of rain which is typically high in the winter season in the Mediterranean region , the water content in bare soil increases, and this may also explain the increase of backscattering. Consequently, there is little possibility to interpret this last stage of the cultivation.

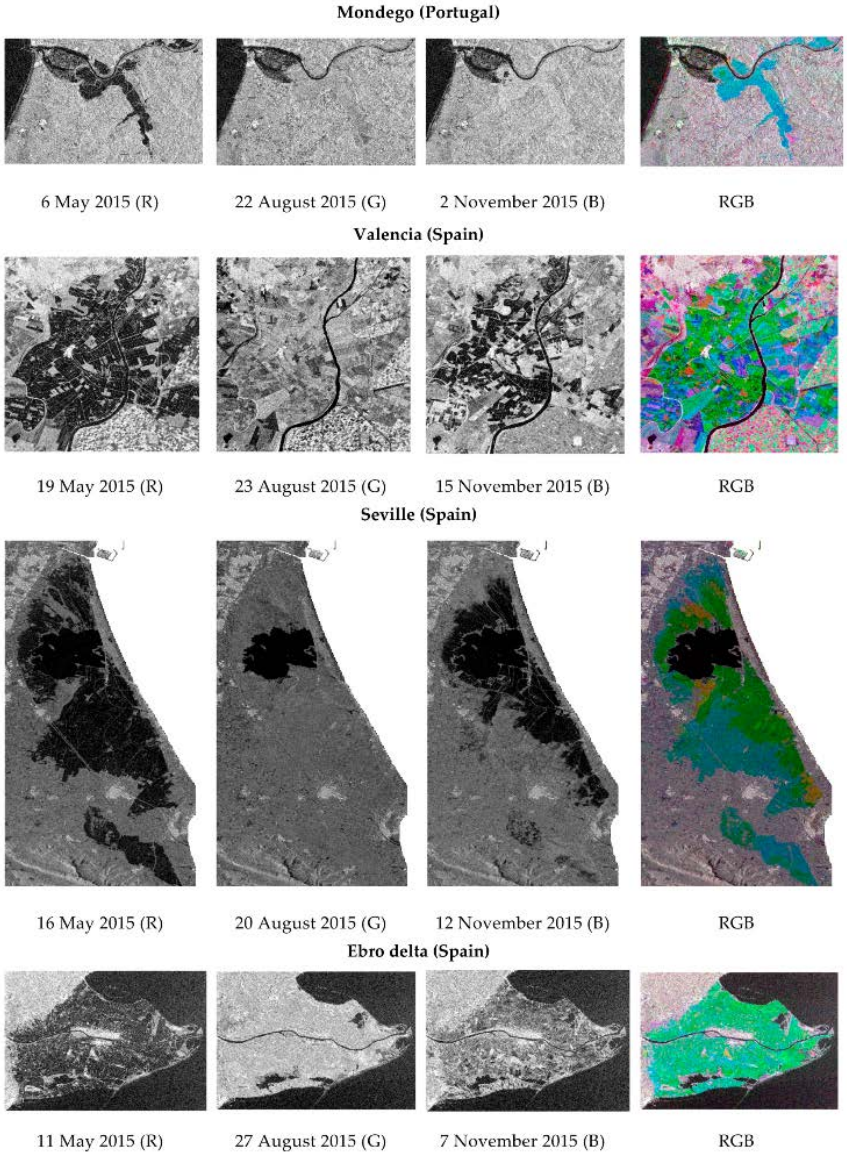

Figure 4.9. Columns 1-3: images of σ^o_{VH} acquired at three dates (from left to right) and, column 4: images of false color composite over the part of study sites.

4.4.2. Thresholds selection

The experimental evaluation of the multi-temporal S-1 backscatter signature from rice fields (as explained in section 4.1) shows that the overall behavior of σ^o_{VH} is comparable to our previous investigations (Nguyen, Gruber et al. 2016). However, the dynamic range over different regions varies due to different incidence angles and farming activities. From Figure 4.9, it is important to note that the response signal patterns from all sample parcels are very consistent. Therefore, we can conclude that these temporal signatures are associated with the rice crop type, and the empirical thresholds of three phenological parameters based on the $\sigma^o_{VH_{potentia\_smooth}}$ values can be used for the identification of rice cropland.

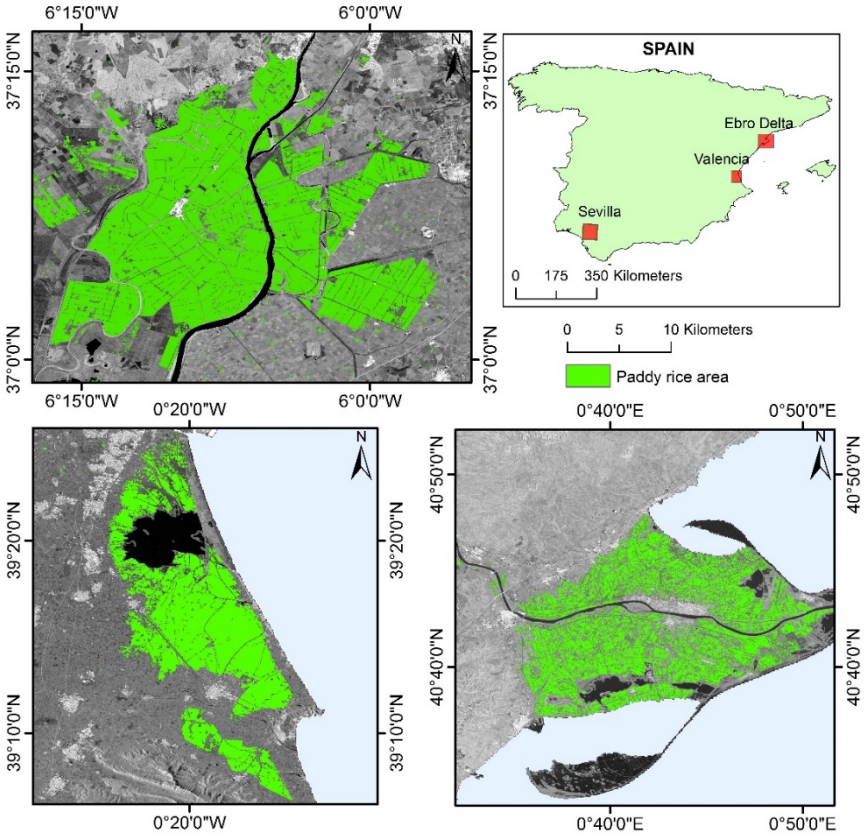

Figure 4.10. Rice cropland mapping in Spain.

4.4.3. Spatial distribution and comparison of S-1 derived rice area with reference data

The temporal backscatter signatures is shown in Figure 6 served to define specific thresholds which were applied to the S-1 time series in order to generate rice area maps for the growing season of 2015. The classification results of rice fields over

eight selected sites in the Mediterranean region are shown in Figure 10. The classification accuracy has been assessed by comparing the classification results to the 2015 rice cropland vector layer for four study sites in Seville (Spain), Valencia (Spain), Lombardia (Italy), and Camargue (France); and CLC (2012) for all study sites. The confusion matrices are presented in Table 1 and Table 2 respectively.

To provide direct comparison, the classification results in all study sites: Seville and Valencia in Spain, and Thessaloniki in Greece were evaluated by using the reference vector dataset from the same year 2015; Lombardia (Italy), and Camargue (France) were evaluated by using higher spatial resolution (SPOT 5, 10 meters); and Earth Imagery and Sentinel-2 data were used to produce reference data to validate the classification results for the rest of study areas (Table 4.2). The Kappa coefficients, rice producer accuracy (omission error), and rice user accuracy (commission error) were, respectively, 0.76, 70.2%, and 82.7% for Mondego, Portugal; 0.87, 86.8%, and 89.2 % for Seville, Spain; 0.85, 81.7%, and 93.3% for Valencia, Spain; 0.79, 70.3 and 95.3% for Ebro delta, Spain ; 0.85, 80.2%, and 94.0% for Camargue, France; 0.82, 79.8%, and 86.2% for Lombardia, Italy; 0.79, 74.1%, and 94.0% for Thessaloniki, Greece; and 0.76, 71.1%, and 84.1 for Marmara-Thrace, Turkey (Table 4.1). The lower accuracy level was observed in Mondego, Portugal, Ebro delta, Spain, Thessaloniki, Greece and Marmara-Thrace, Turkey, because of most rice fields in these regions associated with the small farms, and scattered throughout the mixed agricultural landscape and, thus, were easily omitted with non-rice classes. One potential source of error lies in the time difference between the reference data and the Sentinel-1 image acquisition. For example, the reference data were produced by digitizing homogenous sites of rice fields based on the image visualization and interpretation of existing high-resolution Google Earth imagery and Sentinel-2 optical data, while the classification maps were produced from 2015 S-1A data. Moreover, a number of different of farming activities during the growing season (rice varieties, water level in the fields, density of rice plants in the fields), SAR acquisitions period, could also cause an increase in mapping errors. Although the proposed approach can properly detect most rice areas, some land cover types with high variation in

backscatter values (e.g. wetland or seasonal water body areas) can cause commission errors.

Table 4.2. Confusion matrices of the accuracy assessment.

		Mondego, Portugal			
	class	**non-rice**	**rice**	**total**	**user accuracy**
S-1	**non-rice**	4251	71	4322	98.4%
	rice	35	167	202	82.7%
	total	4286	238	4524	
	producer accuracy	99.2%	70.2%		Kappa = 0.76

		Seville, Spain			
	class	**non-rice**	**rice**	**total**	**user accuracy**
	non-rice	10057	140	10197	98.6%
	rice	111	919	1030	89.2%
S-1	**total**	10168	1059	11227	
	producer accuracy	98.9%	86.8%		Kappa = 0.87

		Valencia, Spain			
	class	**non-rice**	**rice**	**total**	**user accuracy**
	non-rice	6344	176	6520	97.3%
	rice	56	786	842	93.3%
S-1	**total**	6400	962	7362	
	producer accuracy	99.1%	81.7%		Kappa = 0.85

		Ebro delta, Spain			
	class	**non-rice**	**rice**	**total**	**user accuracy**
	non-rice	5637	256	5893	95.6%
	rice	30	606	636	95.3%
S-1	**total**	5667	862	6529	
	user accuracy	99.5%	70.3%		Kappa = 0.79

		Camargue, France			
	class	**non-rice**	**rice**	**total**	**user accuracy**
	non-rice	8915	252	9167	97.3%
	rice	65	1023	1088	94.0%
S-1	**total**	8980	1275	10255	
	producer accuracy	99.3%	80.2%		Kappa = 0.85

Table 4.2. Confusion matrices of the accuracy assessment (cont.).

		Lombardia, Italy			
	class	**non-rice**	**rice**	**total**	**user accuracy**
	non-rice	3392	356	3748	90.5%
	rice	56	1404	1460	86.2%
S-1	**total**	3448	1760	5208	
	producer accuracy	98.4%	79.8%		Kappa= 0.82

		Thessaloniki, Greece			
	class	**non-rice**	**rice**	**total**	**user accuracy**
	non-rice	8915	357	9272	96.2%
	rice	65	1023	1088	94.0%
S-1	**total**	8980	1380	10360	
	producer accuracy	99.3%	74.1%		Kappa = 0.79

		Marmara-Thrace, Turkey			
	class	**non-rice**	**rice**	**total**	**user accuracy**
	non-rice	22975	453	23428	98.1%
	rice	210	1112	1322	84.1%
S-1	**total**	23185	1565	24750	
	producer accuracy	99.1%	71.1%		Kappa = 0.76

Table 4.3. Comparisons of rice crop extraction accuracies from time series S-1 data with Corine Land cover products (CLC 2012).

Sites, country	Kappa	Overall accuracy %	Rice commission %	Rice omission %
	Comparison with CLC 2012 after smoothing and with original CLC 2012 (in (Jonsson and Eklundh 2002))			
Seville, Spain	0.85 {0.70}	93.4 {88.1}	11.8 {9.3}	9.3 {31.9}
Valencia, Spain	0.93 {0.82}	98.9 {92.7}	3.8 {2.0}	9.5 {22.6}
Ebro delta, Spain	0.88 {0.52}	94.3 {77.7}	2.6 {2.8}	10.7 {49.2}
Camargue, France	0.46 {0.37}	87.8 {86.5}	17.7 {18.0}	62.3 {71.2}
Lombardia, Italy	0.6 {0.5}	83.9 {81.3}	12.6 {12.6}	37.3 {53.3}
Thessaloniki, Greece	0.57 {0.37}	83.5 {79.9}	29.8 {30.7}	34.1 {63.0}
Marmara-Thrace, Turkey	0.74 {0.52}	97.3 {94.5}	16.4 {11.3}	31.21 {60.5}
Mondego, Portugal	0.65 {0.43}	95.4 {98.9}	31.2 {40.7}	34.3 {65.7}

For all the study sites, CLC from 2012 were also used for comparison and checking the consistency of classification results over all study areas. Despite the limitations of the CLC data (e.g. there was a three years difference between CLC and S-1 datasets) the results suggest that the application of S-1 time series data for rice area mapping has produced consistent results for all the test sites with overall

accuracies (in quotation {}) ranging from 77.7% to 98.9% (kappa average at 0.53). The average accuracies at Camargue (France), Thessaloniki (Greece) and Mondego (Portugal) are lower than that of Seville and Valencia (Spain). The results showed relatively high error rate for both commission and omission measure (see Table 4.3 for details). The best results were achieved over Seville and Valencia (Spain) with kappa of 0.70 (Rice omission 31.9 %) and 0.82 respectively (Rice omission 22.6%), which is significantly higher than over the other regions. The worst performance (Kappa 0.37, overall accuracy: 79.9%) was reported from Thessaloniki (Greece) with the highest commission errors (63.0%) and omission error (nearly 30.7%). In order to better match the spatial scale between the classification map produced and the CLC 2012 validation layer, the classification results were smoothed by gap filling using a 10x10 window. The reason for this step is to compensate the smoothness level between the classified map and the CLC 2012 validation layer. The CLC 2012 product is consist of large homogeneous polygons which includes the small roads and fields boundaries, which are major source of error in the validation process. After smoothing the classified rice map a significant improvement in the overall accuracy and the kappa value is observed (Table 4.3). The comparison results in the Table 3 show that the poor results of accuracy comparison are not due to the errors classification output, but due to the coarser resolution of the CLC 2012 product.

4.5. Conclusions

In this paper we investigated a phenology-based approach to map rice crop at a continental scale by using space-borne C-band SAR data. Time series of S-1A IW mode with 20 m spatial resolution and VH polarization covering eight sites in the Mediterranean region were used. The results show that the proposed approach is efficient and operationally feasible for extracting rice cropland areas with high accuracy (above 70%) at 20 m spatial resolution (single-polarization) by using S-1A time series.

Our results show that dense SAR time series are critical for monitoring rice areas, which also gave an insight into the farmers' management practices within each rice cropping system.

This study emphasizes the use of annual SAR time series to generate a timely, accurate and high-resolution rice cropland spatial extent. It will be very helpful to assist decision making in the identification of rice areas for intensification, and areas for the development of irrigation as one of the necessary steps in dealing with food security related issues. Despite some current limitations of gaps in S-1A data acquisitions, this study suggests that the current and future SAR systems such as S-1B can be used complementarily to provide valuable spatial, thematic and temporal information about rice crop areas in the Mediterranean region and worldwide.

One limitation highlighted by the research is the need for ancillary information in the time of land preparation and water supply to improve the classification in areas where the temporal signature for rice is unusual. Acquiring to such data would help to improve the accuracy of rice cropland monitoring at the continental scale using S-1 time series.

CHAPTER 5

DISCUSSION AND OUTLOOK

The focus of this thesis was to utilize C-band SAR-based time-series analysis for agricultural rice monitoring. Multiple SAR images acquired from two different SAR missions (i.e., Envisat and Sentinel-1) have been used to derive seasonal rice parameters. C-band SAR data are freely available, provide global long-term coverage, and are relatively consistent. Given the significant amount of existing data records, C-band SAR-based time-series analysis shows a high potential for long-term and global rice monitoring.

This thesis is based on qualitative visual as well as regression analyses which aim to delineate rice cultivated areas and to identify seasonal dynamics over large regions from C-band SAR imagery on a seasonal/ and yearly basis. The achieved analysis accuracy is acceptable in all case studies (i.e., the overall accuracy exceeds 70%).

This thesis consists of three case studies and uses backscatter profiles from one historical C-band SAR mission (i.e., Envisat ASAR WSM, HH polarization) and one current C-band SAR mission (i.e., Sentinel-1, VH polarization). The experiments were performed in two regions, namely the Mekong Delta and the Mediterranean. Results highlight the use of C-band SAR-based time-series analysis as a powerful tool for producing high-quality rice maps and for deriving rice phenology parameters (i.e., beginning of the season, end of the season, and length of the season) over large areas.

A SAR backscatter climatology (for Envisat ASAR WS mode, HH polarization data in the Mekong Delta) was constructed from five years of data (i.e., 2007 to 2012) by normalizing incidence angles, temporal aggregation, temporal filtering, and a method to deal with different acquisition densities. This mean seasonal cycle of SAR backscatter was utilized for deriving the dominant rice-growing areas, cropping schemes and seasonal parameters in the Mekong Delta. Moreover, the evolution of rice cropland is investigated using temporal SAR backscatter

variations. A straightforward, knowledge-based decision-tree approach was used to discriminate different types of rice-cropping systems. This approach is based on the unique seasonal pattern of rice cultivated area that is apparent in the magnitude of SAR backscatter coefficients throughout the growth cycle.

Due to the higher temporal measurement density and different polarizations, a slightly different approach was followed for data from ESA's Sentinel-1 mission: Instead of combining the multi-year backscatter data in HH-polarization and normalizing incidence angles (as it was done for Envisat ASAR WSM data), single-year (i.e., spring season) single-track images from Sentinel-1 were used. No incidence angle normalization is necessary in this case as incidence angles within these single-track images are almost constant. Multi-temporal backscatter observations were analyzed to investigate the backscattering characteristics of rice at different polarizations (i.e., VV and VH-), where VH polarized observations were found to be more sensitive to rice growth than VV observations.

The potential transferability of the developed phenology-based classification strategy was investigated on a continental scale (i.e., the Mediterranean region). Therefore, a dense image stack of Sentinel-1 backscatter data was used to map rice paddy area over eight study sites in six European countries (i.e., Portugal, Spain, Italy, France, Greece, and Turkey). Results show that the proposed approach is efficient and operationally feasible for delineating rice cropland over large areas (i.e., continental scale).

Besides the strengths of the developed method for rice cropland monitoring, two main weaknesses should be noticed. The first relates to the uncertainties introduced by temporal changes in rice-cropping schemes and other land-cover changes in the study area. For example, in chapter 2, time series of over five years of Envisat WSM SAR data were used to analyze the backscattering behavior. It is expected that such land-cover changes are one of the main error sources causing the low producer accuracy of the rice classification in this case study. The other weakness is that the method requires prior knowledge on specific crop calendars which might vary between different study regions. Nonetheless, in this thesis, the developed method for rice cropland monitoring was applied to various study

regions (i.e., the Mekong Delta, Vietnam and six countries in Mediterranean region). These study regions are representative for the tropical climatic zone in Southeast Asia and for the temperate climatic zone in the Mediterranean. Therefore, the adopted rice crop calendars and soil preparation states are expected to be also applicable for other regions in similar climate regimes.

Based on the results and discussion analyzed in the previous chapter and the conclusions of the research study, the following are recommended for further investigation:

I. Reducing temporal gaps between acquisitions (i.e., 6 days) by combining images from Sentinel-1A and Sentinel-1B. The higher temporal resolution of Sentinel-1A/B data might allow identifying more subtle backscatter coefficient variations to distinguish rice cropland from other types of crop/land covers or different types of rice-cropping systems or to detect drainage events which can occur during the growing period.

II. Investigating the potential of cross ratio images (VH/VV or VV/VH) for rice crop extraction. However, cross-ratio images are sometimes difficult to interpret. For example, at the beginning of the rice season, the depression in VV backscatter is probably related to the disappearance of standing water. The VH signal, on the other hand, seems to be less affected by changes in standing water. This behavior can negatively influence the accuracy of rice area delineation when using such cross-ratio images.

III. The developed SAR-based rice monitoring approach relies on a set of various thresholds (e.g., backscatter thresholds for deriving start of the season, end of the season, and length of the season) which are empirically estimated from reference data-sets. Despite the high accuracy of the results, an optimization of these threshold still provides potential for further improving the classification.

IV. The developed SAR-based rice monitoring approach may be improved to provide seasonal estimates on regional scales and annual evaluations on continental scales with a resolution in the order of 20 meters (i.e., from Sentinel-1). To archive this goal, the approach needs to be further evaluated

and implemented on an appropriate computing infrastructure and tested on large SAR data-sets. The necessary expertise to continue these plans and to access a super-computing facility with near-real-time support will be provided a through cooperation with the Earth Observation Data Centre for Water Resources Monitoring (EODC) at TU Wien. The developed algorithm could be implemented into the SAR processing structure of TU Wien and applied on large SAR data-sets.

V. Despite the high accuracy of the proposed method, it would be worthwhile to investigate the role and importance of the other local characteristics of rice cultivation factors (e.g., water supply conditions and tilling practices) to improve the classification accuracy. Reliable information on a single field scale is required to better explain the influence of tilling practices on backscatter signals and their variations during dry periods. Such information can also help to better specify the rice signatures and may contribute to enhancing the results. Information about land preparation and water supply would also be beneficial to improve the classification in areas where SAR temporal backscatter profiles are unusual.

BIBLIOGRAPHY

ADB (Asian Development Bank), (**2009)**. The economics of climate change in Southeast Asia: a regional review. Manila, Philippines.

Apel, H., N. N. Hung, T. T. Long and V. K. Tri (**2012**). Flood Hydraulics and Suspended Sediment Transport in the Plain of Reeds, Mekong Delta. *The Mekong Delta System: Interdisciplinary Analyses of a River Delta*. Springer Netherlands**:** 221-232.

Aschbacher, J., A. Pongsrihadulchai, S. Karnchanasutham, C. Rodprom, D. R. Paudyal and T. L. Toan (**1995**). Assessment of ERS-1 SAR data for rice crop mapping and monitoring. *International Geoscience and Remote Sensing Symposium*. Firenze, Italy.

Blengini, G. A. and M. Busto (**2009**). The life cycle of rice: LCA of alternative agri-food chain management systems in Vercelli (Italy). *Journal of Environmental Management* 90(3): 1512-1522.

Bouman, M. (**2009**). How much water does rice use. *Rice Today*. 8.

Bouvet, A. and T. Le Toan (**2011**). Use of ENVISAT/ASAR wide-swath data for timely rice fields mapping in the Mekong River Delta. *Remote Sensing of Environment* 115: 1090-1101.

Bouvet, A., T. Le Toan and N. Lam-Dao (**2009**). Monitoring of the rice cropping system in the Mekong Delta using ENVISAT/ASAR dual polarization data. *IEEE Transactions on Geoscience and Remote Sensing* 47: 517-526.

Bridhkitti, A., and T. J. Overcamp (**2012**). Estimation of Southeast Asian Rice Paddy Areas with Different Ecosystems from Moderate-Resolution Satellite Imagery. *Agriculture, Ecosystems and Environment* 146: 113–20.

Brisco, B., R. J. Brown, B. Snider, G. J. Sofko, J. A. Koehler and A. G. Wacker (**1991**). Tillage effects on the radar backscattering coefficient of grain stubble fields. *International Journal of Remote Sensing* 12(11): 2283-2298.

Calha, I. M., C. Machado and F. Rocha (**1999**). Resistance of Alisma plantago aquatica to sulfonylurea herbicides in Portuguese rice fields. *International Symposium on Aquatic Weeds, European Weed Research Society*. Springer Netherlands**:** 289-293.

Chakraborty, M., S. Panigrahy and S. A. Sharma (**1997**). Discrimination of rice crop grown under different cultural practices using temporal ERS-1 synthetic aperture radar data. *ISPRS Journal of Photogrammetry and Remote Sensing* 52(4): 183-191.

Chakraborty, M. and S. Panigrahy (**2000**). A processing and software system for rice crop inventory using multi-date RADARSAT ScanSAR data. *ISPRS Journal of Photogrammetry and Remote Sensing* 55: 119-128.

Chakraborty, M., K. R. Manjunath, S. Panigrahy, N. Kundu and J. S. Parihar (**2005**). Rice crop parameter retrieval using multi-temporal, multi-incidence angle

Radarsat SAR data. *ISPRS Journal of Photogrammetry and Remote Sensing* 59(5): 310-322.

Chang, K. W., Y. Shen, and J. C. Lo (**2005**). Predicting Rice Yield Using Canopy Reflectance Measured at Booting Stage. *Agronomy Journal* 97: 872–8.

ChartsBin. Worldwide Rice Production. http://chartsbin.com/view/1009 (last access: March **2017**).

Chen, C. F., N. T. Son and L. Y. Chang (**2012**). Monitoring of rice cropping intensity in the upper Mekong Delta, Vietnam using time-series MODIS data. *Advances in Space Research* 49(2): 292-301.

Chen, C. F., N. T. Son, L. Y. Chang and C. R. Chen (**2011**). Classification of rice cropping systems by empirical mode decomposition and linear mixture model for time-series MODIS 250m NDVI data in the Mekong Delta, Vietnam. *International Journal of Remote Sensing* 32(18): 5115-5134.

Chen, E. X., Z. Y. Li, B. X. Tan, Y. Pang, X. Tian and B. B. Li (**2007**). Supervised wishart classifier for rice mapping using multi-temporal ENVISAT ASAR APS data. *Envisat Symposium.* Montreux, Switzerland.

Chen, J., H. Lin and Z. Pei (**2007**). Application of ENVISAT ASAR data in mapping rice crop growth in southern China. *IEEE Geoscience and Remote Sensing Letters* 4(3): 431-435.

Choudhury, I. and M. Chakraborty (**2006**). SAR signature investigation of rice crop using RADARSAT data. *International Journal of Remote Sensing* 27(3): 519-534.

Choudhury, I., M. Chakraborty, and J. S. Parihar (**2007**). Estimation of Rice Growth Parameter and Crop Phenology with Conjunctive Use of RADARSAT and ENVISAT. *Proceedings of the Envisat Symposium*, Montreux, Switzerland, April 23–27.

de Miranda, M., Fonseca, M., Lima, A., de Moraes, T. and Aparecido Rodrigues, F. (**2015**). Environmental Impacts of Rice Cultivation. *American Journal of Plant Sciences*, 6, 2009-2018.

De Datta, S. (**1981**). Principles and Practices of Rice Production. New York, NY, USA, *Wiley*.

De Zan, F., & Guarnieri, A. M. (**2006**). TOPSAR: Terrain Observation by Progressive Scans. Geoscience and Remote Sensing. *IEEE Transactions on Geoscience and Remote Sensing,* 44(9): 2352–2360

Dong, J. and X. Xiao (**2016**). Evolution of regional to global paddy rice mapping methods: A review. *ISPRS Journal of Photogrammetry and Remote Sensing* 119: 214-227.

Dong, J., X. Xiao, W. Kou, Y. Qin, G. Zhang, L. Li, C. Jin, Y. Zhou, J. Wang, C. Biradar, J. Liu and B. Moore Iii (**2015**). Tracking the dynamics of paddy rice planting area in 1986–2010 through time series Landsat images and phenology-based algorithms. *Remote Sensing of Environment* 160: 99-113.

Directorate - General for Agricultural and Rural Development (European Commission). http://ec.europa.eu/agriculture/cereals/trade/rice/economic-fact-sheet_en.pdf (last access: September **2016**)

Elert, E. (**2014**). Rice by the numbers: A good grain. *Nature* 514(7524): S50-S51.

European Commission - Joint Research Centre. Earth observation. https://ec.europa.eu/jrc/en/research-topic/earth-observation (last access: March **2017**).

European Environmental Agency (EEA). CLC2006 technical guidelines. https://www.eea.europa.eu/publications/technical_report_2007_17 (last access: March **2017**)

European Environmental Agency (EEA). CLC2012 technical guidelines. http://land.copernicus.eu/user-corner/technical-library/Addendum_finaldraft_v2_August_2014.pdf (last access: March **2017**)

Fairhurst, T., and A. Dobermann (**2002**). Rice in the Global Food Supply. *Better Crops International* 16, Special Supplement: 3–6.

Fan, W., W. Chao, Z. Hong, Z. Bo and T. Yixian (**2011**). Rice Crop Monitoring in South China With RADARSAT-2 Quad-Polarization SAR Data. *Geoscience and Remote Sensing Letters*, IEEE 8(2): 196-200.

Fang, H., B. Wu, H. Liu and X. Huang (**1998**). Using NOAA AVHRR and Landsat TM to estimate rice area year-by-year. *International Journal of Remote Sensing* **19**(3): 521-525.

Ferrero, A. and A. Tinarelli (**2007**). Rice cultivation in the E.U. ecological conditions and agronomical practices. Pesticide Risk Assessment in Rice Paddies : Theory and Pratice. *Elsevier*: Amsterdam: 1-24.

Food and Agricultural Organization of the United Nations (FAO). http://www.fao.org/fileadmin/templates/wsfs/docs/expert_paper/How_to_Feed_the_World_in_2050.pdf (last access: March **2017**).

Food and Agricultural Organization of the United Nations (FAO). http://www.fao.org/docrep/013/i2050e/i2050e.pdf (last access: March **2017**).

Food and Agriculture Organization of Unitd Nations (FAOSTAT). Paddy Rice Production. http://faostat3.fao.org/ (last access: July, **2015**).

Gebhardt, S., J. Huth, L. D. Nguyen, A. Roth and C. Kuenzer (**2012**). A comparison of TerraSAR-X Quadpol backscattering with RapidEye multispectral vegetation indices over rice fields in the Mekong Delta, Vietnam. *International Journal of Remote Sensing* 33(24): 7644-7661.

General Statistic Office of Vietnam (GSO, **2012**). Results of the 2011 Rural, Agricultural and Fishery Census. Hanoi, Vietnam.

General Statistic Office of Vietnam (GSO, **2014**). Statistical Yearbook of Vietnam. Hanoi, Vietnam.

Genovese, G., C. Vignolles, T. Negre and G. Passera (**2001**). A methodology for a combined use of normalised difference vegetation index and CORINE land cover

data for crop yield monitoring and forecasting. A case study on Spain. *Agronomie* 21: 91-111.

Gilbert, M., X. Xiao, D. U. Pfeiffer, M. Epprecht, S. Boles, C. Czarnecki, P. Chaitaweesub, W. Kalpravidh, P. Q. Minh, M. J. Otte, V. Martin and J. Slingenbergh (**2008**). Mapping H5N1 highly pathogenic avian influenza risk in Southeast Asia. *Proceedings of the National Academy of Sciences* 105(12): 4769-4774.

Gong, P., J. Wang, L. Yu, Y. Zhao, Y. Zhao, L. Liang, Z. Niu, X. Huang, H. Fu, S. Liu, C. Li, X. Li, W. Fu, C. Liu, Y. Xu, X. Wang, Q. Cheng, L. Hu, W. Yao, H. Zhang, P. Zhu, Z. Zhao, H. Zhang, Y. Zheng, L. Ji, Y. Zhang, H. Chen, A. Yan, J. Guo, L. Yu, L. Wang, X. Liu, T. Shi, M. Zhu, Y. Chen, G. Yang, P. Tang, B. Xu, C. Giri, N. Clinton, Z. Zhu, J. Chen and J. Chen (**2013**). Finer resolution observation and monitoring of global land cover: first mapping results with Landsat TM and ETM+ data. *International Journal of Remote Sensing* 34(7): 2607-2654.

Inoue, Y., T. Kurosu, H. Maeno, S. Uratsuka, T. Kozu, K. Dabrowska-Zielinska and J. Qi (**2002**). Season-long daily measurements of multifrequency (Ka, Ku, X, C, and L) and full-polarization backscatter signatures over paddy rice field and their relationship with biological variables. *Remote Sensing of Environment* 81(2–3): 194-204.

Inoue, Y. and E. Sakaiya (**2013**). Relationship between X-band backscattering coefficients from high-resolution satellite SAR and biophysical variables in paddy rice. *Remote Sensing Letters* 4(3): 288-295.

International Rice Research Institute (IRRI). Rice Knowledge Bank. http://www.knowledgebank.irri.org/ (last access: July **2015**).

Jia, M., L. Tong, Y. Chen, Y. Wang and Y. Zhang (**2013**). Rice biomass retrieval from multitemporal ground-based scatterometer data and RADARSAT-2 images using neural networks. *Journal of Applied Remote Sensing* 7(1): 073509-073509.

Jonsson, P. and L. Eklundh (**2002**). Seasonality extraction by function fitting to time-series of satellite sensor data. *IEEE Transactions on Geoscience and Remote Sensing* 40(8): 1824-1832.

Kaojarern, S.-A., J. P. Delsol, T. L. Toan and S. P. Kam (**2002**). Assessment of Multi-Temporal Radar Imagery in Mapping Land System for Rainfed Lowland Rice in Northeast Thailand. *Map Asia* 2002.

Koay, J.Y., et al. (**2007**). Paddy fields as electrically dense media: Theoretical modeling and measurement comparisons. IEEE Trans. Geosci. Remote Sens 45(9): 2837–2849.

Koellner, T. and R. W. Scholz (**2006**). Assessment of land use impacts on the natural environment. *The International Journal of Life Cycle Assessment* 13: 32-48.

Koellner, T., L. Baan, T. Beck, M. Brandão, B. Civit, M. Goedkoop, M. Margni, L. M. Canals, R. Müller-Wenk, B. Weidema and B. Wittstock (**2012**). Principles for life cycle inventories of land use on a global scale. *The International Journal of Life Cycle Assessment* 18: 1203-1215.

Kuenzer, C., A. Bluemel, S. Gebhardt, T. V. Quoc and S. Dech (**2011**). Remote Sensing of Mangrove Ecosystems: A Review. *Remote Sensing* 3(5).

Kuenzer, C., I. Campbell, M. Roch, P. Leinenkugel, V. Q. Tuan and S. Dech (**2013**). Understanding the impact of hydropower developments in the context of upstream–downstream relations in the Mekong river basin. *Sustainability Science* 8(4): 565-584.

Kuenzer, C., H. Guo, J. Huth, P. Leinenkugel, X. Li and S. Dech (**2013**). Flood Mapping and Flood Dynamics of the Mekong Delta: ENVISAT-ASAR-WSM Based Time Series Analyses. *Remote Sensing* 5(2).

Kuenzer, C. and K. Knauer (**2013**). Remote sensing of rice crop areas. *International Journal of Remote Sensing* 34(6): 2101-2139.

Kumar, M. D., M. V. K. Sivamohan and N. Bassi (**2012**). Water management, food security and sustainable agriculture in developing economies. *Routledge*: London.

Kurosu, T., M. Fujita and K. Chiba (**1995**). Monitoring of rice crop growth from space using the ERS-1 C-band SAR. *IEEE Transactions on Geoscience and Remote Sensing* 33(4): 1092-1096.

Kurosu, T., M. Fujita and K. Chiba (**1997**). The identification of rice fields using multi-temporal ERS-1 C band SAR data. *International Journal of Remote Sensing* 18(14): 2953-2965.

Lam-Dao, N., T. Le Toan, A. Apan, A. Bouvet, F. Young and T. Le-Van (**2009**). Effects of changing rice cultural practices on C-band synthetic aperture radar backscatter using Envisat advanced synthetic aperture radar data in the Mekong River Delta. *Journal of Applied Remote Sensing* 3(1).

Lam-Dao, N. A., A.; Le-Toan, T.; Young, F.; Le-Van, T.; Bouvet, A (**2009**). Towards an Operational System for Rice Crop Inventory in the Mekong River Delta, Vietnam Using ENVISAT-ASAR data. *The 7th FIG Regional Conference*. Hanoi, Vietnam.

Le Toan, T., F. Ribbes, N. Floury, M. Fujita and T. Kurosu (**1997**). Rice crop mapping and monitoring using ERS-1 data based on experiment and modeling results. *IEEE Transactions on Geoscience and Remote Sensing* 35: 41-56.

Leinenkugel, P., C. Kuenzer, N. Oppelt and S. Dech (**2013**). Characterisation of land surface phenology and land cover based on moderate resolution satellite data in cloud prone areas — A novel product for the Mekong Basin. *Remote Sensing of Environment* 136: 180-198.

Li, K., B. Brisco, S. Yun and R. Touzi (**2012**). Polarimetric decomposition with RADARSAT-2 for rice mapping and monitoring. *Canadian Journal of Remote Sensing* 38(2): 169-179.

Li, Y., Q. Liao, X. Li, S. Liao, G. Chi and S. Peng (**2003**). Towards an operational system for regional-scale rice yield estimation using a time-series of Radarsat ScanSAR images. *International Journal of Remote Sensing* 24(21): 4207-4220.

Li, Z., G. Sun, M. Wooding, Y. Pang, Y. Dong, E. Chen and B. Tan (**2004**). Rice Monitoring using Envisat ASAR Data in China. *Envisat & ERS Symposium*. Salzburg, Austria

Liew, S. C., P. Chen, S. P. Kam, T. P. Tuong, V. Q. Minh and H. Lim (**1998**). Rice crops monitoring in the Mekong river delta using combined ERS and RADARSAT synthetic aperture radar. *IEEE International Geoscience and Remote Sensing Symposium*. Seattle, WA, USA.

Liew, S. C., S.-p. Kam and T.-p. Tuong (**1998**). Application of multitemporal ERS-2 synthetic aperture radar in delineating rice cropping systems in the Mekong River Delta, Vietnam. *IEEE Transactions on Geoscience and Remote Sensing* 36(5): 1412-1420.

Ling, F., Z. Li, E. Chen, X. Tian, L. Bai and F. Wang (**2010**). Rice areas mapping using ALOS PALSAR FBD data considering the Bragg scattering in L-band SAR images of rice fields. *IEEE International Geoscience and Remote Sensing Symposium*. Honolulu, Hawaii, USA.

Liu, Y., Chen, K.S., Xu, P., and Li, Z.L., (2016). Modeling and Characteristics of Microwave Backscattering From Rice Canopy Over Growth Stages. *IEEE Transactions on Geoscience and Remote Sensing* 54(11): 6757-6770.

Loew, A., R. Ludwig and W. Mauser (**2006**). Derivation of surface soil moisture from ENVISAT ASAR wide swath and image mode data in agricultural areas. *IEEE Transactions on Geoscience and Remote Sensing* 44(4): 889-899.

Lopez-Sanchez, J. M., J. D. Ballester-Berman and I. Hajnsek (**2011**). First Results of Rice Monitoring Practices in Spain by Means of Time Series of TerraSAR-X Dual-Pol Images. *IEEE Journal of Selected Topics in Applied Earth Observations and Remote Sensing* 4(2): 412-422.

Lopez-Sanchez, J. M., F. Vicente-Guijalba, J. D. Ballester-Berman and S. R. Cloude (**2014**). Polarimetric Response of Rice Fields at C-Band: Analysis and Phenology Retrieval. *IEEE Transactions on Geoscience and Remote Sensing* 52(5): 2977-2993.

Martin, S. Bhatt, P. W. Gething, J. J. Farrar, S. I. Hay and H. Yu (**2014**). Predicting the risk of avian influenza A H7N9 infection in live-poultry markets across Asia. *Nature Communications* 5: 4116.

Manzanilla, D.O., Paris, T.R., Vergara, G.V., Ismail, A.M., Pandey, S., Labios, R.V., Tatlonghari, G.T., Acda, R.D., Chi, T.T.N/. Duoangsila, K., Siliphouthone, I., Manikmas, M.O.A. & Mackill, D.J. (**2011**). Submergence risks and farmers' preferences: Implications for breeding Sub1 rice in Southeast Asia. *Agricultural Systems*,104: 335–347.

Masutomi, Y., K. Takahashi, H. Harasawa and Y. Matsuoka (**2009**). Impact assessment of climate change on rice production in Asia in comprehensive consideration of process/parameter uncertainty in general circulation models. *Agriculture, Ecosystems & Environment* 131(3–4): 281-291.

McNairn, H. and B. Brisco (**2004**). The application of C-band polarimetric SAR for agriculture: a review. *Canadian Journal of Remote Sensing* 30(3): 525-542.

Monfreda, C., N. Ramankutty, and J. A. Foley (**2008**). Farming the Planet: 2. Geographic Distribution of Crop Areas, Yields, Physiological Types, and Net Primary Production in the Year 2000. *Global Biochemical Cycles* 22: 1–19.

Mosleh, K. M., K. Q. Hassan and H. E. Chowdhury (**2015**). Application of Remote Sensors in Mapping Rice Area and Forecasting Its Production: A Review. *Sensors* 15(1).

Naeimi, V., P. Leinenkugel, D. Sabel, W. Wagner, H. Apel and C. Kuenzer (**2013**). Evaluation of Soil Moisture Retrieval from the ERS and Metop Scatterometers in the Lower Mekong Basin. *Remote Sensing* 5(4).

Nelson, A., M. Boschetti, G. Manfron, F. Holecz, F. Collivignarelli, L. Gatti, M. Barbieri, L. Villano, P. Chandna and T. Setiyono (**2014**). Combining moderate-resolution time-series RS data from SAR and optical sources for rice crop characterisation : examples from Bangladesh. *Land applications of radar remote sensing* (*InTech)*: Rijeka, Croatia,.

Nguyen, B. D., K. Clauss, S. Cao, V. Naeimi, C. Kuenzer and W. Wagner (**2015**). Mapping Rice Seasonality in the Mekong Delta with Multi-Year Envisat ASAR WSM Data. *Remote Sensing* 7(12).

Nguyen, D., W. Wagner, V. Naeimi and S. Cao (**2015**). Rice-planted area extraction by time series analysis of ENVISAT ASAR WS data using a phenology-based classification approach: A case study for Red River Delta, Vietnam. *ISPRS - International Archives of the Photogrammetry, Remote Sensing and Spatial Information Sciences*. Berlin, Germany.

Nguyen, D. B., A. Gruber and W. Wagner (**2016**). Mapping rice extent and cropping scheme in the Mekong Delta using Sentinel-1A data. *Remote Sensing Letters* 7(12): 1209-1218.

Nguyen, T. T. H., C. A. J. M. de Bie, A. Ali, E. M. A. Smaling and T. H. Chu (**2012**). Mapping the irrigated rice cropping patterns of the Mekong delta, Vietnam, through hyper-temporal spot NDVI image analysis. *International Journal of Remote Sensing* 33(2): 415-434.

Nyquist, H. (**1928**). Certain Topics in Telegraph Transmission Theory. *Transactions of the American Institute of Electrical Engineers* 47(2): 617-644.

Özküralpli, İ. and F. Sunar (**2007**). Monitoring Crop Growth In Rice Padies In The Thrace-Meriç Basin With Multitemporal Radarsat-1 Satellite Images. *Proceedings of the ISPRS Commission VII—Conference on Information Extraction From SAR and Optical Data, with Emphasis on Developing Countries*. Istanbul, Turkey.

Panigrahy, S., M. Chakraborty, S. A. Sharma, N. Kundu, S. C. Ghose and M. Pal (**1997**). Early estimation of rice area using temporal ERS-1 synthetic aperture radar data a case study for the Howrah and Hughly districts of West Bengal, India. *International Journal of Remote Sensing* 18(8): 1827-1833.

Panigrahy, S., K. R. Manjunath, M. Chakraborty, N. Kundu and J. S. Parihar (**1999**). Evaluation of RADARSAT Standard Beam data for identification of potato and rice crops in India. *ISPRS Journal of Photogrammetry and Remote Sensing* 54(4): 254-262.

Panigrahy, S., V. Jain, C. Patnaik and J. S. Parihar (**2012**). Identification of Aman Rice Crop in Bangladesh Using Temporal C-Band SAR – A Feasibility Study. *Journal of the Indian Society of Remote Sensing* 40(4): 599-606.

Patel, N. K., T. T. Medhavy, C. Patnaik and A. Hussain (**1995**). Multi temporal ERS-1 SAR data for identification of rice crop. *Journal of the Indian Society of Remote Sensing* 23(2): 33.

Pathe, C., W. Wagner, D. Sabel, M. Doubkova and J. B. Basara (**2009**). Using ENVISAT ASAR Global Mode Data for Surface Soil Moisture Retrieval Over Oklahoma, USA. *IEEE Transactions on Geoscience and Remote Sensing* 47(2): 468-480.

Pei, Z., S. Zhang, L. Guo, H. McNairn, J. Shang and X. Jiao (**2011**). Rice identification and change detection using TerraSAR-X data. *Canadian Journal of Remote Sensing* 37(1): 151-156.

Peng, D., A. R. Huete, J. Huang, F. Wang and H. Sun (**2011**). Detection and estimation of mixed paddy rice cropping patterns with MODIS data. *International Journal of Applied Earth Observation and Geoinformation* 13(1): 13-23.

Pingali, P. L., M. Hossain and R. V. Gerpacio (**1997**). Asian Rice Bowls: The Returning Crisis? Wallingford: CAB International; Manila: The International Rice Research Institute

Potin, P., P. Bargellini, H. Laur, B. Rosich and S. Schmuck (**2012**). Sentinel-1 mission operations concept. *IEEE International Geoscience and Remote Sensing Symposium (IGARSS)*. Munich, Germany.

Prasad, A. K., L. Chai, R. P. Singh and M. Kafatos (**2006**). Crop yield estimation model for Iowa using remote sensing and surface parameters. *International Journal of Applied Earth Observation and Geoinformation* 8(1): 26-33.

Prather, M., D. Ehhalt, F. Dentener, R. Derwent and A. Grubler (**2001**). Atmospheric chemistry and greenhouse gases. Climate Change 2001: The Scientific Basis. *IPCC Third Assessment Report*. Geneva, Switzerland**:** 239-289.

Premalatha, M. and P. P. Nageswara Rao (**1994**). Crop acreage estimation using ERS-1 SAR data. *Journal of the Indian Society of Remote Sensing* 22(3): 139-147.

Quoc Vo, T., C. Kuenzer and N. Oppelt (**2015**). How remote sensing supports mangrove ecosystem service valuation: A case study in Ca Mau province, Vietnam. *Ecosystem Services* 14: 67-75.

Renaud, F. G., J. P. M. Syvitski, Z. Sebesvari, S. E. Werners, H. Kremer, C. Kuenzer, R. Ramesh, A. Jeuken and J. Friedrich (**2013**). Tipping from the Holocene to the Anthropocene: How threatened are major world deltas? *Current Opinion in Environmental Sustainability* 5(6): 644-654.

Reynolds, C. A., M. Yitayew, D. C. Slack, C. F. Hutchinson, A. Huete and M. S. Petersen (**2000**). Estimating crop yields and production by integrating the FAO Crop Specific Water Balance model with real-time satellite data and ground-based ancillary data. *International Journal of Remote Sensing* 21(18): 3487-3508.

Ribbes, F. and T. L. Toan (**1996**). Use of ERS-1 SAR data for ricefield mapping and rice crop parameters retrieval. *IEEE International Geoscience and Remote Sensing Symposium*. Lincoln, NE, USA.

Ribbes, F. (**1999**). Rice field mapping and monitoring with RADARSAT data. *International Journal of Remote Sensing* 20(4): 745-765.

Rice Knowledge Bank. Rice Rrowing Environments. http://www.knowledgebank.irri.org/submergedsoils/index.php/rice-growing-environments/lesson-1 (access: March **2017**)

Ricepedia. Growth phases. http://ricepedia.org/rice-as-a-plant/growth-phases (access: March **2017**)

Rodríguez Díaz, J. A., E. K. Weatherhead, J. W. Knox and E. Camacho (**2007**). Climate change impacts on irrigation water requirements in the Guadalquivir river basin in Spain. *Regional Environmental Change* 7(3): 149-159.

Rossi C., Erten E (**2015**). Paddy-rice monitoring using TanDEM-X. *IEEE Trans. Geosci. Remote Sens*. 53:900–910.

Rosenqvist, A. (**1999**). Temporal and spatial characteristics of irrigated rice in JERS-1 L-band SAR data. *International Journal of Remote Sensing* 20(8): 1567-1587.

Roy, P., T. Ijiri, D. Nei, T. Orikasa, H. Okadome, N. Nakamura and T. Shiina (**2009**). Life cycle inventory (LCI) of different forms of rice consumed in households in Japan. *Journal of Food Engineering* 91(1): 49-55.

Roy, P., D. Nei, T. Orikasa, Q. Xu, H. Okadome, N. Nakamura and T. Shiina (**2009**). A review of life cycle assessment (LCA) on some food products. *Journal of Food Engineering* 90(1): 1-10.

Sakamoto, T., M. Yokozawa, H. Toritani, M. Shibayama, N. Ishitsuka and H. Ohno (**2005**). A crop phenology detection method using time-series MODIS data. *Remote Sensing of Environment* 96(3–4): 366-374.

Santasombat, Y. (**2015**). Impact of China's Rise on the Mekong Region. *Palgrave Macmillan US*.

Sass, R. L., F. M. Fisher, A. Ding and Y. Huang (**1999**). Exchange of methane from rice fields: National, regional, and global budgets. *Journal of Geophysical Research: Atmospheres* 104(D21): 26943-26951.

Sass, R. L. and R. J. Cicerone (**2002**). Photosynthate allocations in rice plants: Food production or atmospheric methane?. *Proceedings of the National Academy of Sciences of the United States of America* 99(19): 11993-11995.

Schmitt, A. and B. Brisco (**2013**). Wetland Monitoring Using the Curvelet-Based Change Detection Method on Polarimetric SAR Imagery. *Water* 5(Vv): 1036-1051.

Shannon, C. E. (**1998**). Communication in the Presence of Noise. *Proceeding of IEEE* 86(2): 447-457.

Shao, Y., C. Wang, X. Fan and H. Liu (**1997**). Estimation of rice growth status using RADARSAT data. *IEEE International Geoscience and Remote Sensing*. Singapore, Singapore.

Shao, Y., X. Fan, H. Liu, J. Xiao, S. Ross, B. Brisco, R. Brown and G. Staples (**2001**). Rice monitoring and production estimation using multitemporal RADARSAT. *Remote Sensing of Environment* 76(3): 310-325.

Showman, G.A. (**2010**). Principles of Modern Radar, in ed. by Mark A. Richards, James A.Scheer, and William A. Holm, Scitech Publishing, vol. *Volume I -Basic Principles, chap*. 21. An Overview of Radar Imaging.

Silva, E., S. Batista, P. Viana, P. Antunes, L. Serôdio, A. T. Cardoso and M. J. Cerejeira (**2006**). Pesticides and nitrates in groundwater from oriziculture areas of the 'Baixo Sado' region (Portugal). *International Journal of Environmental Analytical Chemistry* 86(13): 955-972.

Singha, M., B. Wu and M. Zhang (**2017**). Object-based paddy rice mapping using HJ-1A/B data and temporal features extracted from time series MODIS NDVI data. *Sensors* 17(1).

Son, N.-T., C.-F. Chen, C.-R. Chen, H.-N. Duc and L.-Y. Chang (**2014**). A Phenology-Based Classification of Time-Series MODIS Data for Rice Crop Monitoring in Mekong Delta, Vietnam. *Remote Sensing* 6(1).

Soo Chin, L., K. Suan-Pheng, T. To-Phuc, C. Ping, M. Vo Quang and L. Hock (**1998**). Application of multitemporal ERS-2 synthetic aperture radar in delineating rice cropping systems in the Mekong River Delta, Vietnam. *IEEE Transactions on Geoscience and Remote Sensing* 36(5): 1412-1420.

Statista Inc. http://www.statista.com/statistics/255947/top-rice-exporting-countries-worldwide-2011/ (last access: March **2016**).

Suga, Y. and T. Konishi (**2008**). Rice crop monitoring using X, C and L band SAR data. *Proc. SPIE 7104, Remote Sensing for Agriculture, Ecosystems, and Hydrology (*X). Cardiff, Wales, United Kingdom.

Tan, Q. T. Q., J. H. J. Hu, S. B. S. Bi and Z. L. Z. Liu (**2004**). A study on rice field edge extraction in Radarsat SAR images. *IEEE International Geoscience and Remote Sensing Symposium 6*: 2-5. Anchorage, AK, USA.

Tao, F., Y. Hayashi, Z. Zhang, T. Sakamoto and M. Yokozawa (**2008**). Global warming, rice production, and water use in China: Developing a probabilistic assessment. *Agricultural and Forest Meteorology* 148(1): 94-110.

Thu, P. M. and J. Populus (**2007**). Status and changes of mangrove forest in Mekong Delta: Case study in Tra Vinh, Vietnam. *Estuarine, Coastal and Shelf Science* 71(1–2): 98-109.

Toan, T. L., H. Laur, E. Mougin and A. Lopes (**1989**). Multitemporal and dual-polarization observations of agricultural vegetation covers by X-band SAR images. *IEEE Transactions on Geoscience and Remote Sensing* 27(6): 709-718.

Toan, T. L., F. Ribbes, L. F. Wang, N. Floury, K. H. Ding, J. A. Kong, M. Fujita and T. Kurosu (**1997**). Rice crop mapping and monitoring using ERS-1 data based on experiment and modeling results. *IEEE Transactions on Geoscience and Remote Sensing* 35(1): 41-56.

Ulaby, F. T., R. K. Moore and A. K. Fung (**1982**). Microwave remote sensing: active and passive. Volume II. *Radar remote sensing and surface scattering and emission theory*.

University NAVSTAR Consortium (UNAVCO). Synthetic Aperture Radar (SAR) Satellites. http://www.unavco.org/instrumentation/geophysical/imaging/sar-satellites/sar-satellites.html (access: March **2017**)

van der Sande, C. J., S. M. de Jong and A. P. J. de Roo (**2003**). A segmentation and classification approach of IKONOS-2 imagery for land cover mapping to assist flood risk and flood damage assessment. *International Journal of Applied Earth Observation and Geoinformation* 4: 217-229.

Van Groenigen, K.J., van Kessel, C., Hungate, B.A (**2012**). Increased greenhouse-gas intensity of rice production under future atmospheric conditions. *Nature Climate Change* 3: 288-291.

Wagner, W., G. Lemoine and H. Rott (**1999**). A Method for Estimating Soil Moisture from ERS Scatterometer and Soil Data. *Remote Sensing of Environment* 70(2): 191-207.

Wang, C., J. Wu, Y. Zhang, G. Pan, J. Qi and W. A. Salas (**2009**). Characterizing L-Band Scattering of Paddy Rice in Southeast China With Radiative Transfer Model and Multitemporal ALOS/PALSAR Imagery. *IEEE Transactions on Geoscience and Remote Sensing* 47(4): 988-998.

Wang, C., Wu, J., Zhang, Y., Pan, G., Qi, J., and Salas, W.A (**2009**). Characterizing L-band scattering of paddy rice in southeast china with radiative transfer model and multitemporal ALOS/PALSAR imagery. IEEE Trans. Geosci. Remote Sens 47(4): 988–998.

Wang, H., J. Chen, Z. Wu and H. Lin (**2012**). Rice heading date retrieval based on multi-temporal MODIS data and polynomial fitting. *International Journal of Remote Sensing* 33(6): 1905-1916.

Wang, L., J. A. Kong, K. H. Ding, T. L. Toan, F. Ribbes-Ballarin and N. Floury (**2005**). Electromagnetic scattering model for rice canopy based on Monte Carlo simulation. *Progress In Electromagnetics Research* 52: 153-171.

Wang, L., C. Song, Y. Song, Y. Guo, X. Wang and X. Sun (**2010**). Effects of reclamation of natural wetlands to a rice paddy on dissolved carbon dynamics in the Sanjiang Plain, Northeastern China. *Ecological Engineering* 36(10): 1417-1423.

Weng, X.-Y., C.-J. Zheng, H.-X. Xu and J.-Y. Sun (**2007**). Characteristics of photosynthesis and functions of the water–water cycle in rice (Oryza sativa) leaves in response to potassium deficiency. *Physiologia Plantarum* 131(4): 614-621.

Wikipedia. Earth observation. https://en.wikipedia.org/wiki/Earth_observation (last access: March **2017**).

WorldFacts.. 10 Largest Rice Producing Countries. http://www.worldatlas.com/articles/the-countries-producing-the-most-rice-in-the-world.html (last access: March **2017**).

Xiao, X., S. Boles, S. Frolking, C. Li, J. Y. Babu, W. Salas and B. Moore Iii (**2006**). Mapping paddy rice agriculture in South and Southeast Asia using multi-temporal MODIS images. *Remote Sensing of Environment* 100(1): 95-113.

Xiao, X., S. Boles, S. Frolking, W. Salas, B. Moore, C. Li, L. He and R. Zhao (**2002**). Observation of flooding and rice transplanting of paddy rice fields at the site to landscape scales in China using VEGETATION sensor data. *International Journal of Remote Sensing* 23(15): 3009-3022.

Xiao, X., S. Boles, J. Liu, D. Zhuang, S. Frolking, C. Li, W. Salas and B. Moore Iii (**2005**). Mapping paddy rice agriculture in southern China using multi-temporal MODIS images. *Remote Sensing of Environment* 95(4): 480-492.

Xie, Y., Z. Sha and M. Yu (**2008**). Remote sensing imagery in vegetation mapping: a review. *Journal of Plant Ecology* 1(1): 9-23.

Yan, X., H. Akiyama, K. Yagi and H. Akimoto (**2009**). Global estimations of the inventory and mitigation potential of methane emissions from rice cultivation conducted using the 2006 Intergovernmental Panel on Climate Change Guidelines. *Global Biogeochemical Cycles* 23(2).

Yang, S. B., S. H. Shen, X. Y. Zhao, W. Gao, T. J. Jackson, J. Wang and N. B. Chang (**2012**). Assessment of RADARSAT-2 quad-polarization SAR data in rice crop mapping and yield estimation. *Remote Sensing and Modeling of Ecosystems For Sustainability IX* 8513(06). San Diego, California.

Yonezawa, C., M. Negishi, K. Azuma, M. Watanabe, N. Ishitsuka, S. Ogawa and G. Saito (**2012**). Growth monitoring and classification of rice fields using multitemporal RADARSAT-2 full-polarimetric data. *International Journal of Remote Sensing* 33(18): 5696-5711.

Yu, G., S. Yang, X. Zhao and S. Shen (**2010**). Application of ENVISAT ASAR Data to Rice Monitoring in Jiangsu Province, China. *International Conference on Multimedia Technology*. Ningbo, China.

Zhang, Y., C. Wang, J. Wu, J. Qi and W. A. Salas (**2009**). Mapping paddy rice with multitemporal ALOS/PALSAR imagery in southeast China. *International Journal of Remote Sensing* 30(23): 6301-6315.

Zhang, Y., Liu, X., Su, S., and Wang, C (**2014**). Retrieving canopy height and density of paddy rice from Radarsat-2 images with a canopy scattering model. Int. J. Appl. Earth Observ. Geoinf 28: 170–180.